ESTIMATION OF EPICARDIAL ELECTRICAL POTENTIALS FROM BODY SURFACE MEASUREMENTS BASED ON A DIGITAL SIMULATION OF THE HUMAN THORAX

A thesis submitted for the Degree of

Doctor of Philosophy

in the University of London

by

George Chiao-Chi Lo

June 1977

Engineering in Medicine Laboratory

Department of Electrical Engineering

Imperial College of Science and Technology

London SW7

ABSTRACT

The forward problem in electrocardiography has been attacked using a digital computer model of the human torso that took into account the heart muscles, intracardiac blood-mass, lungs, liver, great vessels, spine, sternum and anisotropic skeletal muscles. Physically, this model can be thought of as an assembly of discrete blocks of conductors. By assigning an alpha-numeric character to each conductor block according to its electrical properties, the entire torso anatomy is represented as coded images in the computer. The potential distributions in the model are calculated by the method of finite-differences. The set of finite-difference equations approximating the field distribution is constructed by means of the numerical-analogue developed in this study. These equations are solved iteratively using the Gauss-Seidel method. A rapid convergence of the solution is achieved by iterating firstly on a coarser model and then improving the accuracies of the solution on the finer model. The validity of this model was demonstrated by comparing simulated body-surface distributions with those observed on live subjects.

For applications to the inverse problem, a matrix of transfer coefficients relating the potentials on 26 epicardial segments to the potentials on 26 body-surface sites were calculated from this model. Using this transfer matrix, epicardial maps were reconstructed from in-vivo

body-surface measurements. The stability of the inverse solutions was found to be greatly improved by

a) carefully selecting the 26 body-surface sites in order to minimize the condition number of the transfer matrix.

b) spatial smoothing of the surface data before inversion.

c) performing the inverse calculations using an iterative process.

A comparison between the calculated epicardial potentials and in-vitro data showed the results to be consistent.

This study has demonstrated the feasibility of an unconstrained, evenly-determined inverse solution based on epicardial potentials.

CONTENTS

ACKNOWLEDGEMENTS

I wish to thank my supervisor, Dr. D. M. Monro, for the advice and guidance he has given me throughout this project. I am also indebted to him for making available the necessary funds and computing facilities during this period of research.

I extend my gratitude to Professor B. M. Sayers, Dr. P. J. Bourdillion and my colleagues, in particular Mr. P. Cheung, Mr. M. Thai-Thein-Neigh and the late Mr. J. Branch for the many hours of fruitful discussions.

The constant encouragements from my parents and my wife, Jennifer, during this period of research has meant much to me.

Finally, I wish to acknowledge CIBA Laboratories, Horsham, England for their generous support.

CHAPTER 1

INTRODUCTION

This dissertation describes the development of a numerical method for determining epicardial potentials from electrode measurements taken on the body surface. Non-invasive studies of this kind belong to the class of problems in electrocardiography known as the 'Inverse Problem'. Ideally, the inverse problem is concerned with the reconstruction of a physiologically realistic cardiac generator from electrical potentials recorded on the body surface. A prerequisite to such an attempt is a valid quantitative relationship between the heart sources and the body-surface potentials which they generate. To obtain such a relationship constitutes the so called 'Forward Problem'. In this study, the forward solution is found using a digital computer model of the human torso. By simulating the conduction pathways in the human body on a digital computer, the corresponding body surface distribution for any given source configuration can be calculated. Hence, the required source-surface relationship.

The forward problem has in the past, been attacked in a great variety of ways. These included analytical attempts in which the human torso is assumed to be a homogeneous conductor with highly idealized geometries such as spheres, spheroids, cylinders, etc. (Yeh and Martinek, 1957; Okada, 1956). Solutions obtained using such over-simplified models are grossly inadequate for the purpose of realistic inverse studies.

In order to obtain a more accurate relationship between the heart sources and body surface potentials, other workers constructed tank models that took into account body shape and various internal inhomogeneities. In such studies, a torso-shaped container made of some non-conducting material is filled with an electrolyte, usually a saline solution. The desired internal inhomogeneities are then simulated by introducing some porous structures so as to create regions of different resistivity inside the saline-filled container. Burger and Van Milaan (1946) used sand-bags and corks to simulate the lungs and the spine. A most ingeneous idea of using a 3-dimensional matrix of interlocking plastic rods to vary the saline-spaces inside the matrix structure was proposed by Rush (1971). By trimming the edges of the rods, the density ratio of insulating plastic to the conducting saline solution in each structure could therefore be controlled. The twice life-size model he constructed which took into account the heart muscle, the cardiac blood-mass, The lungs, the liver, the great vessels, the spine, the ribs, the subcutaneous fat and the anisotropic skeletal muscles must be the most detailed modelling of the human torso that has ever been attempted. Although analogue devices of this kind are capable of a high degree of realism, they are on the other hand, expensive to build and cumbersome to use. Once constructed, their geometries or resistivity ratios cannot be easily altered. For this reason, it is unlikely that models of this kind will be used extensively for electrocardiographic investigations that involve changes in either the torso geometry or the tissue resistivities.

Human subjects have also been used in forward studies. Body-surface mapping of pacemaker impulses on cardiac patients with implanted catheters have provided much insight into the nature of the transmission of electrical signals in the human body (Hamer, Boyle and Sowton, 1965). Studies of this kind however, are limited as the investigator has little or no control over the positioning of the catheter electrodes inside the patients. Nevertheless, these results provide invaluable data for testing the validity of other models. Cadavers offer a greater scope for more systematic investigations, but the results obtained are difficult to interpret due to the changes in tissue resistivity after death.

The availability of large high-speed digital computers makes it possible to attack this problem numerically. The earliest of such attempts was made Gelernter and Swihart (1964). Using what is essentially an intuitive approach, they derived an integral equation for the charges that accumulate at the interfaces between regions of different conductivities. From these charges, the potential at any surface point can be calculated from Coulomb's law. The idea of such a solution is to replace the single integral equation by a set of linear algebraic equations. These equations relate the unknown charge density on an elemental surface area to the charge density on every other surface elements. By solving these equations iteratively on a digital computer the unknown surface charge densities are calculated.

An alternative integral equation was later proposed by Barr et al.(1966). Unlike the Gelernter-Swihart equation which was formulated in terms of charge densities, theirs was formulated directly in terms of the interface potentials. The integral equation was then approximated by a set of linear equations that relates the potential value at one surface point to the potential at every other surface point. As in the previous method, these equations were solved iteratively using a digital computer.

Much of the work done to promote the integral-equation method of solving the forward problem was carried out by Barnard, Duck, Lynn and Timlake (1967). They made two important contributions that were to improve on the Gelernter-Swihart technique. First, they derived a more accurate discrete approximation for the integral equation which they claimed to possess better convergence properties. Secondly, they introduced a deflation technique to speed up the convergence rate of the iterative process. Using the improved technique, they successfully calculated the body-surface potentials due to current dipole sources located inside a torso-shaped volume-conductor which included lungs and intracardiac blood-mass.

In spite of these extensive developments in the integral-equation technique for solving forward problems, the solutions obtained so far correspond to the simplest analogue models. The reason of this lies in the limitations of the integral-equation techniques: In theory, these techniques could be used to calculate the potential distribution for volume-conductors of any geometrical shapes and combinations of internal inhomogeneities. In practice, the rapidly increasing costs of both human and computational resources with shape complexity and internal inhomogeneities limits all calculations to the simplest volume-conductor configurations. Moreover, anisotropicity in the volume-conductor cannot be accounted by the integral-equation methods.

An alternative numerical approach based on the more common but well established method of finite-differences is considered in this study. Unlike the integral-equation approach, the solution obtained by finite-differences consists of point values that are distributed throughout the entire volume of the conductor. It appears at first sight that this method would require even greater computational resources since it involves solution over the entire 3-dimensional volume instead of only over the 2-dimensional boundary surfaces in the case of integral-equation approach. But as pointed out by Terry (1967), in the finite-difference formulation, the potential at each volume-point is only related to those of its nearest neighbours. In the case of the integral-equation formulation, the potential at each surface-point interacts directly with those at every other surface-points. Therefore, although the matrix of the linear equations formulated by the finite-difference method is considerably larger than the matrix of linear equations formulated by the integral-equation method, it is on the other hand extremely 'sparse'. That is, it contains a very high density of zero elements. Numerically, it can be shown that such a matrix is better suited to an iterative process. Moreover, a theorem due to Collatz (see Hilderbrand, 1968) guarantees the convergence of the finite-difference equations when either the Jacobi or the Gauss-Seidel iteration is used. The matrices derived from the integral-equations tend to be rather unstable in practice.

The reason why the finite-difference method has not previously found its way into the forward solution is that this method was orginally developed for solving simple field problems in engineering and physics. It has not been sufficiently developed to tackle the immensely more complex field problems encountered in human electrophysiology. Except for simple field configurations, the mathematical formulation of the finite-difference equations is extremely difficult and in many cases, unknown. This problem was overcome in this study by considering a straightforward resistive-network analogue which leads to convenient finite-difference equations. Being an analogue device, it can be used to solve extremely complicated field problems with the greatest conceptual ease. Its main limitations like any other analogue devices are the costs and the length of time required to construct the model. However, by borrowing the simple physical concept of the network analogue, it is possible to derive finite-difference equations for the most complex field configurations without encountering any mathematical difficulties. In essence, what has been accomplished is the development of a 'numerical-analogue' for calculating volume-conductor fields. This technique is so called because the solutions are obtained numerically on a digital computer but with a representation similar to an analogue model.

Unlike the forward problem in which the accuracy depends only on how realistic a model is used, the inverse problem on the other hand has no unique solution. Over a century ago, Helmholtz demonstrated that a given potential distribution on the surface of a volume-conductor could arise from an infinite variety of sources. Therefore, almost any kind of generators can be used to represent the electromotive forces in the heart. The earliest attempt to describe the heart activities used a single dipole which is fixed in location but allowed to vary in direction and magnitude. The inadequacies of this simple model have long been recognized. In spite of this, it has remained until today, the basis of the clinical ECG. In order to generate a more complete description of the spatial and temporal behaviour of the electrical activities within the heart, the fixed dipole was replaced by more sophisticated source configurations such as the moving dipole (Gabor and Nelson, 1954), the multipole (Yeh et al, 1958; Geselowitz, 1960) and the multiple-dipole (Fischmann and Barber, 1963; Bellman et al, 1964; Lynn et al, 1967). The moving dipole as implied, is a single dipole that is allowed the freedom of position. Its locations are indicative of the areas of major activities. The multipole has no obvious physiological siginificance. Nevertheless, it describes the body-surface distributions in a very compact manner. By far the most attractive is the multiple-dipole model. Here, a finite number of dipoles are located at significant sites throughout the myocardium. Each dipole would therefore represent the net electrical activities in its vicinity. Thus if the correct values of the moment of each dipole could be determined, it would surely be of great assistance to the clinical detection of cardiac disorders.

More recently, there has been a growing interest in determining epicardial potentials as a possible inverse solution (Martin & Pilkington, 1972; Barr and Spach, 1976). This approach has two distinct advantages: In the first instance, no prior assumption as to the physiological nature of the generator is necessary. In the case of the multiple-dipole model, the direction of each dipole has to be carefully chosen in accordance with the propagation of the depolarization waves. Secondly, inverse solutions based on epicardial potentials can be compared directly with potential measurements taken on the heart surface. No such direct comparison between the dipole moments and experimental data exists.

The important question however, is whether knowledge of epicardial potentials contribute to useful clinical information. Isochronous maps of epicardial excitation obtained by Durrer et al. (1965) showed a delay in the activation time for right ventricular hypertrophy. Taccardi et al.(1971) compared the epicardial potentials obtained before and after coronary occlusions. In all the cases, they observed a potential minimum located in the ischaemic region during the TQ interval. This minimum persisted for part of the QRS interval and was later replaced by a maximum which lasted throughout the ST and T interval. And just before the end of the T interval, this maximum disappeared and was once replaced by a minimum. In a recent study by Spach et al.(1975), they discovered two distinct features in the epicardial distributions during ectopic sequences. These were a unidirectional spread of the excitation wave from the ectopic focus during the early QRS complex and a dominance of repolarization positive potentials near the ectopic site during the ST-T interval. All these and many other similar studies clearly suggest a wealth of clinically useful information to be contained in epicardial distributions.

The greatest stumbling block to a clinically acceptable inverse solution however, remains the inability of present day techniques to resolve with sufficient accuracies the heart sources from body-surface recordings. When the multiple-dipole model was first tested by earlier workers, serious errors were demonstrated in the solutions. The magnitude of the dipole moments were either unrealistically large or the directions of the dipoles were in contradiction with known plysiological events. In order to obtain solutions in closer agreements with physiology, contraints were imposed. The most commonly applied is that of fixing the orientation of each dipole to the direction of the propagation of the depolarization wave-fronts. The most extensively developed model of this kind is that of Lynn et al.(1967). In addition to constraining the dipole directions, they further restrict the dipole movements in the solution to be non-negative, thus avoiding inward pointing dipoles which are considered to be unphysiological in the normal case at least. Other constraints included forcing each dipole to follow a given time history (Bellman et al.1964) or prescribing the dipole moment to be either 'on' or 'off' at the appropriate periods in the heart cycle (Horan and Flowers, 1967; Barr et al.,1970). The stability of an epicardial-potential inverse solution was considered by Martin and Pilkington (1972). From their investigations using a system of concentric spheres as the model for the torso, they concluded that it is not feasible to determine epicardial potentials from surface measurements using an unconstrained solution. And in a second paper (Martin et al, 1975), they discussed the use of a statistical constraint in calculating epicardial potentials.

Applying constraints to inverse solutions however, are not without their disadvantages. Surely, the ultimate objective of an inverse solution is to aid clinical detection of cardiac abnormalities. To force an inverse solution to accept what is normal may risk excluding the very abnomalities that are to be detected. An example is the case of cardiac abnomalities in which the excitation spreads inwards from the epicardium. To use a multiple-dipole solution constrained to point outwards only is clearly unrealistic in this situation.

The purpose in this study therefore, is to investigate the feasibility of an unconstrained inverse solution based on epicardial potentials. The research to achieve this goal consists of two parts: The first of which is concerned with deriving a valid forward solution and the second, an investigation of the various factors that might influence the stability of the inverse calculations. It is hoped that an accurately configured forward solution combined with a carefully structured inverse calculation will enable a stable and unconstrained inverse solution to be found.

CHAPTER 2

MATHEMATICAL STATEMENT OF THE PROBLEM

Much attention in electrocardiographic studies have been directed to two fundamental problems. These are the 'Forward problem' and the 'Inverse problem'.

The forward study is concerned with calculating the body surface potential distribution due to a given source configuration located in the myocardium. The inverse study on the other hand is concerned with the determination of the activities of the heart generators (hence the physiological state of the heart) from available potential measurements on the body surface.

Statement of the Problem

These problems may be stated mathematically as follows: Suppose the contribution to the potential at the point i on the body surface from a unit strength generator (assumed to be fixed in direction) in the j myocardial location is T_{ij} (Fig.2.1). Then the potential v_i at the point i on the surface due to an arbitrary source distribution $(s_1, s_2, s_3, \ldots s_n)$ is given by,

$$v_i = \sum_{j=1}^{n} T_{ij}\, s_j \tag{2.1}$$

where $s_1, s_2, s_3, \ldots s_n$ are the values of the strength of the generators in the myocardial locations 1,2,3,...n. Similarly,

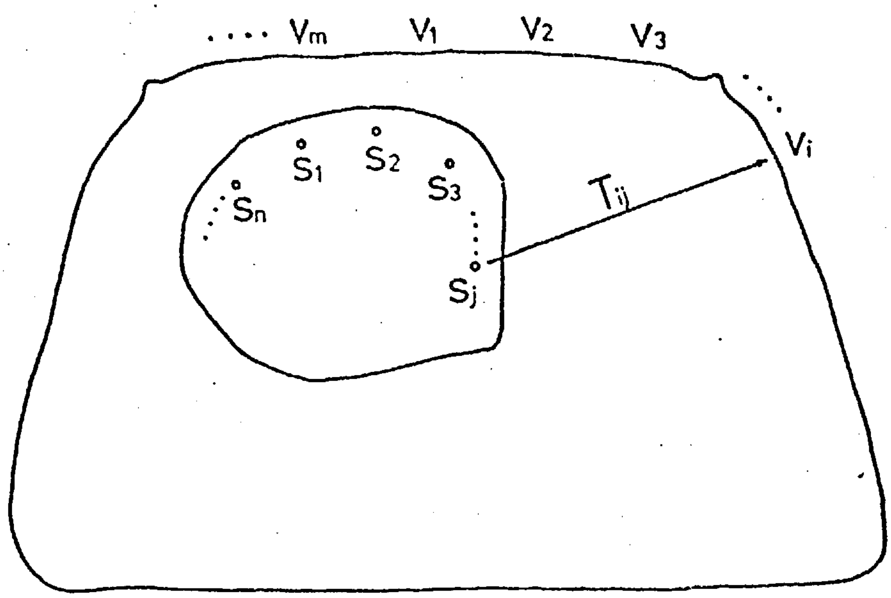

Fig.2.1 : Myocardial to body surface transfer relationship

the potential at any other surface point can be calculated by superposing the contributions from all the heart generators. Thus for m surface points on the body, the potentials at these points can be related to the source generators using the matrical equation,

$$\underline{v} = T\underline{s} \tag{2.2}$$

where $\underline{v} = (v_1, v_2, v_3, \ldots v_m)$ is a column vector containing the values of the body surface potentials, $\underline{s} = (s_1, s_2, s_3, \ldots s_n)$ is a column vector of the generator strengths and T is a matrix of dimension (m×n) containing the transfer coefficients between the heart generators and the point locations on the body surface.

The purpose in the forward study is to compute the matrix T which is clearly a function of the geometrical and electrical properties of the human torso. Once T is calculated, it is then possible to determine the generator strengths $\underline{s}$ for any given set of surface potentials $\underline{v}$. The latter constitutes the inverse problem which can be expressed mathematically as,

$$\underline{s} = T^{-1}\underline{v} \qquad (m=n) \tag{2.3}$$

Method of Overdetermination

Ideally, n surface measurements suffice to determine n unknown heart generators. In practice, measurements are subjected to errors which often result in gross uncertainties in the solution. For this reason, the system in Eqn. 2.2 is generally made considerably overdetermined. That is, taking more measurements than the number of generators (m>n). Clearly, an overdetermined system cannot be solved by direct inversion. On the other hand, it is always possible to find the best approximate solution in the sense that the square of the length of the residual vector,

$$\underline{r} = T\underline{s} - \underline{v} \tag{2.4}$$

is a minimum (the principle of least square). Minimizing $|r|^2$ yields,

$$T^T T\underline{s} = T^T \underline{v} \tag{2.5}$$

(see Lanczos, 1961).

The remarkable property of Eqn. 2.5 is that no matter how strongly overdetermined is the original system, it will always have a unique solution given by,

$$\underline{s} = (T^T T)^{-1} T^T \underline{v} \tag{2.6}$$

CHAPTER 3

CALCULATION OF VOLUME-CONDUCTOR FIELDS

3.1 Introduction

The aggregate of the passive tissues that support the flow of currents resulting from the electrical activity in the heart is generally referred to as the 'volume-conductor'. The electrical potential everywhere in the volume-conductor satisfies Poisson's equation (Plonsey, 1969)

$$\nabla^2 u = F(x,y,z) \tag{3.1}$$

where $F(x,y,z)$ is the distribution of the cardiac generators. The regions external to the myocardium are assumed to be free from any electrical generators. In these regions, Eqn. 3.1 reduces to

$$\nabla^2 u = 0 \tag{3.2}$$

which is Laplace's equation.

The problem of solving these equations is a classical one in mathematical physics known as the 'boundary value' problem. Except for a few of the simplest field configurations, these equations have no known analytical solutions. For this reason, various approximate methods of solution have to be used. These may broadly be classified into numerical techniques and analogue simulations.

Before the advent of digital computers, analogue devices dominated the solution of boundary value problems. In analogue simulation, the original problem is replaced by an analogue model which approximates its behaviour. The purpose of constructing the analogue may be to increase or decrease the physical dimension of the original system in order to facilitate investigation, to improve the accessibility of the system to probing devices by replacing, for example, a solid medium by some fluid equivalent, or merely to avoid damaging the system due to the invasive nature of the investigation. Although conceptually very simple, analogue devices tend to be rather cumbersome to use and expensive to build. Once constructed, their geometries and other physical parameters cannot be easily altered.

With large, high-speed digital computers becoming more readily available, numerical techniques have largely replaced the more cumbersome analogue devices. The approach here is to approximate the single continuous partial-differential equation by a set of discrete linear algebraic equations which can then be handled on a computer. The main attraction of a numerical method lies in its speed and economy in obtaining a solution using general purpose computing equipment which is widely available. Of particular importance is the relative ease with which any parameter of the problem may be altered. On the other hand, the task of deriving an accurate yet manageable replacement for the original differential equation can be most formidable. Indeed, solutions to some of the more complex field problems still rely to a large extend on analogue methods.

This chapter describes the development of a 'numerical-analogue' for calculating volume-conductor fields. The technique is so called because the solutions are obtained numerically using a computer but with a representation conceptually similar to a discrete analogue model. In this way, the advantages of both numerical technique and analogue simulation are realized.

3.2 The Method of Finite-Difference

The finite-difference method is one of the most well established numerical technique for solving potential field problems. Solutions obtained using this method provide potential values at discrete points (nodes) which are spaced in some ordered manner throughout the whole of the field region. The idea of the solution is as follows: At each node, the potential which is initially unknown, is approximately related to the potentials of the neighbouring nodes by a linear algebraic equation. In this way, the single partial-differential equation is modelled by a set of linear equations which can be solved simultaneously for the unknown potentials.

Approximation of the Laplacian

Consider for simplicity a two dimensional, linear, homogeneous and isotropic conducting medium S, superimposed on which is a uniform grid of interval h (Fig. 3.1). At an arbitrary node O, the potential must satisfy the equation

$$\left.\frac{\partial^2 u}{\partial x^2}\right|_o + \left.\frac{\partial^2 u}{\partial y^2}\right|_o = 0 \qquad (3.3)$$

where u is the unknown potential function, and x and y are the Cartesian coordinates of space.

The object of the exercise here is to approximate Eqn. 3.3 by a linear algebraic equation expressed in terms of the potentials at the nodes 1,2,3 and 4. This can be achieved by expanding the potentials at nodes 1,2,3 and 4 about the potential at node O

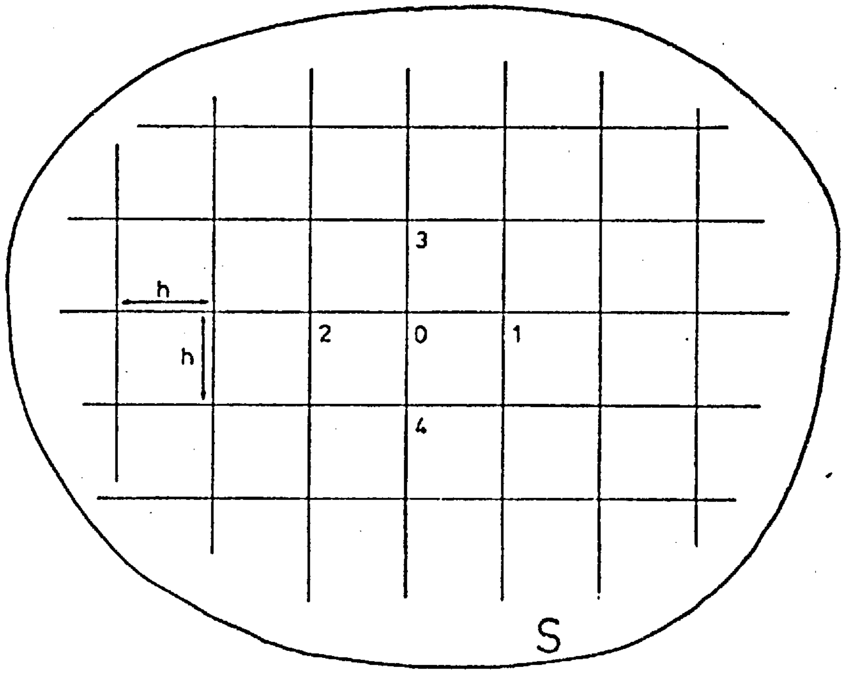

Fig. 3.1: Finite-difference representation in a uniform field region S.

using Taylor's series:

$$u_1 = u_0 + hu'_x + \frac{h^2}{2!}u''_{xx} + \frac{h^3}{3!}u'''_{xxx} + \frac{h^4}{4!}u''''_{xxxx} + \ldots\ldots$$

$$u_2 = u_0 - hu'_x + \frac{h^2}{2!}u''_{xx} - \frac{h^3}{3!}u'''_{xxx} + \frac{h^4}{4!}u''''_{xxxx} + \ldots\ldots$$

$$u_3 = u_0 + hu'_y + \frac{h^2}{2!}u''_{yy} + \frac{h^3}{3!}u'''_{yyy} + \frac{h^4}{4!}u''''_{yyyy} + \ldots\ldots$$

$$u_4 = u_0 - hu'_y + \frac{h^2}{2!}u''_{yy} - \frac{h^3}{3!}u'''_{yyy} + \frac{h^4}{4!}u''''_{yyyy} + \ldots\ldots$$

(3.4)

Adding the first two equations and ignoring the terms to the power four and above yields,

$$h^2 u''_{xx} \doteq u_1 + u_2 - 2u_0 \qquad (3.5)$$

Similarly, for the last two equations,

$$h^2 u''_{yy} \doteq u_3 + u_4 - 2u_0 \qquad (3.6)$$

On substituting Eqn. 3.5 and Eqn. 3.6 into Eqn. 3.3, the required finite-difference approximation for the potential at the node 0 is derived:

$$u_1 + u_2 + u_3 + u_4 - 4u_0 = 0 \qquad (3.7)$$

The error introduced by neglecting the higher order terms in the Taylor series is of the order of h^2. Therefore, provided h is small, Eqn. 3.7 is a good approximation of Eqn. 3.3.

Solution of Laplace Equation as a set of Simultaneous Equations

The following example demonstrates the solution of a simple field problem using the method of finite-differences. Consider a conducting square with its four sides held at potential values V_a, V_b, V_c and V_d respectively (Fig. 3.2). Applying the finite-difference approximation in Eqn. 3.7 to each of the grid points in the conductor yields a set of linear algebraic equations which can be expressed in the following matrical form:

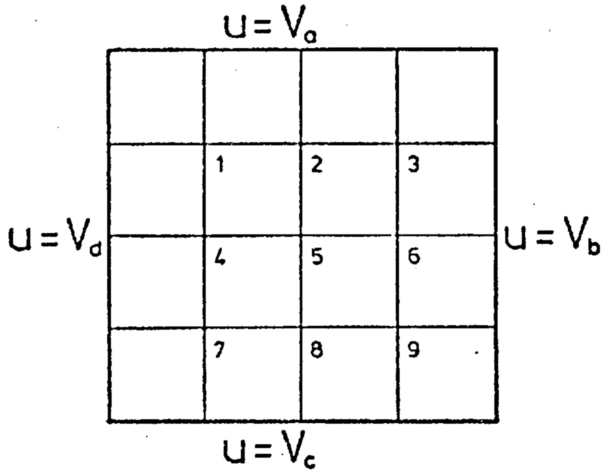

Fig.3.2: Example illustrating the finite-difference method of solution in a conducting square.

$$\begin{bmatrix} +4 & -1 & & -1 & & & & & \\ -1 & +4 & -1 & & -1 & & & & \\ & -1 & +4 & & & -1 & & & \\ -1 & & & +4 & -1 & & -1 & & \\ & -1 & & -1 & +4 & -1 & & -1 & \\ & & -1 & & -1 & +4 & & & -1 \\ & & & -1 & & & +4 & -1 & \\ & & & & -1 & & -1 & +4 & -1 \\ & & & & & -1 & & -1 & +4 \end{bmatrix} \begin{bmatrix} u_1 \\ u_2 \\ u_3 \\ u_4 \\ u_5 \\ u_6 \\ u_7 \\ u_8 \\ u_9 \end{bmatrix} = \begin{bmatrix} V_a + V_d \\ V_a \\ V_a + V_b \\ V_d \\ 0 \\ V_b \\ V_c + V_d \\ V_c \\ V_b + V_c \end{bmatrix} \qquad (3.8)$$

It is easily verified that this set of equations is non-singular and can therefore be solved simultaneously for the unknowns, $u_1, u_2, u_3, \ldots u_9$.

Limitations of the Finite-Difference Method

The finite-difference approximation derived in Eqn. 3.7 applies only to nodes at the interior of a homogeneous conductor.

In the case of those nodes on the surface of the conductor or the boundaries between different media, The finite-difference equations are quite different. Therefore if a finite-difference computer program is to be useful, it must be able to identify the various nodal conditions and generate the appropriate finite-difference equation for each node in the conductor. For a simple problem where the field boundaries are straight lines or plane surfaces, identification of the various type of nodes is a straight forward matter. Moreover, numerous general finite-difference equations exist and are easily implemented to generate the required set of linear equations.

However, applications of the finite-difference method to the solution of volume-conductor field problems are somewhat limited. The reasons for this are two-fold: The first is that boundaries separating regions of different conductivity are not just simple plane surfaces but highly convoluted ones. To define these surfaces in the computer alone constitutes a major task of organization. The second reason is that many of the nodal configurations encountered in the volume-conductor have no known finite-difference equations. Although it is possible to simplify the problem by removing these nodal configurations, the validity of the solution is then in question.

3.3 The Resistive-Network Analogue

The idea of the resistive-network analogue consists essentially of approximating the original distributed field region by a network of interconnected resistors. The mechanism of the solution is in principle identical to the finite-difference method, although the original developments are entirely independent.

The Basic Network

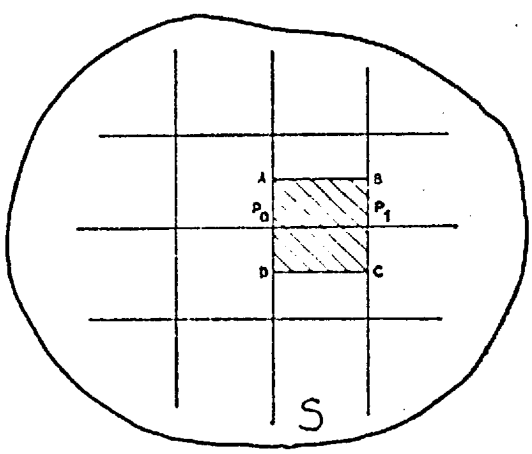

Fig.3.3: A discrete approximation of the current pathways between P_0 and P_1 by an elemental block ABCD.

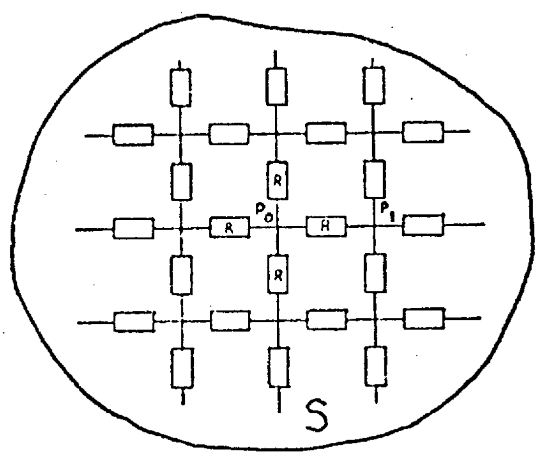

Fig.3.4: A resistive-network approximation of a distributed field region S.

Consider the distributed conductor S, superimposed on which is a uniform grid (Fig. 3.3). If the flow of current between points P_0 and P_1 is assumed to be supported solely by the block conductor ABCD, then it is possible to remove this block and replace in its place, a resistor R having the same resistance value as that across the opposite sides AD and BC of the block without affecting too significantly, the overall pattern of current flow in S. Repeating this process to every adjacent grid points in S, the entire continuous conductor is replaced by a network of discrete components (Fig. 3.4).

The error introduced by this discretization process clearly depends on the grid size. In the limit as the grid interval is made smaller and smaller, the network analogue becomes once more the continuous, distributed conductor.

Nodal Equation

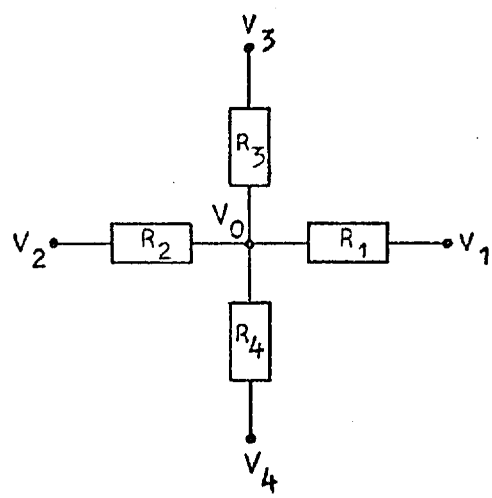

Fig.3.5: Basic network structure.

The resistive-network analogue was developed largely on an intuitive basis. In essence, its solution mechanism is similar to that of the finite-difference method. This is demonstrated by applying Kirchoff's law to the current flowing into node 0 in the network in Fig. 3.5, giving

$$\frac{V_1 - V_0}{R_1} + \frac{V_2 - V_0}{R_2} + \frac{V_3 - V_0}{R_3} + \frac{V_4 - V_0}{R_4} = 0 \qquad (3.9)$$

In the case of a homogeneous, isotropic conductor, $R_1 = R_2 = R_3 = R_4$. Eqn. 3.9 now becomes

$$V_1 + V_2 + V_3 + V_4 - 4V_0 = 0 \qquad (3.10)$$

which is identical to the finite-difference equation derived in Eqn. 3.7.

It can be shown that such similarity exists for all nodal configurations. Indeed, the resistive-network can be regarded as computing mechanism with the resistors connected in such a way that the operations indicated by the finite-difference equations are carried out.

Limitations of the Resistive-Network Analogue

The network analogue may be an extremely versatile device for solving field problems, but the number of resistors required to construct an adequate network representation of the volume-conductor makes this approach totally impractical for present study. Moreover, the interior of a 3-dimensional network structure cannot be easily accessed. This makes investigation and repositioning of any internal generators extremely difficult.

3.4 A Proposed Numerical-Analogue

The numerical-analogue to be developed in this section consists of a hybrid between the finite-difference method and the resistive-network analogue. The purpose is to simplify the implementation of the finite-difference method for calculating volume-conductor fields. This is achieved in two distinct stages. The first of which is concerned with the efficient organization of the volume-conductor data on the digital computer. In the second stage, a general finite-difference equation is derived using what is essentially a network representation of the conductor.

3.4.1 Discrete Representation of a Volume-Conductor

One of the main factors limiting the use of numerical techniques in solution of volume-conductor fields is the difficulty in representing a complex geometrical shape on the computer. In the case where the boundaries of the given conductor are straight lines (Fig. 3.6), defining these boundaries is a simple matter. However, with more convoluted

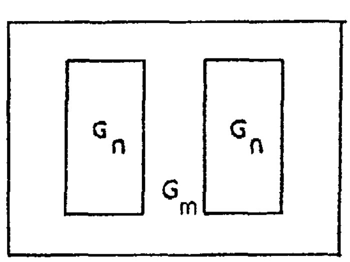

Fig.3.6: Conductor with rectilinear boundaries.

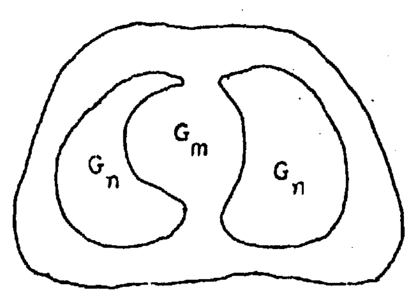

Fig.3.7: Conductor with more complicated boundary shapes.

boundary shapes as shown in Fig. 3.7, the exercise of describing the geometries rapidly becomes more difficult.

The most common and straightforward approach of defining such shapes on the computer is to use the position coordinates of a series of points distributed along the boundaries (Fig. 3.8). Such a method becomes extremely tedious when the number of points is large.

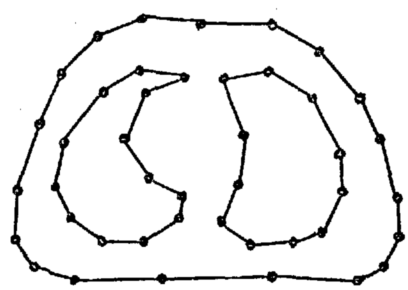

Fig.3.8: Piece-wise approximation of the conductor boundary.

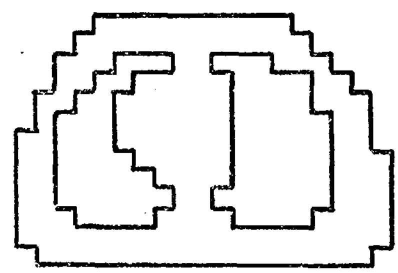

Fig.3.9: A discrete representation of the conductor.

The method proposed in this section consists of replacing the original conductor by a discrete approximation as shown in Fig. 3.9. The discretization process is most easily performed with the aid of a graph paper superimposed on top of the conductor. By assigning an alpha-numeric character corresponding

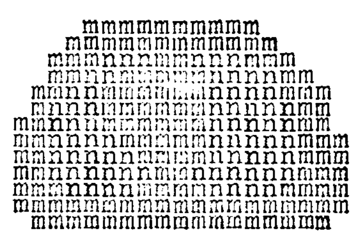

Fig.3.10: Coded image of the discrete conductor.

to the electrical property in each 'cell' in Fig. 3.9, the conductor is therefore represented in a coded form (Fig. 3.10), which is readily entered into the computer. The efficiency of data input can further be improved by compressing the data in each row in the following manner:

Row Data: --AAAAAABBBBAAAAAAAABBBAA......

Input Format: 2-,6A,4B,8A,3B,......

meaning 2 bits of blanks, 6 bits of conductor with property A, 4 bits with property B and so on.

Representation in Three-Dimensions

These ideas are easily extended to three dimensions. Instead of approximating the conductor by small conducting squares, here, the volume-conductor is represented as cubes. Fig. 3.11 shows an impression of a discretized human torso.

The discretization process is essentially the same as before and is organized as follows:

1) Divide the 3-D conductor into horizontal slabs of thickness equal to the digitization interval (Fig. 3.12b).
2) Digitize each slab by means of a 2-D grid superimposed on top of that slab (Fig. 3.12c).
3) Finally, construct the coded image for each slab by assigning the appropriate alpha-numeric code to each discrete cube (Fig. 3.12d).

In this way, the entire 3-D volume-conductor is represented as successive planes of coded images in the computer.

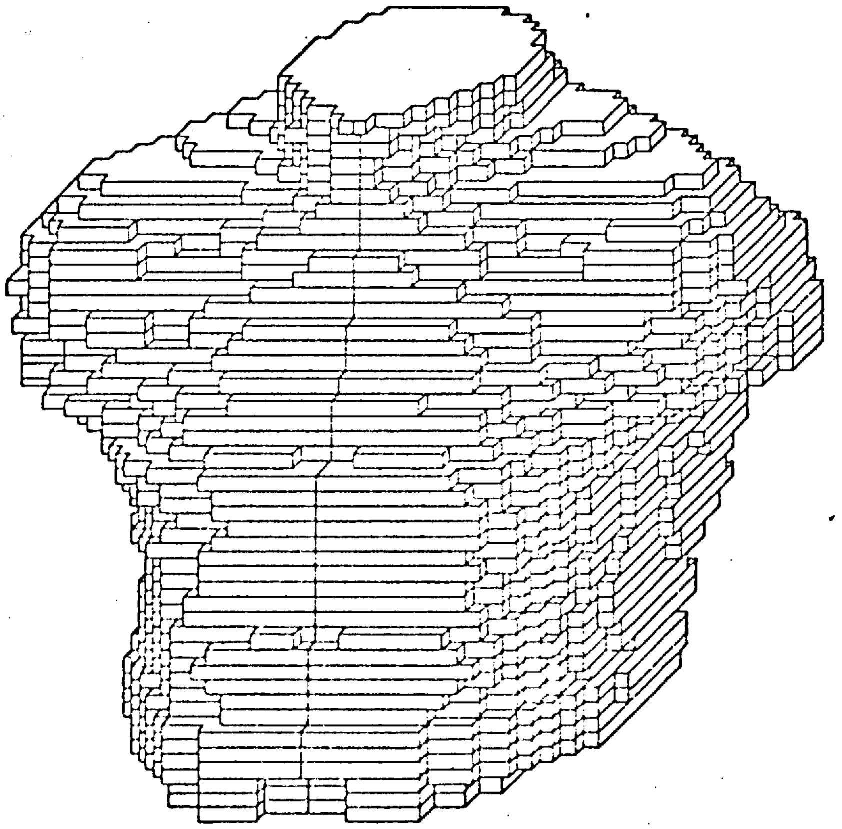

Fig.3.11: A physical impression of a discretized human torso

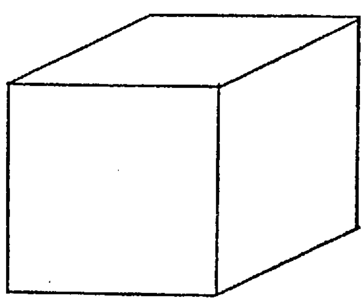

Fig.3.12a

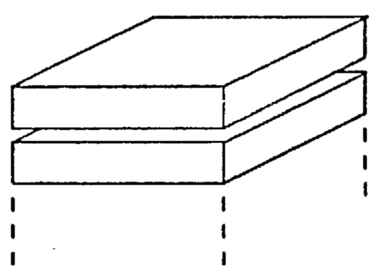

Fig.3.12b

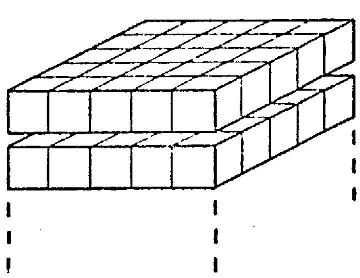

Fig.3.12c

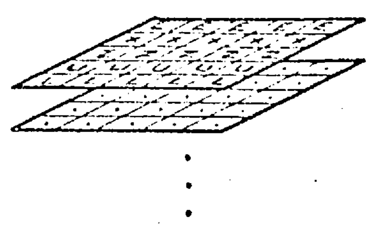

Fig.3.12d

Fig.3.12: Illustration of the stages in the discretization of a three dimensional volume-conductor.

3.4.2 Generalized Finite-Difference Equation

This section describes the development of a generalized finite-difference equation for setting up the linear equations necessary to model the volume-conductor numerically.

Consider the general nodal configuration in a 2-dimensional discretized conductor (Fig. 3.13), where A,B,C and D are four neighbouring elemental conductors with different electrical properties. The finite-difference equation for this nodal configuration has the general form:

$$K_1u_1 + K_2u_2 + K_3u_3 + K_4u_4 - (K_1+K_2+K_3+K_4)u_0 = 0 \tag{3.11}$$

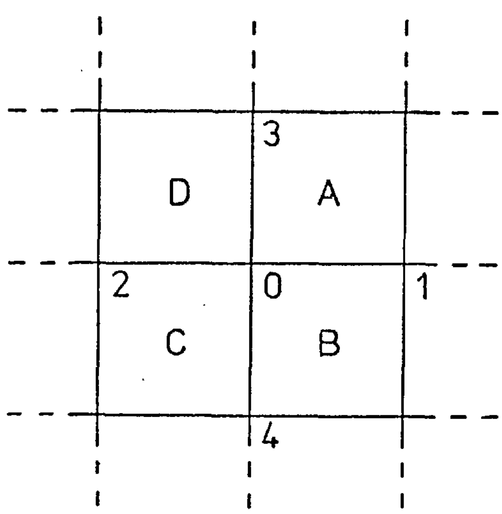

Fig.3.13: A general nodal configuration.

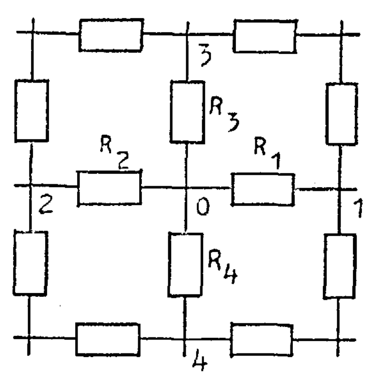

Fig.3.14: A general network configuration.

To derive the coefficients K_1,K_2,K_3,K_4 in Eqn. 3.11 using the mathematical approach described in Sec. 3.2 is extremely tedious. On the other hand, a resistive network analogue for this nodal configuration can easily be constructed (Fig. 3.14). The only problem that remains is to determine the values of the resistances R_1, R_2, R_3 and R_4 which can then be substituted into the nodal equation in Eqn. 3.9 to obtain the required finite-difference formula:

$$\frac{1}{R_1}u_1 + \frac{1}{R_2}u_2 + \frac{1}{R_3}u_3 + \frac{1}{R_4}u_4 - \left(\frac{1}{R_1}+\frac{1}{R_2}+\frac{1}{R_3}+\frac{1}{R_4}\right)u_0 = 0 \tag{3.12}$$

Notice that the resistance values of the network analogue are just the reciprocals of the finite-difference coefficients in Eqn. 3.11. It would therefore be more appropriate to consider the conductances $G_1 = \frac{1}{R_1}$, $G_2 = \frac{1}{R_2}$, $G_3 = \frac{1}{R_3}$ and $G_4 = \frac{1}{R_4}$ instead of the resistances in the network analogue. This, as will become clearer, greatly simplifies the developments to be discussed in the remaining parts of this section.

Coefficients for the Basic Equation

Recalling from Section 3.3 that the conductance G_1 approximates the current pathway WXYZ between P_0 and P_1 (Fig. 3.15). However, this block consists of one half WXP_1P_0 with property A and the other half P_0P_1YZ with property B. In this case, it would be more sensible to regard G_1 as a parallel combination of two conductances G_A and G_B, where G_A represents the conduction pathway WXP_1P_0 between P_0 and P_1, and G_B represents the pathway P_0P_1YZ. Similarly, all other conductances in the network analogue can be represented in this manner. The purpose of using such a representation is

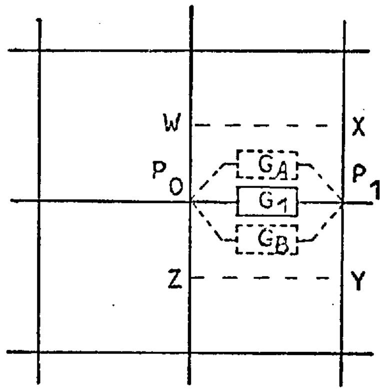

Fig.3.15: Replacement of G_1 by two parallel components G_A and G_B.

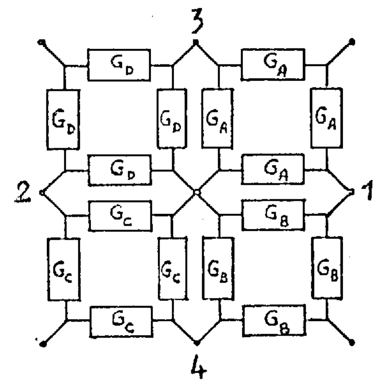

Fig.3.16: Network illustrating the relationship between the individual component and the elemental conductors A,B,C,D in Fig.3.13.

that it is now possible to relate each elemental discrete conductor to an elemental network configuration (Fig. 3.16). The importance of this will be realized in the later developments in this section.

The immediate advantage however, is that the finite-difference equation for the nodal configuration in Fig. 3.13 can be easily derived from the network analogue in Fig. 3.16 to be:

$$(G_A+G_B)u_1 + (G_C+G_D)u_2 + (G_A+G_D)u_3 + (G_B+G_C)u_4 - 2(G_A+G_B+G_C+G_D)u_0 = 0 \qquad (3.13)$$

Expressed in this form, the finite-difference equation for any arbitrary node 0 can be computed given the conductivities of the four surrounding elemental blocks A,B,C and D.

Equation for Non-Uniform Grid

The use of a regularly distributed finite-difference grid is often in practice, inefficient. Whereas a given grid interval may not be adequate to represent certain parts of the field region, it may on the other hand be unnecessarily fine in other parts. In order to minimize the number of nodes (hence the size of the system of linear equations) for a required accuracy, non-uniform grids are often used so that the grid densities may be adjusted to suit the local field condition.

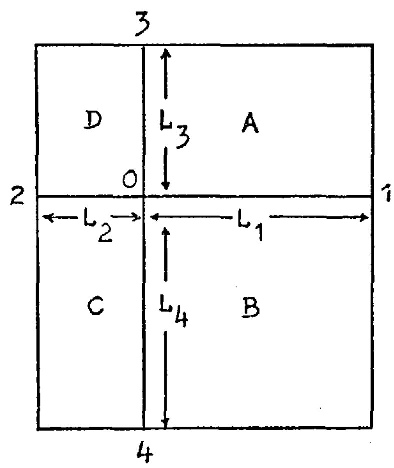

Fig.3.17: Non-uniform grid

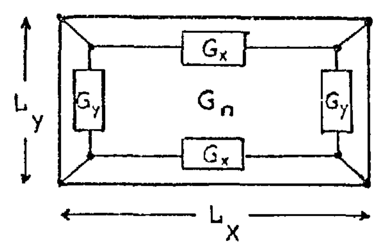

Fig.3.18: Equivalent Network for a rectangular elemental conductor

Consider a non-uniformly distributed grid configuration, Fig. 3.17. Each discrete element A,B,C,D ..... may no longer be a square. Consider the element n, whose x and y dimensions are L_x and L_y respectively (Fig. 3.18). If the conductivity of the element is G_n, then it can be shown that the values of the x and y components in the equivalent network are:

$$G_x = \frac{L_y}{L_x} G_n \,, \qquad G_y = \frac{L_x}{L_y} G_n \tag{3.14}$$

The finite-difference equation for the nodal configuration in Fig. 3.17 can therefore be expressed as:-

$$\frac{1}{L_1}(L_3G_A+L_4G_B)u_1 + \frac{1}{L_2}(L_4G_C+L_3G_D)u_2 + \frac{1}{L_3}(L_1G_A+L_2G_D)u_2$$
$$+ \frac{1}{L_4}(L_1G_B+L_2G_C)u_4 - [\,]u_0 = 0 \qquad (3.15)$$

where the quantity $[\,]$ denotes the sum of the coefficients of u_1, u_2, u_3, u_4.

Equation for Anisotropic Conductor.

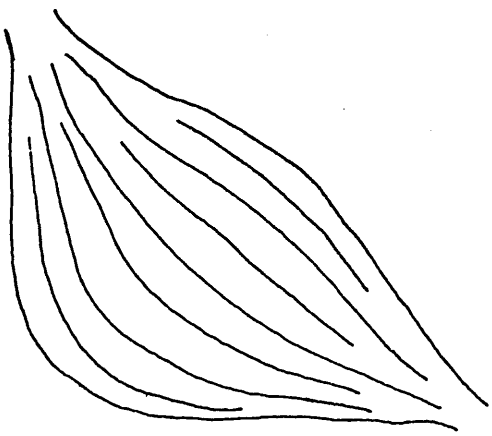

Fig.3.19: A sketch of a typical muscle layer. The 'flow-lines' indicate high conductive pathways.

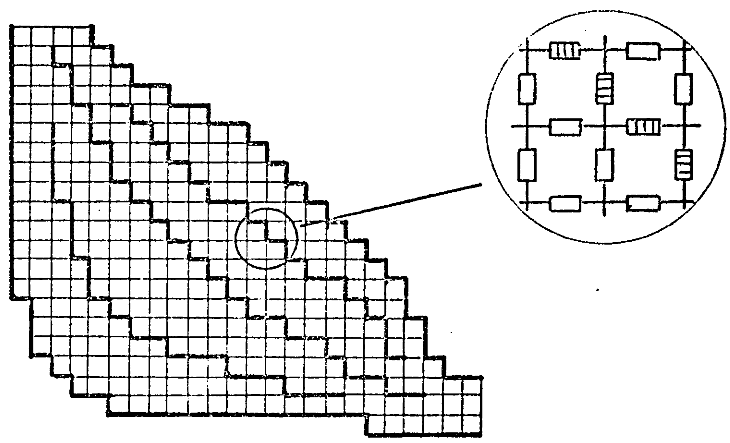

Fig.3.20: A discrete representation of the anisotropic muscle layer. The heavy lines indicate pathways connected by high conductive components.

Occassionally, it may occur that the given conductor is anisotropic. In the case where the conductivity varies from one principal axis to another, the difficulty is easily dealt with. A more difficult situation arises when the variation in conductivity follows no consistent direction. Such anisotropicities occur for example in skeletal muscles where the conductivity along the muscle fibres is an order of magnitude greater than in the transverse direction and there is no specific direction in which these fibres lie. A sketch of a typical muscle layer is shown in Fig. 3.19. The 'flow-lines' indicate pathways of high conductivity.

The method proposed here to simulate such anisotropicity is a natural extension to the numerical-analogue. The field concerned is discretized and approximated in the usual network form. Highly conductive pathways are then laid into the network to create the effects of anisotropicity. These are represented by the heavy thick lines in Fig. 3.20. It is clearly seen that the smaller the discretization interval is made, the more accurate will be the approximation.

Consider the network in Fig. 3.20 with a high conductive pathway through it. Such a network can be constructed using discrete elements whose equivalent networks consist of different conductive components (Fig. 3.21). To derive the

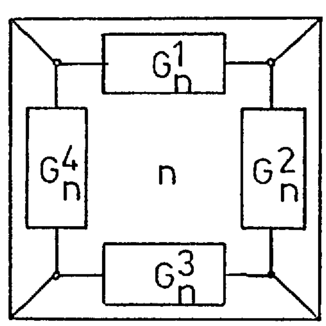

Fig.3.21: System for identifying each component in an anisotropic elemental conductor.

finite-difference equation in this case requires each individual conductance to be identified. This can be achieved by labelling the conductances in each element as indicated in Fig. 3.21. The finite-difference equation now becomes:

$$\frac{1}{L_1}(L_3G_A^3+L_4G_B^1)u_1 + \frac{1}{L_2}(L_4G_C^3+L_3G_D^1)u_2 + \frac{1}{L_3}(L_1G_A^4+L_2G_D^2)u_3$$

$$\frac{1}{L_4}(L_1G_B^4+L_2G_C^2)u_4 - [\,]u_0 = 0 \qquad (3.16)$$

where $[\,]$ denotes the sum of the coefficients of u_1, u_2, u_3, u_4.

Equation in 3-Dimensions

The developments described above are easily extended to 3-dimensions. Here, each discrete elemental conductor is represented by a 3-dimensional network structure as shown in Fig. 3.22. It is however, not essential to identify each individual conductance in this network for calculating volume-

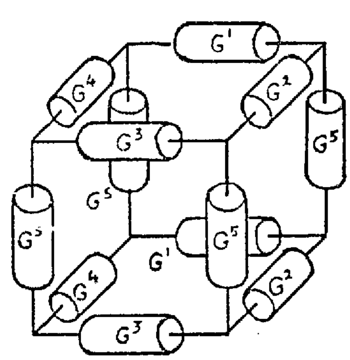

Fig. 3.22: Equivalent network for a three-dimensional elemental conductor.

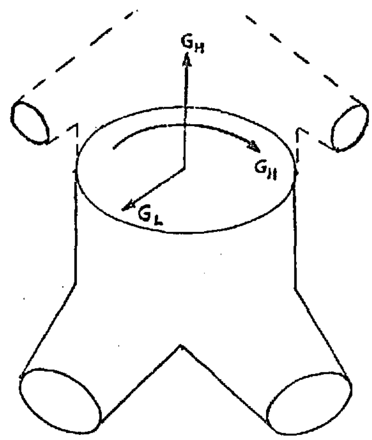

Fig.3.23: Diagram illustrating the directions of anisotropicities in the upright human torso.

conductor fields. The reason is that the anisotropicity in the upright torso occurs only in the horizontal planes (Fig. 3.23). Therefore, it is only necessary to define the five ratios, $G_n^1:G_n^2:G_n^3:G_n^4:G_n^5$ for an elemental conductor n as defined in Fig. 3.22. The finite-difference equation for a

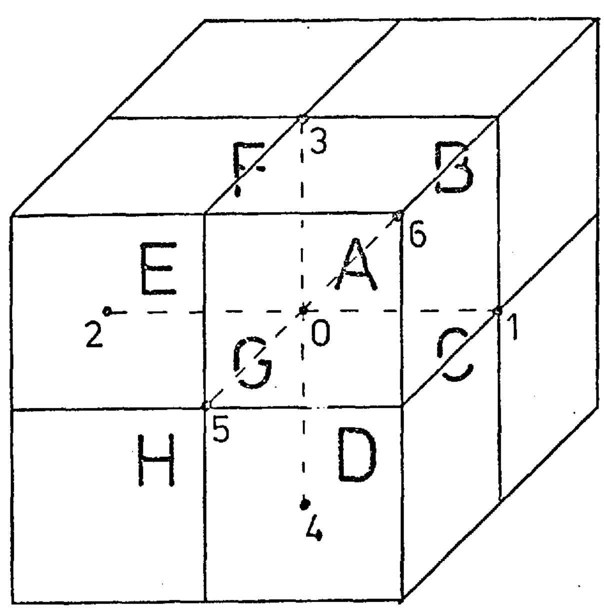

Fig.3.24: Nodal configuration in a three-dimensional volume-conductor.

node O at the corner of eight neighbouring cubes A,B,C,D,E,F,G and H (Fig. 3.23) is therefore given by,

$$\frac{1}{L_1}(L_3L_5G_A^1+L_3L_6G_B^3+L_4L_6G_C^3+L_4L_5G_D^1)u_1$$
$$+\frac{1}{L_2}(L_3L_5G_E^1+L_3L_6G_F^3+L_4L_6G_G^3+L_4L_5G_H^1)u_2$$
$$+\frac{1}{L_3}(L_1L_5G_A+L_1L_6G_B+L_2L_6G_F+L_2L_5G_E)u_3$$
$$+\frac{1}{L_4}(L_1L_5G_D+L_1L_6G_C+L_2L_6G_G+L_2L_5G_H)u_4$$
$$+\frac{1}{L_5}(L_1L_3G_A+L_1L_4G_D+L_2L_4G_H+L_2L_3G_E)u_5$$
$$+\frac{1}{L_6}(L_1L_3G_B+L_1L_4G_C+L_2L_4G_G+L_2L_3G_F)u_6$$
$$-[\,]u_0 = 0 \qquad (3.17)$$

where $[\,]$ denotes the sum of the coefficients of $u_1,u_2,\ldots.u_6$.

3.5 Solution by Iteration

The solution of a partial-differential equation using the finite-difference method has been reduced to the solution of a set of simultaneous equations which can be expressed in the matrical form,

$$A\underline{u} = \underline{b} \tag{3.18}$$

where A is a matrix of the finite-difference coefficients, $\underline{u}$ is a column vector containing the unknown potentials and $\underline{b}$ is a column vector of known values. The resultant matrix A is often very large (an order of 10,000 is necessary for an adequate representation of the torso volume-conductor). However, A is also extremely 'sparse'. That is, it contains a high density of zero elements. In a 3-dimensional conductor, the maximum number of non-zero elements in each row of the A matrix is seven. A typical configuration of a matrix formulated

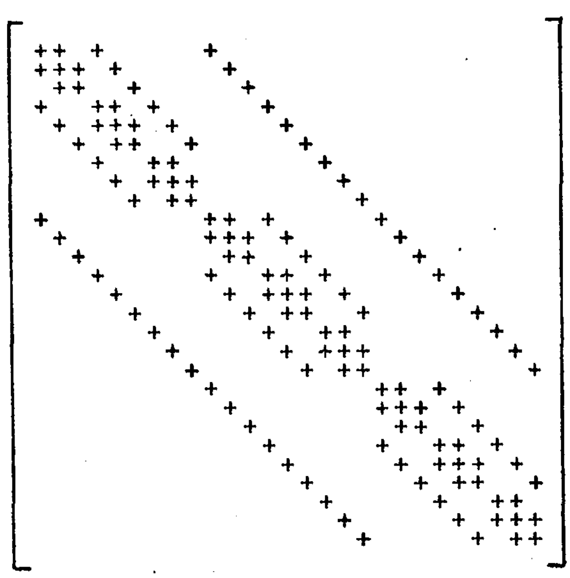

Fig.3.25: A typical matrix configuration formulated by the finite-difference method.

by finite-differences is shown in Fig. 3.25, only that it is usually of much larger order.

It is clearly seen that to attempt to solve such a system of equations using a direct method of elimination would rapidly 'fill-up' those places which are initially zero. And to attempt to implement such a method on a computer is uneconomical on storage locations. For this reason, an iterative method in which the sparsity of the matrix is fully exploited, is generally used.

Jacobi and Gauss-Seidel Iteration

Variations of iterative procedures applicable to the system in Eqn. 3.18 are numerous. The most well known being the Jacobi and the Gauss-Seidel schemes. In the Jacobi iteration, the solution is found by successive applications of the process:

$$\begin{aligned} u_1^{k+1} &= \frac{1}{a_{11}}(b_1 - a_{12}u_2^k - a_{13}u_3^k - \cdots\cdots - a_{1n}u_n^k) \\ u_2^{k+1} &= \frac{1}{a_{22}}(b_2 - a_{21}u_1^k - a_{23}u_3^k - \cdots\cdots - a_{2n}u_n^k) \\ &\vdots \\ u_n^{k+1} &= \frac{1}{a_{nn}}(b_n - a_{n1}u_1^k - a_{n2}u_2^k - \cdots\cdots - a_{n,n-1}u_{n-1}^k) \end{aligned} \tag{3.19}$$

where k is the index of iteration.

The Gauss-Seidel method is a refinement of the Jacobi process. It consists of replacing in each stage of the iteration, the most recently available estimates:

$$u_1^{k+1} = \frac{1}{a_{11}}(b_1 - a_{12}u_2^k - a_{13}u_3^k \cdots\cdots - a_{1n}u_n^k)$$

$$u_2^{k+1} = \frac{1}{a_{22}}(b_2 - a_{21}u_1^{k+1} - a_{23}u_3^k \cdots\cdots - a_{2n}u_n^k)$$

$$\vdots$$

$$u_n^{k+1} = \frac{1}{a_{nn}}(b_n - a_{n1}u_1^{k+1} - a_{n2}u_2^{k+1} \cdots - a_{n,n-1}u_{n-1}^{k+1}) \tag{3.20}$$

This scheme has two distinct advantages over the previous one in that the solution converges much more rapidly and the instantaneous updating of the estimates means that it requires only half the storage locations of the Jacobi method. Invariably, the Gauss-Seidel scheme is preferred.

Convergence Theorem

An iterative scheme is only useful if the process converges to the true solution. The condition for the convergence of the Jacobi and the Gauss-Seidel methods are given in a theorem due to Collatz (see Hildebrand, 1968), which states that for an $(n \times n)$ system, the iterative processes will converge if A possesses the following two properties:

1) The matrix A does not contain a $(p \times q)$ submatrix of zeros such that $p+q \geqslant n$.
2) The magnitude of each diagonal element in A must be at least as large as the sum of the off-diagonal elements in that row, and in at least

one case, is larger than that sum.

The matrix formulated by finite-difference method does not have any zero element in its diagonal. Therefore, it cannot possess a (p×q) submatrix of zeros with $p+q \geqslant n$. Moreover, the diagonal element in each row is formed from the negative sum of the off-diagonal elements in that row. In solving this system, the boundary condition requires that the potential of at least one node be known. This means the removal of at least one row and one column of the matrix A. Consequently the second condition is also satisfied.

Therefore, the solution of the finite-difference equations is guaranteed to converge when either the Jacobi or the Gauss-Seidel iterative scheme is used.

Acceleration of Convergence.

It is seen clearly from the processes in Eqn. 3.19 and Eqn. 3.20 that when A is sparse, the 'propagation' of the solution will be extremely slow. In other words, a large number of iterations is required for the solution to settle to a satisfactory accuracy. The extrapolated Gauss-Siedel method provides a very simple but nonetheless effective way to accelerate the convergence of the solution. Here, a new value of the estimate is extrapolated from two most recent estimates in the following manner:

$$\bar{u}_i^{k+1} = u_i^k + w(u_i^{k+1} - u_i^k) \qquad (3.21)$$

where $\bar{u}_i^{k+1}$ is the extrapolated estimate and w the 'acceleration factor'. For 1>w<2, the convergence rate is increased. And for some value w_{opt} which is different for each problem, the convergence becomes most rapid. This optimum acceleration factor can be estimated using the empirical formula (see Binns and Lawrenson, 1973),

$$w_{opt} = \frac{2}{1 + (1-c)^{\frac{1}{2}}} \tag{3.22}$$

where c is defined as the limiting value of the ratio of the absolute values of the maximum changes in the estimate occuring on successive iterations when the acceleration factor is unity:

$$c = \underset{k \to \infty}{\mathrm{Lt}} \frac{\max \left| u_i^{k+1} - u_i^k \right|}{\max \left| u_i^k - u_i^{k-1} \right|} \tag{3.23}$$

Although any arbitrary value may be used as the initial estimate for $u_1^{(0)}, u_2^{(0)}, u_3^{(0)}, \ldots u_n^{(0)}$, on the other hand a considerable amount of computing time can be saved if these initial estimates are made as close to the final solution as possible. This gives rise to a scheme to speed up convergence by obtaining firstly, an approximate solution on a coarse grid and then using this solution as the initial estimate for the final system.

Convergence error

There is no means by which the error at each step of the iteration can be calculated. However, an upper bound to the error e_m in the solution can be estimated using the following formula (see Milne, 1953),

$$e_m = \frac{rR^2}{4h^2} \qquad (3.24)$$

where R is the radius of a sphere which just encloses the volume-conductor, h is the grid interval and r is the maximum residual in the solution.

3.6 Program Organization

A complete description of the computer program for implementing the numerical-analogue is given in Appendix A. The program is organized into four phases of operations which are briefly described below:

PHASE1 - The purpose of PHASE1 is to read and unpack the volume-conductor data and store them on file TAPE1. The program assumes the input data to be arranged in the manner described in Sec. 3.4.1.

PHASE2 - This phase scans the coded data on TAPE1 and generates the finite-difference nodes for the conductor. These are stored on file TAPE2.

PHASE3 - PHASE3 is concerned with constructing the set of finite-difference equations using data on TAPE1 and TAPE2. These equations are stored on file TAPE3.

PHASE4 - This phase reorganizes the data on TAPE3 for efficient iteration. The potential at each node is calculated using the Gauss-Seidel method. The solution is stored on file TAPE4.

3.7 Simple Validation Studies

The validity of the numerical-analogue is investigated in this section by comparing the solutions obtained using this method with those obtained analytically.

Dipole in a Sphere

The formula derived by Frank (1952) to calculate the potential distribution inside a homogeneous conducting sphere due to two point current sources provides an ideal volume-conductor solution against which the validity of the numerical-analogue can be demonstrated.

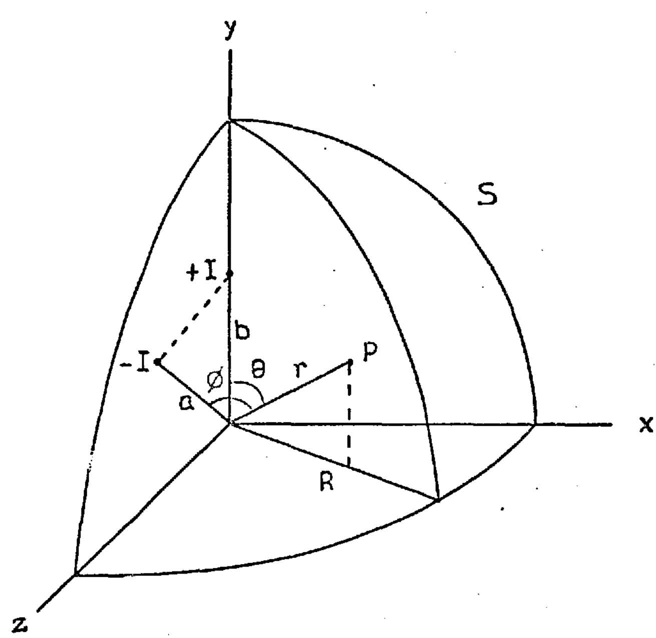

Fig.3.26: Two point current sources arbitrarily located inside a homogeneous conducting sphere, one octant of which is shown.

Consider two point current sources +I and -I arbitrarily located inside a homogeneous conducting sphere S of radius R and conductivity G. The potential at any point within S can be determined from the formula,

$$V = \frac{I}{4\pi G}\left(\frac{1}{r_b} - \frac{1}{r_a} + \frac{R}{br_{bi}} - \frac{R}{ar_{ai}} + \frac{1}{R}\,\mathrm{Ln}\left[\frac{r_a + R - a\cos\emptyset}{r_b + R - b\cos\Theta}\right]\right) \tag{3.25}$$

where

$$r_a = (r^2 + a^2 - 2ra\cos\emptyset)^{\frac{1}{2}}$$

$$r_b = (r^2 + b^2 - 2rb\cos\Theta)^{\frac{1}{2}}$$

$$ar_{ai} = (R^4 + r^2a^2 - 2Rra\cos\emptyset)^{\frac{1}{2}}$$

$$br_{bi} = (R^4 + r^2b^2 - 2Rrb\cos\Theta)^{\frac{1}{2}}$$

and the parameters R, r, a, b, $\emptyset$, and Θ are as specified in Fig. 3.26.

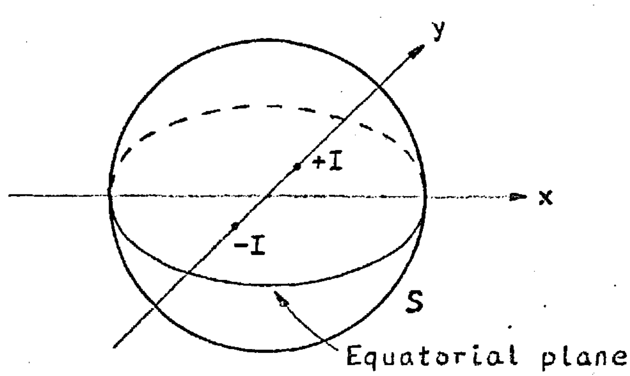

Fig.3.27: Two symmetrically placed current sources, +I and -I in the equatorial plane of a conducting sphere S.

The distribution for the case of two current sources symmetrically placed in the equatorial plane (Fig. 3.27)

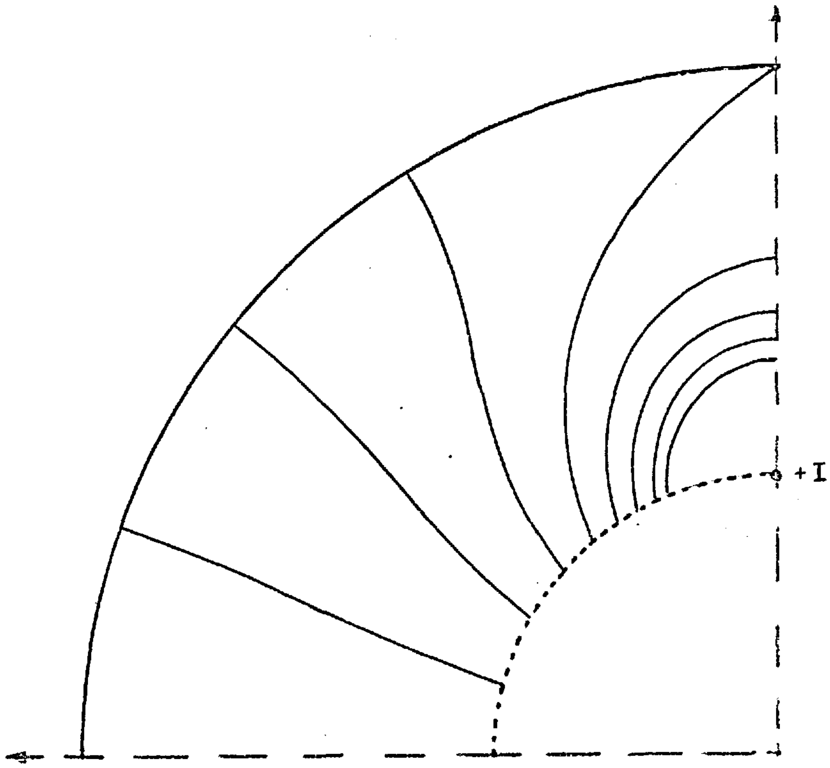

Fig.3.28: Potential distribution in one-quarter of the equatorial plane for the source configuration in Fig.3.27 calculated using Eqn.3.25.

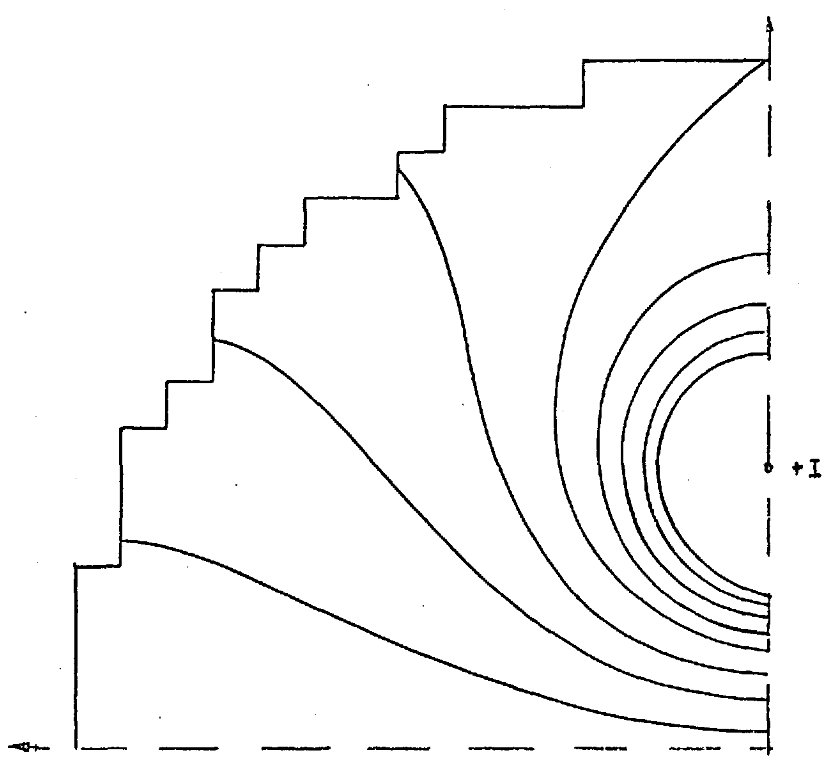

Fig.3.29: Numerical-analogue solution of the potential distribution for the source configuration in Fig.3.27.

is shown in Fig. 3.28. Because of the symmetry of the isopotentials about the x and y axes, only one-quarter of the equatorial plane is shown. The dotted circle shows the region inside which Eqn. 3.25 has no solution.

The same problem is now attacked using the numerical-analogue. A discrete spherical conductor is constructed from elemental cubes of dimension $\frac{R}{15}$. The potential distribution calculated by the numerical-analogue for the same source configuration is shown in Fig. 3.29.

Notice that in spite of the rather coarse representation of the sphere, the solution obtained still agrees very closely with the one obtained analytically.

Boundary Condition

It is well known that when an isopotential line crosses a boundary between two regions of different conductivity, it must be 'refracted' according to the relation,

$$\frac{\tan \theta_1}{\tan \theta_2} = \frac{g_1}{g_2} \tag{3.26}$$

where g_1 and g_2 are the conductivities of the two regions, θ_1 and θ_2 are the angles which the tangents to the isopotential make with the boundary at the point of crossing (Fig. 3.30).

This boundary condition provides a simple means of testing the validity of the numerical-analogue solution of inhomogeneous fields. Fig. 3.31a and Fig. 3.31b show the potential

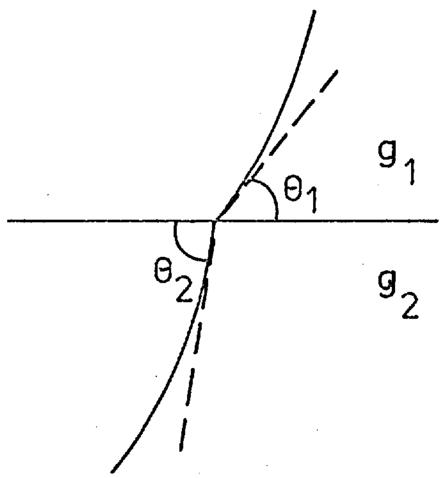

Fig.3.30: 'Refraction' of isopotential line at the boundary between two different media.

distributions in one plane through two inhomogeneous conductors. In both cases, it is seen that the isopotentials crossing the inhomogeneity interfaces satisfy the relation in Eqn. 3.26.

Anisotropicity

A demonstration of the validity of the numerical-analogue for calculating anisotropic fields is now discussed. Consider the case in which the conductivities in the principal axes, x, y, and z are all different. The Laplacian for such an anisotropic conductor is,

$$g_x\frac{\partial^2 u}{\partial x^2} + g_y\frac{\partial^2 u}{\partial y^2} + g_z\frac{\partial^2 u}{\partial z^2} = 0 \qquad (3.27)$$

where g_x, g_y and g_z are the conductivities in the x, y and z directions respectively. The problem in Eqn. 3.27 can be transformed into one involving isotropicity using the transformation,

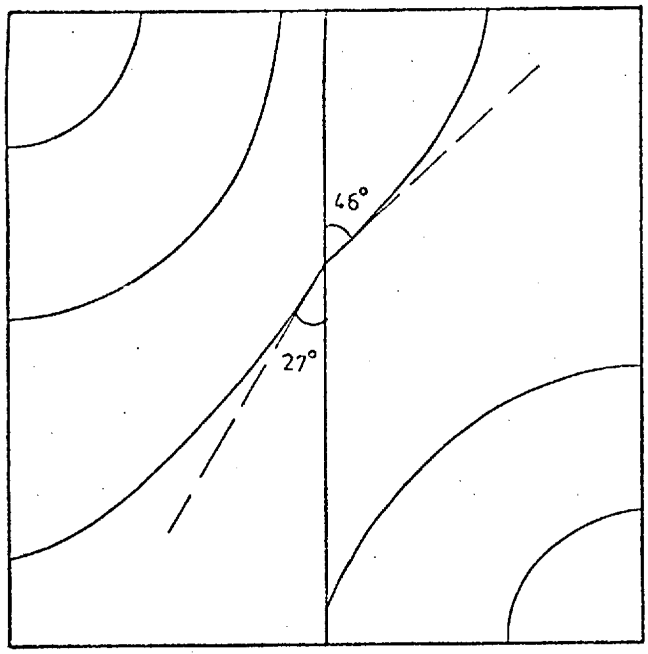

$$\frac{g_1}{g_2} = 0.5$$

$$\frac{\tan\theta_1}{\tan\theta_2} = 0.49$$

$g_1 = 1.0$ $g_2 = 2.0$

Fig.3.31a

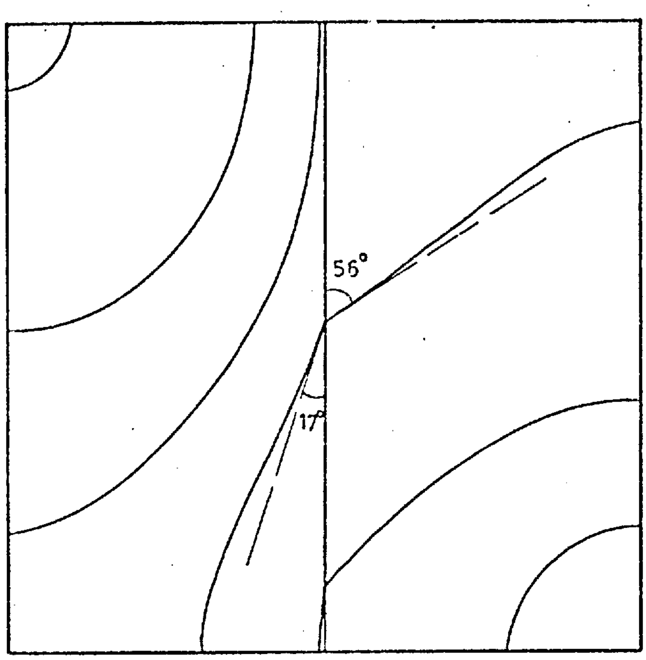

$$\frac{g_1}{g_2} = 0.2$$

$$\frac{\tan\theta_1}{\tan\theta_2} = 0.206$$

$g_1 = 1.0$ $g_2 = 5.0$

Fig.3.31b

Fig.3.31: Calculations of conductivity ratios from the angles the isopotentials make with the boundaries separating two regions of different conductivities.

$$x' = \frac{(g_y g_z)^{\frac{1}{2}}}{g} x \quad , \quad y' = \frac{(g_x g_z)^{\frac{1}{2}}}{g} y \quad , \quad z' = \frac{(g_x g_y)^{\frac{1}{2}}}{g} z \tag{3.28}$$

where x', y' and z' are the new systems of coordinates. The potential gradients are related by

$$\frac{\partial u}{\partial x'} = \frac{\partial u}{\partial x}\frac{\partial x}{\partial x'} = \frac{g}{(g_y g_z)^{\frac{1}{2}}}\frac{\partial u}{\partial x} \tag{3.29}$$

$$\frac{\partial^2 u}{\partial x'^2} = \frac{g^2}{(g_y g_z)}\frac{\partial^2 u}{\partial x^2} \tag{3.30}$$

Similarly,

$$\frac{\partial^2 u}{\partial y'^2} = \frac{g^2}{(g_x g_z)}\frac{\partial^2 u}{\partial y^2} \quad , \quad \frac{\partial^2 u}{\partial z'^2} = \frac{g^2}{(g_x g_y)}\frac{\partial^2 u}{\partial z^2} \tag{3.31}$$

Substituting Eqn. 3.30 and Eqn. 3.31 into Eqn. 3.27, yields

$$\frac{g_x g_y g_z}{g^2}\left(\frac{\partial^2 u}{\partial x'^2} + \frac{\partial^2 u}{\partial y'^2} + \frac{\partial^2 u}{\partial z'^2}\right) = 0 \tag{3.32}$$

which clearly is an expression for an isotropic conductor.

In this exercise, a numerical-analogue solution for an anisotropic conductor is computed. The isopotentials through a plane of the conductor is shown in Fig. 3.32. The same problem on the other hand, can be solved assuming isotropicity by using the coordinate transformation:

$$x' = \sqrt{6}\, x \quad , \quad y' = \sqrt{3}\, y \quad , \quad z' = \sqrt{2}\, z \tag{3.33}$$

which means calculating the potentials in an equivalent

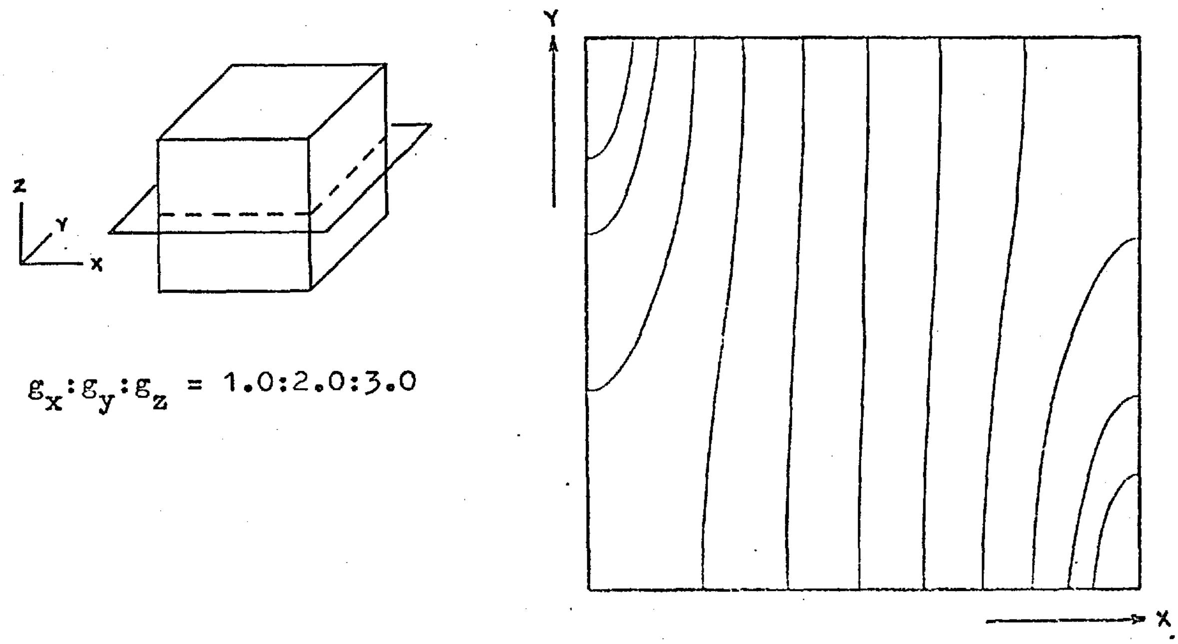

Fig.3.32: Numerical-analogue solution for an anisotropic conductor.

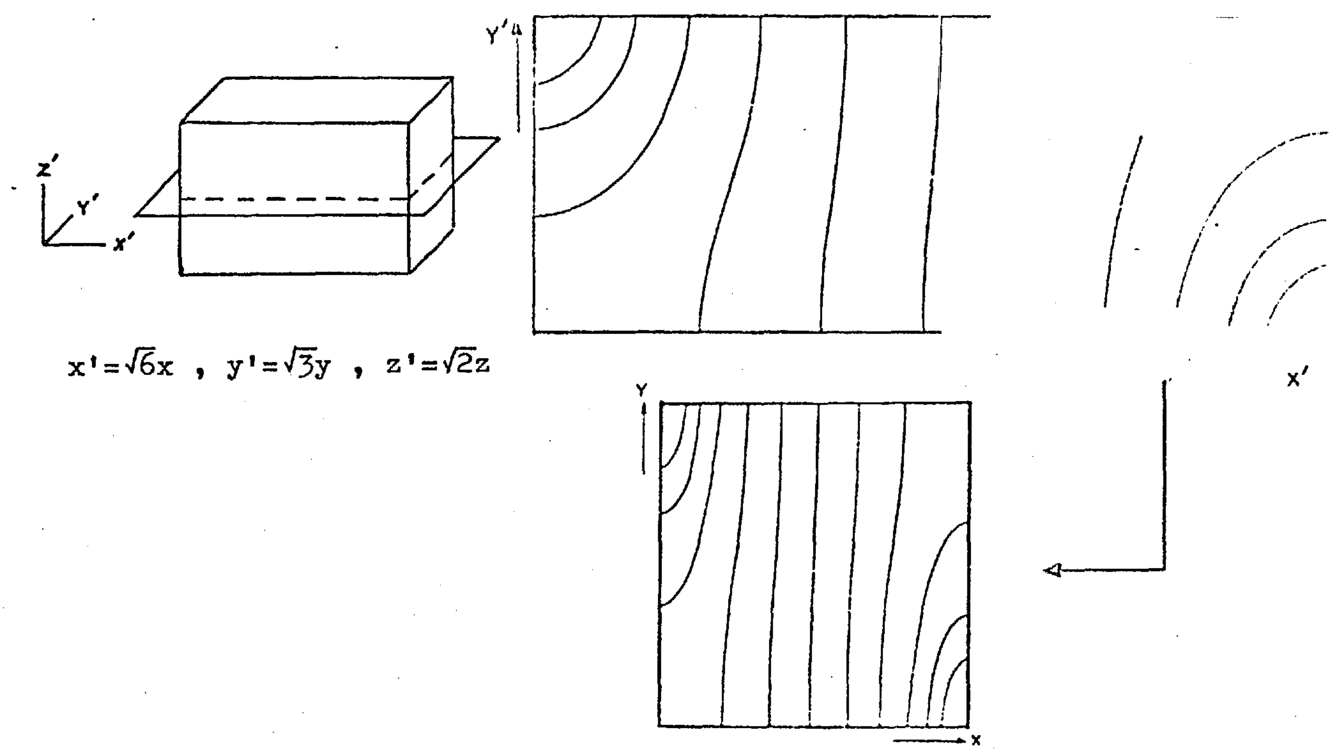

Fig.3.33: Solution to the same problem in Fig.3.32 obtained by calculating the potential distribution in an equivalent isotropic conductor. The required solution is derived by an inverse co-ordinate transformation.

isotropic conductor with dimensions $\sqrt{6} : \sqrt{3} : \sqrt{2}$ (Fig. 3.33). The solution to the original problem is derived by a simple inverse transformation.

It is seen clearly that the solutions obtained by the two independent methods agree.

3.8 Conclusion

The development of a numerical-analogue for calculating volume-conductor fields was described in this chapter. The method is distinct from the finite-difference method and the resistive-network analogue in that it combines the latter two methods in such a way that the advantages of both methods are realized.

The validity of the numerical-analogue was also demonstrated by comparing its solutions with those obtained by other means.

CHAPTER 4

A DISCRETE ANATOMICAL MODEL OF THE HUMAN THORAX

4.1 Introduction

In the preceeding chapter, a numerical procedure for calculating the electrical fields in a volume-conductor has been described. Now, a valid digital representation of the human thorax must be derived for applications to the forward problem in electrocardiography.

The choice of an appropriate sampling grid is fundamental to this problem. Ideally, the grid interval should be made as small as possible for two reasons: The first is that the errors introduced by the finite-difference approximation vanish in the limit as the grid interval is made smaller and smaller. Secondly, a fine grid allows greater geometrical details to be resolved, hence a more realistic representation of the human torso. In practice, the limitations of speed and storage of a given computer will ultimately limit the resolution of the chosen grid.

Furthermore, it is not necessarily sensible to exploit the available computing resources to the limit for the reason that the accuracy of the solutions does not depend on the grid size alone, but also on the values of the tissue conductivities used in the simulation. In the present study, these values are taken from published sources. The problem here lies in the difficulties of estimating the accuracies of the published data due to the inconsistencies between results obtained by different groups of investigators (see Appendix B). The differences ranges from 70% for liver to some 400% for muscular tissues. Moreover, repeated measurements for the same tissue obtained by Rush et. al.(1963) showed deviations in the results ranging from 14% for liver to 30% for muscles.

It is therefore difficult to justify the applications of vast computing resources for the purpose of minimizing the errors due to grid size when the validity of published conductivities is somewhat questionable. For this reason, it is more sensible to emphasize when constructing the torso model, on the economy of achieving a solution rather than on the numerical accuracies.

4.2 Anatomical Data

The data on which the model is based is obtained from an atlas of the anatomical cross-sections of human body prepared by Symmington (1956). These cross-sections were made from a male cadaver sectioned at approximately one inch interval. For the purpose of this study, two additional cross-sections in between the planes of the atlas were interpolated by hand. Cross-sections corresponding to the torso slabs shown in Fig. 4.1 were digitized using the grid configuration shown in Fig. 4.2. The complete specification of the digitized torso cross-sections is shown in Fig. 4.3a and Fig. 4.3b. The corresponding coded images of these cross-sections can be found in Appendix C.1.

The coded image for a model digitized at a coarser grid of one-half inch is also given in Appendix C (Appendix C.2). The purpose of using two models is to reduce the computational time required to obtain a solution. This is achieved by iterating firstly on the coarse model and then using this solution as the initial guess for the potential function in the finer model. In this way, the problem of slowly converging solution for the fine model is overcome.

The conductivity ratios for the codings used in the model are given in Table 4.1. These were derived from the set of tissue resistivity data obtained by Rush et al.(1963). The reasons for using their data is that firstly, this is the most recently available and also one of the most complete set of measurements. Secondly, their measurements were made with electrocardiographic applications specifically in mind.

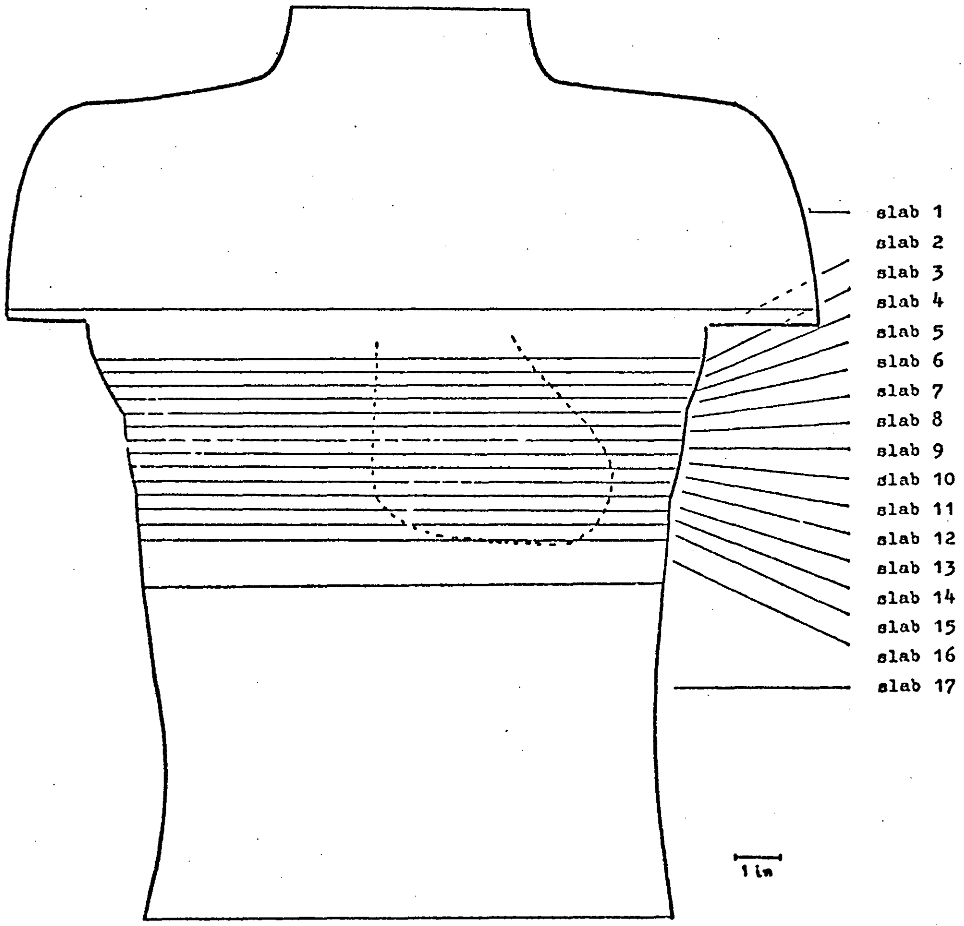

Fig.4.1: Diagram illustrating the various slabs used in the discrete model.

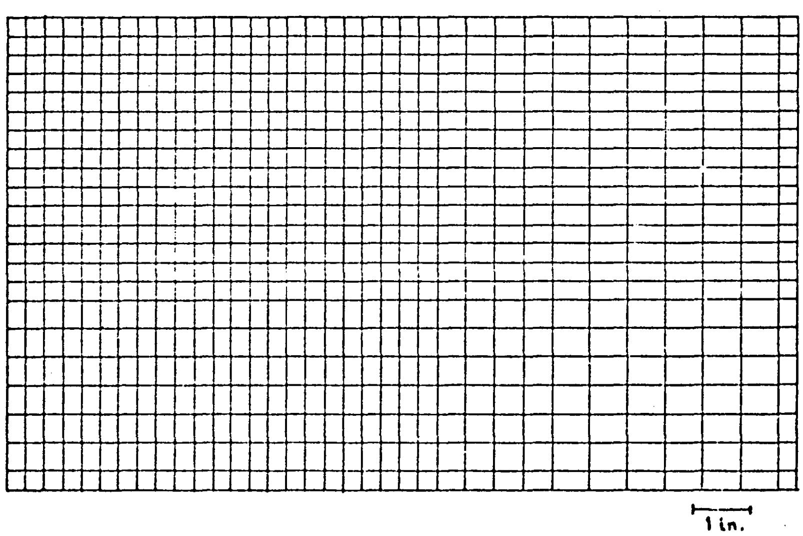

Fig.4.2: Configuration of the sampling grid.

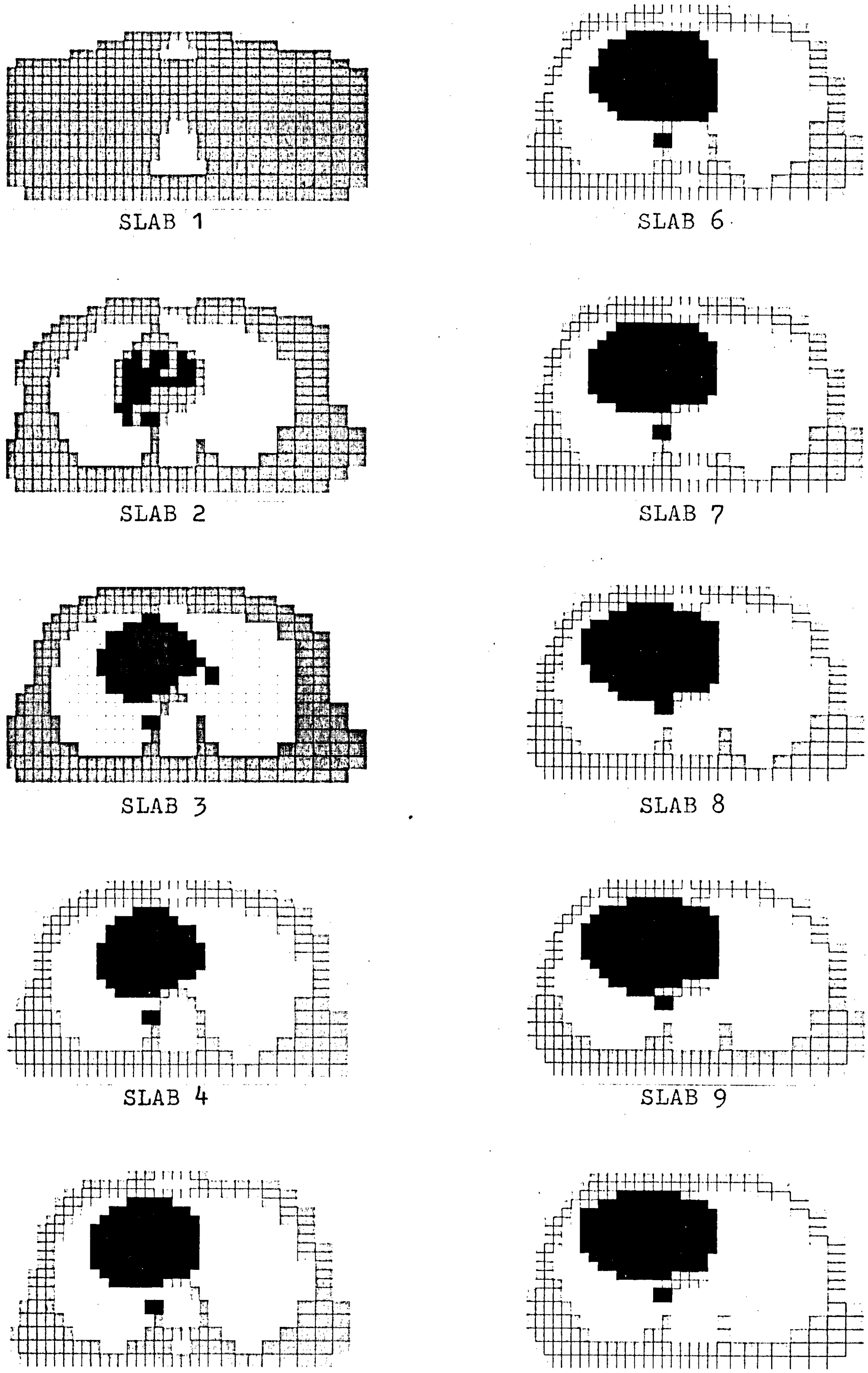

Fig.4.3a: Slab 1 to Slab 10 of the discretized torso sections.

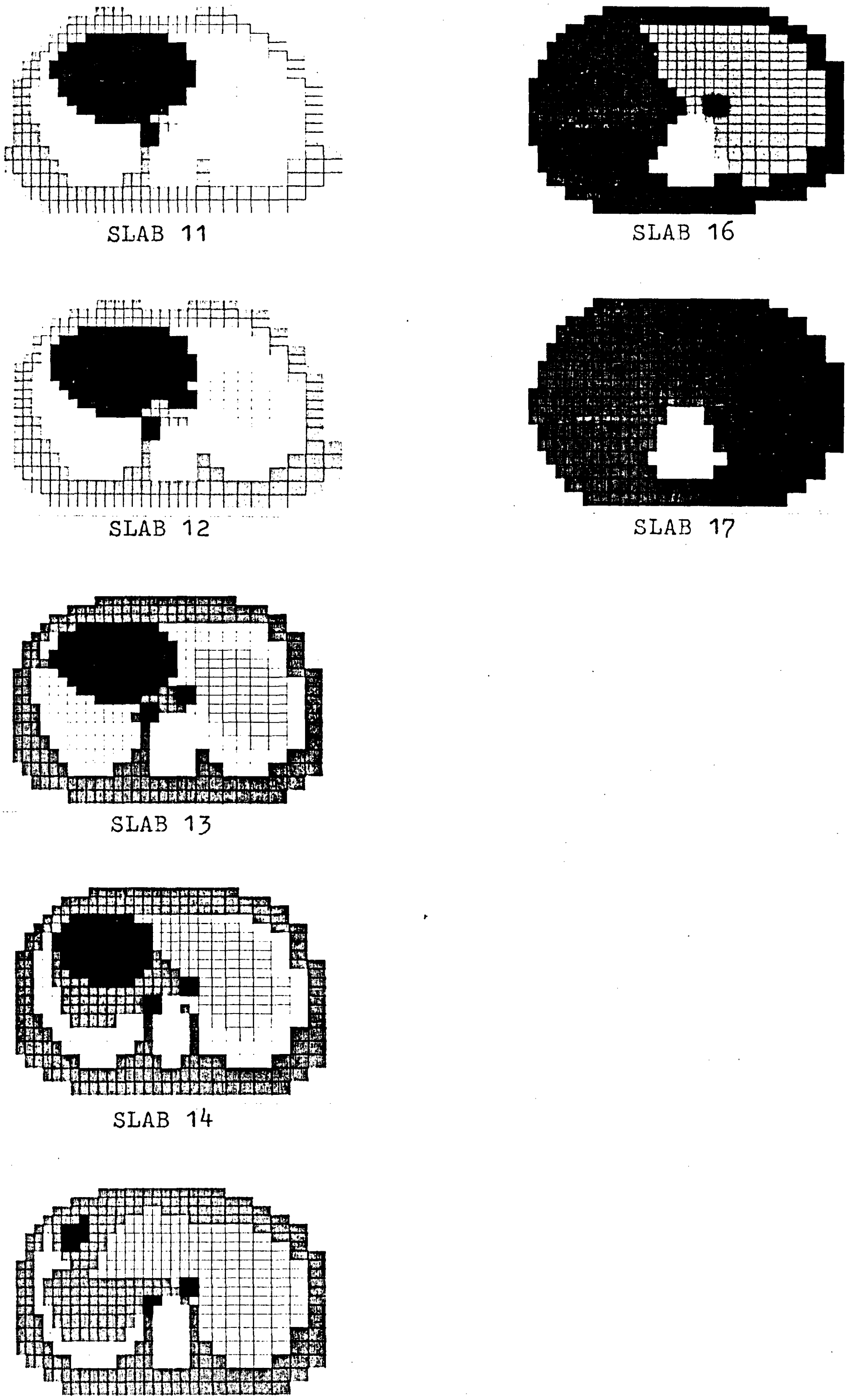

Fig.4.3b: Slab 11 to Slab 17 of the discretized torso sections.

Table 4.1: Table of codings and their conductivity ratios.

TISSUE	RESISTIVITY (ohm-cm)	CODING	CONDUCTIVITY RATIO				
Human Trunk	463	T	1.0				
Blood	162	M/V	2.8				
Heart	377*	H	1.2				
Lung	2100	L	0.2				
Liver	700	R	0.6				
Skeletal Muscle	2300 high 150 low	(Refer to Fig.3.22 for anisotropic representation)					
			G^1	G^2	G^3	G^4	G^5
		1	3.0	3.0	0.2	0.2	3.0
		2	0.2	3.0	3.0	0.2	3.0
		3	0.2	0.2	3.0	3.0	3.0
		4	3.0	0.2	0.2	3.0	3.0
		5	3.0	0.2	3.0	0.2	3.0
		6	0.2	3.0	0.2	3.0	3.0

* The resistivity of the heart is taken to be the geometric mean of the high and low values given by Rush et al.(1963).

4.3 Adequacy of the Sampling Grid

There is no simple analytical means of determining the magnitude of the errors introduced by the finite grid size. The only practical method is to compare the solutions obtained at various grid sizes. Using the solutions obtained at two different grid sizes, the exact solution can be estimated by Richardson's extrapolation method (see Vitkovitch, 1966) which is briefly described below.

Assuming that the potential function does not contain derivatives higher than the order four, then the error introduced by the finite-difference approximation for a grid size h_a is,

$$u_o - u_a = \frac{M_4 h_a^2}{4} \qquad (4.1)$$

where u_a is the potential at a given node, u_o is the exact potential and M_4 is the magnitude of the fourth order derivative. Similarly, the error due to the grid size h_b is,

$$u_o - u_b = \frac{M_4 h_b^2}{4} \qquad (4.2)$$

Eliminating the quantity M_4 from the above equations gives:

$$u_o = \frac{h_a^2 u_b - h_b^2 u_a}{h_a^2 - h_b^2} \qquad (4.3)$$

From the extrapolated exact solution, the error introduced by either grid size can therefore be estimated.

Inorder to economize on computional resources, the investigation that follows will be restricted to a two-dimensional cross-sectional model of the human torso.

Fig. 4.4 shows the same torso cross-section digitized at different grid sizes, three of which, Fig. 4.4a, Fig. 4.4b and Fig. 4.4c are digitized using regular grids of one-sixth inch, one-third inch and one-half inch respectively. The fourth, Fig. 4.4d is digitized using an irregular grid with the sampling density greater around the cardiac region, because here the potential function varies the most rapidly.

The electrical potential distribution for each model is calculated for the same source configuration. In each case, the iteration is terminated when the upper bound for the error in the solution as determined from Eqn. 3.24 is less than 0.001%. The maximum difference between the solution obtained using the one-sixth inch grid and the one-third inch grid is of the order of 3%. Substituting this into Eqn. 4.3 gives an estimated discretization error of some 1% for the one-sixth inch model and 4% for the one-third inch one. Similarly, error for the one-half inch model is estimated to be some 10%. As the grid interval for Fig. 4.4d is irregular, it it not possible to use this technique to estimate its discretization error. However, since the maximum difference between the solution for this model and that for the one-third inch one is only some 0.3%, it is therefore unlikely that the error here would be greater than 4.5%.

The computional time required for each of these solutions is shown in Table 4.2. When the grid size is reduced from one-third inch to one-sixth inch, the computional time is increased by a staggering amount of 1600%. The corresponding improvement in

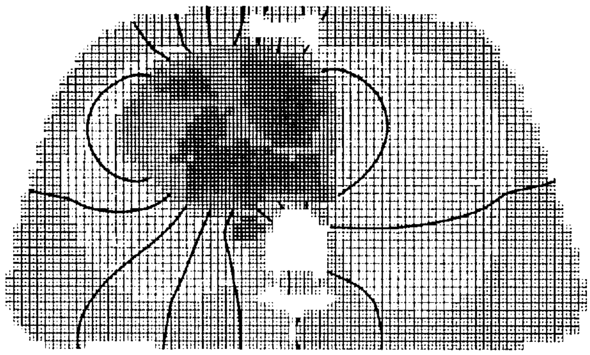

Fig.4.4a: One-sixth inch grid.

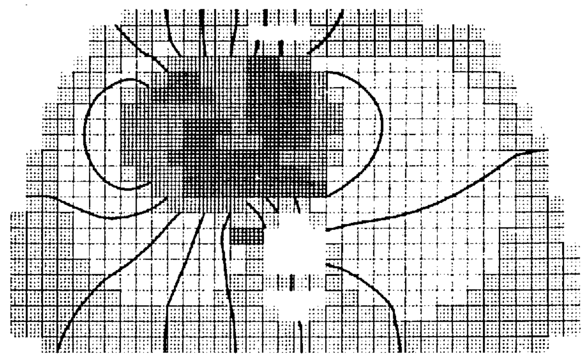

Fig.4.4b: One-third inch grid.

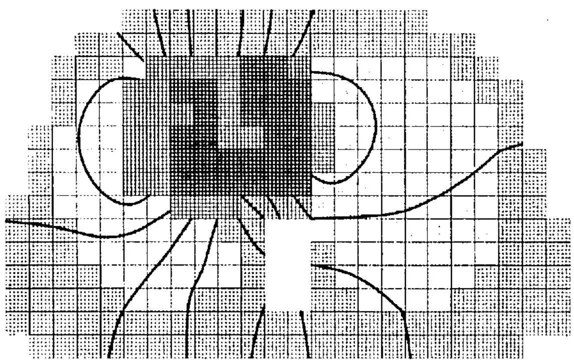

Fig.4.4c: One-half inch grid.

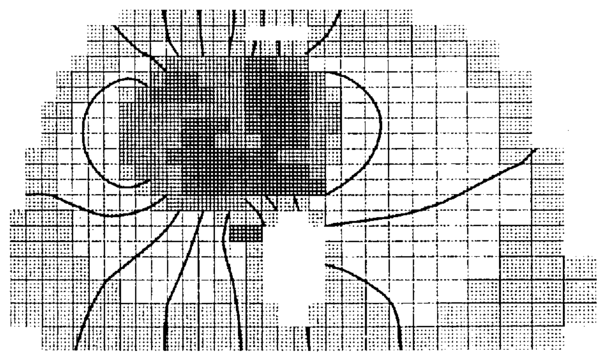

Fig.4.4d: Irregular grid.

Fig.4.4: Digitization of the same torso section using different grid sizes. The heavy thick lines are isopotentials due to a sinusoidally varying potential distribution on the heart surface.

Table 4.2: Computational time and estimated error for different grid sizes.

GRID SIZE (inch)	COMPUTATIONAL TIME (sec.)	ESTIMATED ERROR (%)
One-sixth	80	1
One-third	5	4
One-half	1	10
Irregular	2.5	5

the numerical accuracy on the other hand is only some 4% which hardly justifies the large difference in the computional costs. A further reduction of 50% in the computional cost can be achieved by using the irregular grid in Fig. 4.4d.

Although this investigation is carried out using two-dimentional models, the results nevertheless do provide useful indications as to the adequacies of the discrete three-dimensional torso model described in the previous section.

4.4 Effects of the Various Internal Inhomogeneities

The discrete model of the human torso developed in Section 4.2 includes all the internal inhomogeneities that could be resolved by the grid. It is relevant to enquire whether all the inhomogeneities are necessary. If not, then clearly it would be sensible to simplify the model accordingly.

For this investigation the surface distribution for five models with varying degree of complexity in their anatomies were used. These are shown in Fig. 4.5.

It is observed that the introduction of intracardiac blood-mass enhances greatly the magnitudes of the surface maximum and minimum. This observation is in close agreement with the results obtained by Barnard et al.(1967). Two interesting features are observed when the lungs are introduced. The first is a slight clockwise rotation of the surface potentials and the second is a 'focusing' effect towards the front of the torso. The rotation of the potentials can be explained by the difference in mass between the left and the right lungs, while the focusing effect can be accounted for by the low resistive pathways through the gaps separating the two lungs. A further rotation of the isopotentials is observed when the liver is introduced. This once again, is due to the non-uniform displacement of currents in the torso. The effects of the spine, the sternum and the great vessels are to increase the irregularities in the isopotentials. A drastic change in the pattern of the surface potentials is observed when the aniso-tropicity of the skeletal muscles is introduced. This includes a

SURFACE POTENTIAL DISTRIBUTIONS FOR DIFFERENT MODELLING ASSUMPTIONS

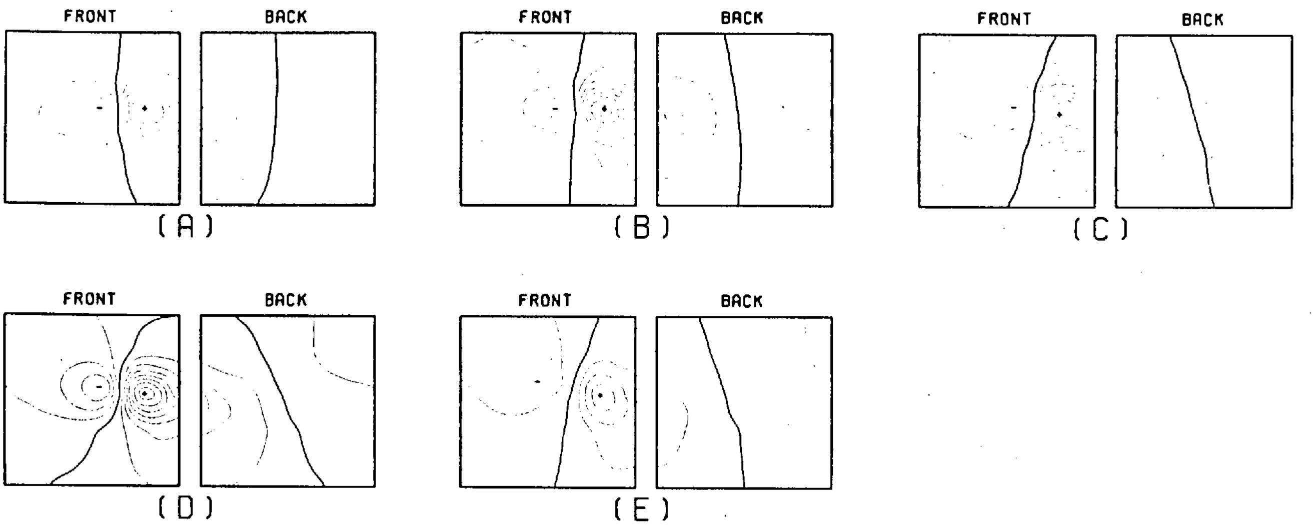

MODELLING ASSUMPTIONS

(A) - HOMOGENEOUS ISOTROPIC TORSO-SHAPED VOLUME CONDUCTOR
(B) - AS (A) + INTRACARDIAC BLOOD MASS
(C) - AS (B) + LUNGS
(D) - AS (C) + G.VESSELS. SPINE. LIVER AND SKEL.MUSCLE
(E) - AS (D) BUT WITH ANISOTROPIC SKEL. MUSCLE

Figure 4.5

reduction in the magnitudes of the surface potentials and an increase in separation of the maximum and minimum. This is not unexpected since the effect of a low resistive pathway parallel to the body surface is to disperse any localized concentration of the surface currents.

Since it is shown that all the inhomogeneities contribute to the body surface potentials in a significant manner, it can therefore be argued that the data accumulated in Section 4.2 are justified in the complexities of the internal inhomogeneities.

4.5 Comparison of Simulated and Observed Surface Potentials

In this section, the data of the torso model accumulated in this chapter is used to calculate catheter potentials on the body surface of cardiac patients with pacemakers implanted in their right ventricles. These simulated surface potentials are then compared with those actually measured on the patients' torsos.

The measurements of Hamer et al.(1965) from implanted pacing catheters provide an ideal basis for comparison. They recorded from several cardiac patients with implanted pacemakers in their right ventricles, the magnitudes of the pacemaker impulses at various sites on the patients' torsos. From these recordings, they reconstructed isopotential maps of what is effectively a dipole source located in the right ventricle.

From their information of the locations and orientations of the catheter tips in the patients, the corresponding surface distributions were computed using the torso model derived in this chapter. The simulated surface potential distributions and those reconstructed by Hamer et al.(1965) are shown in Fig. 4.6. It is seen that a close agreement in all the major features between the two sets of distributions can be found. This indicates quite strongly the validity of the model data accumulated in this chapter.

COMPARISONS BETWEEN SIMULATED AND EXPERIMENTALLY OBSERVED CATHETER POTENTIALS

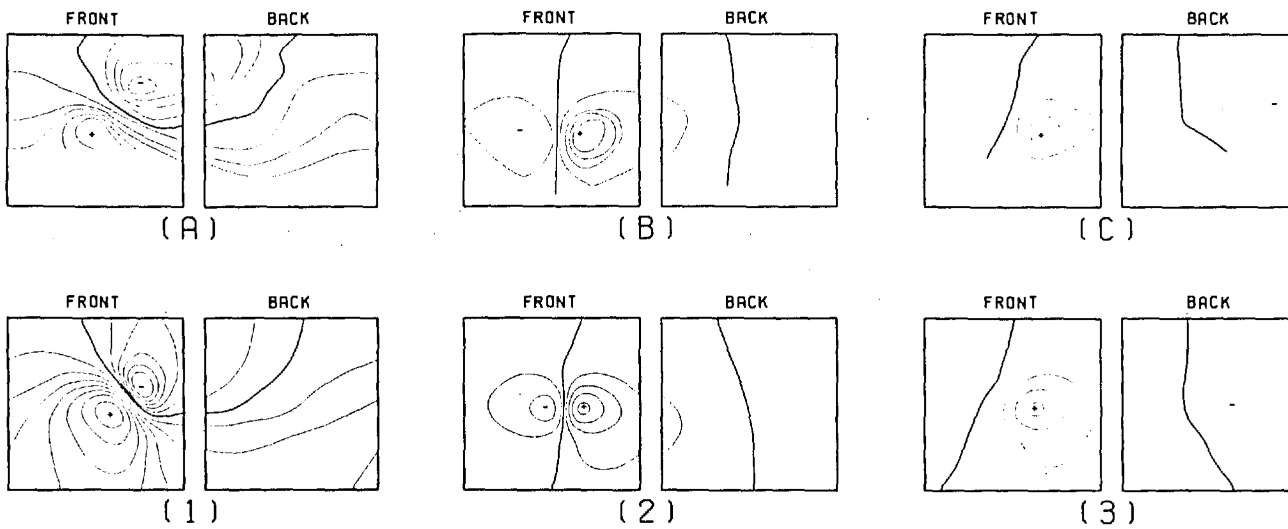

(A),(B),(C) - BODY SURFACE POTENTIAL DISTRIBUTION PRODUCED BY CATHETER IMPULSES (REDRAWN FROM HAMER, BOYLE AND SOWTON, 1965)

(1),(2),(3) - SURFACE DISTRIBUTION OBTAINED BY SIMULATION

Figure 4.6

4.6 Conclusion

A digital computer model of the human torso which took into account the intra-cardiac blood-mass, the great vessels, the heart muscle, the lungs, the liver, the spine, the sternum and the anisotropic skeletal muscles has been derived. The validity of this model was demonstrated by comparing surface potentials computed from the model with those obtained experimentally.

In order to speed up the convergence of the solution, a coarser model was also constructed so that an initial estimate of the solution could be obtained economically. Using this estimate as the initial guess in the finer model, the number of iterations required to achieve the solution is greatly reduced.

CHAPTER 5

AN INVESTIGATION ON THE FEASIBILITY OF AN UNCONSTRAINED INVERSE SOLUTION

5.1 Introduction

The purpose of this chapter is to investigate the feasibility of an unconstrained inverse solution based on recovering epicardial potentials from surface measurements. Previous workers (Barnard et al., 1967; Brody and Hight, 1972; Martin and Pilkington, 1972) have demonstrated the inherent difficulties in such an approach due to the highly ill-conditioned property of the heart-surface transfer matrix T defined in Chapter 2. The effect is that presence of small perturbations in the measurement vector $\underline{v}$ in the equation,

$$T\underline{s} = \underline{v} \tag{5.1}$$

will lead to serious errors to be observed in the solution vector $\underline{s}$. They also attempted overdetermination of the problem but met with little success in obtaining a valid solution.

In order to overcome this problem, various constraints were imposed by past workers on their inverse solutions. These constraints are usually based on some prior knowledge of the valid solution. For example, Barnard et al.(1967) constrained the dipole moments of their multiple-dipole solution to be non-negative, so avoiding solutions with 'inward pointing' dipoles which are held to be physiologically unrealistic in normal cases. Another form of constraint which was introduced by Martin and Pilkington (1972) in their epicardial solutions assumed a prior knowledge of the statistics of the solution vectors.

However, a constrained approach is not without its disadvantages. Clearly, the ultimate objective in the inverse solution is to aid diagnosis and detection of abnormalities. To constrain the solution in order to fit what is a valid result for the normal may risk excluding solutions which are correct for the abnormal. For example, in certain cardiac abnormalities, the excitation spreads outside-in which clearly would be misrepresented by a solution that constrains the dipoles to point outwards.

It is for this reason that this chapter is devoted to the study of the heart-surface transfer relationship in the hope that such investigations may lead to a formulation of an unconstrained inverse solution.

5.2 The Torso as a Spatial Filter

The distribution of body-surface potentials g(p) can be related to the epicardial distribution f(s) by the integral equation,

$$g(p) = \int_S K(p,s)f(s)ds \qquad (5.2)$$

where K(p,s) represents the body transfer characteristics and the integration is over the heart surface. The problem in inverse electrocardiography is to infer f(s) from knowledge of g(p). Ideally, this is achieved by a simple inverse transformation of Eqn. 5.2. In practice however, g(p) is obtained by measurements which are subjected to errors such as positional uncertainties, physiological noise and measurement errors. The result can be to cause the solution to oscillate wildly.

Twomey (1965) proposed an elegant technique for investigating problems of this kind. He showed that the success of inferring f(s) from g(p) when the latter is subjected to noise depends on the shape of K(p,s). This is most clearly illustrated by the Fourier transform of the kernel K(p,s):

Spectral Kernel

Consider the Fourier transform pair,

$$f(s) = \int_{-\infty}^{\infty} F(w)e^{-jws}ds \qquad (5.3)$$

$$F(w) = \int_{-\infty}^{\infty} f(s)e^{jws}ds \qquad (5.4)$$

Substituting Eqn. 5.3 in Eqn. 5.2 qives,

$$g(p) = \int_S K(p,s) \left[\int_{-\infty}^{\infty} F(w) e^{jws} dw \right] ds \qquad (5.5)$$

As the function K(p,s) must vanish outside the area of integration, the limits of integration can be extended to $\pm\infty$. And reversing the order of integration yields,

$$g(p) = \int_{-\infty}^{\infty} \Phi(p,w) F(w) dw \qquad (5.6)$$

where

$$\Phi(p,w) = \int_{-\infty}^{\infty} K(p,s) e^{jws} ds \qquad (5.7)$$

known as the spectral kernel is the Fourier transform of K(p,s) with respect to the variable s.

In most physical systems, K(p,s) is a smooth function of s. The corresponding spectral kernel $\Phi(p,w)$ becomes a function which decreases rapidly with increasing $|w|$. A simple example to illustrate the rapidly declining function of $\Phi(p,w)$ in the volume-conductor was given by Martin and Pilkington (1972).

Case of Two Concentric Spheres

They considered the case of a highly idealized model of the torso represented by two concentric spheres embedded in an infinitely homogeneous medium (Fig. 5.1). The inner sphere represents the heart while the outer sphere represents the torso.

For any given distribution of potential V_s on the surface of the inner sphere, the potential V_p generated on the outer sphere can be calculated using Poisson's Integral equation:

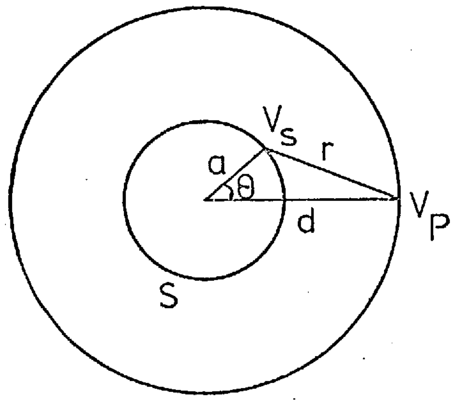

Fig.5.1: Two concentric spheres of radius a and d embedded in an infinitely homogeneous medium.

$$V_p = \int_S \frac{(d^2 - a^2)V_s}{4\pi a r^3}\, ds \qquad (5.8)$$

where

$$r = (a^2 + d^2 - 2ad\cos\theta)^{\frac{1}{2}} \qquad (5.9)$$

Because of the symmetry of the system, Eqn. 5.8 can be reduced to an integration over one variable by making use of the relation,

$$\delta s = 2\pi a^2 \sin\theta\ \delta\theta \qquad (5.10)$$

The kernel of this system then becomes

$$K(c,\theta) = \frac{(c - c^3)\sin\theta}{2(1 + c^2 - 2c\cos\theta)^{3/2}} \qquad (5.11)$$

where the constant c is the ratio a/d.

A family of the spectral kernel for the various a/d ratios is shown in Fig. 5.2. Clearly, the spectral kernel has the

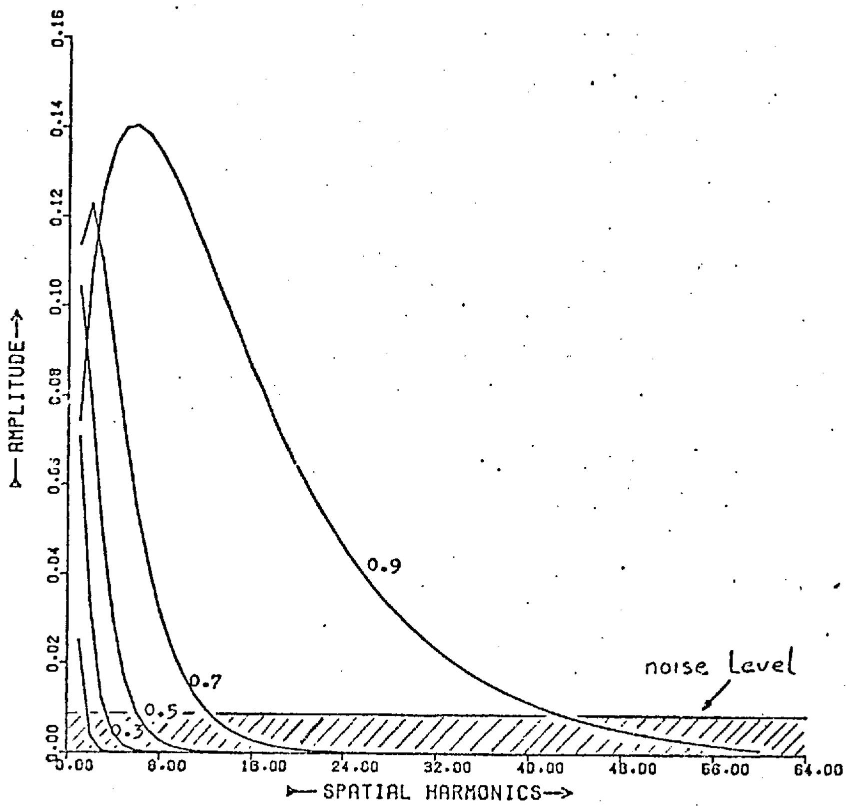

Fig.5.2: A family of spectral Kernel for various a/d ratios.

characteristics of a 'low-pass' filter. The degree of filtering depends on the distance from the source to the surface.

Interpretation

Inspite of the rapidly decreasing values of $\Phi(p,w)$ as $|w|$ increases, in theory the values only become vanishingly small. Therefore provided the system is totally free from noise and $g(p)$ can be measured precisely, the function $f(s)$ can be accurately retrieved. In practice however, the system is subjected to noise which is represented by the shaded region in Fig. 5.2. The consequence of this is that the information which can be extracted is now limited to some frequence range $(-q,+q)$ for which $\Phi(p,w)$ is greater than the noise level. The number of independent parameters that can be inferred from $g(p)$

according to Shannon's sampling theorem is 2q. Attempt to infer more parameters is to seek information outside the filter 'window' which will only lead to large high frequency oscillations in the solution.

To summarize:

1) A volume-conductor has the characteristic of a 'low-pass' spatial filter. The further the source is from the surface, the greater is the filtering effect.
2) Consequently, only a filtered version of the epicardial potential function can be inferred.
3) For a 'useful' bandwidth of qHz, not more than 2q independent epicardial generators can be determined.
4) To attempt to infer more epicardial generators will only lead to high frequency oscillations in the solution.

The arguments of this section provide no indication as to the feasibility of an inverse solution, nor do they allow a measure of the errors likely to occur in the solution. Nevertheless, they illustrate the mechanism by which epicardial potentials are transferred to the body surface and outline the inherent limitations of inverse solutions.

5.3 System Eigenvalues as Weight Factors

A more quantitative way to investigate the effect of noise on inverse solution is to consider the eigenvalues of the system transfer matrix T. The system equation (Eqn. 5.1) can be rewritten to account for noise:

$$T(\underline{s}+\underline{f}) = (\underline{v}+\underline{e}) \tag{5.12}$$

where $\underline{e}$ is the error vector associated with the measurements of $\underline{v}$, and $\underline{f}$ is the resultant error vector in the solution $\underline{s}$. The crucial question here is whether the relative smallness of $\underline{e}$ will result in relatively small $\underline{f}$. The answer to this question depends on the relative magnitudes of the system eigenvalues.

Orthogonal Transformation

Consider the error relation,

$$T\underline{f} = \underline{e} \tag{5.13}$$

Assuming for the moment that T is symmetric. Under this condition, T can be diagonalized by a proper rotation of the reference system (see Lanczos, 1961):

$$U^T T U = D \tag{5.14}$$

where U is an orthogonal matrix and D is a diagonal matrix containing all the system eigenvalues,

$$D = \begin{bmatrix} d_1 & & & & \\ & d_2 & & & \\ & & \cdot & & \\ & & & \cdot & \\ & & & & d_n \end{bmatrix} \tag{5.15}$$

The rotated system now becomes,

$$D\underline{f}' = \underline{e}' \tag{5.16}$$

where $\underline{e}' = U^T\underline{e}$, $\underline{f}' = U^T\underline{f}$.
The length of the error vectors are not affected by this transformation. That is, $|e| = |e'|$ and $|f| = |f'|$.

Error Magnification

The importance of the system eigenvalues in determining the errors in the solution is demonstrated clearly by the relation,

$$f_i' = \frac{e_i'}{d_i} \tag{5.17}$$

The problem arises when d_i is very small. The result of dividing the error e_i' by a very small number is a very large value of f_i' . As shown by Lanczos (1961), the critical quantity here is the ratio of the largest to the smallest eigenvalues,

$$C = \frac{d_{max}}{d_{min}} \tag{5.18}$$

which is known as the 'condition number' of the system. This number provides an upper bound to the magnification of the percent error in the solution. The greater the condition number, the less likely is the chance of a successful solution in the presence of noise.

Non-Symmetric System Matrix

The case where T is non-symmetric is complicated by the fact that the eigenvalues are likely to be complex. This problem is overcome by premultiplying the system matrix by its transpose:

$$T^{T}T(\underline{s}+\underline{f}) = T^{T}(\underline{v}+\underline{e}) \qquad (5.19)$$

The effect of this as mentioned in Chapter 2 is to minimize the length of the residual vector in the solution. If the system is evenly-determined in the first instance (that is T is square), then this minimization has no effect on the solution. The importance of this operation however is that the new system matrix $T^{T}T$ is once again symmetric and thus amenable to the error analysis described in this section.

5.4 Optimization of the System Resolution

The 'low-pass' filter characteristic of the volume-conductor implies that the magnitude of the condition number will depend on the dimension of the system matrix. The smaller the system matrix, the smaller will be the condition number. This is because in a small system, information is extracted from the low-frequency region of the spatial filter where the signal-to-noise ratio is large. This leads to the impression that the only means of achieving a stable unconstrained inverse solution is to reduce the size of the system matrix until the condition number is sufficiently small. As will be demonstrated in this section, a carefully selected configuration of the measurement locations can greatly improve the system condition number.

Position for Maximum Resolution

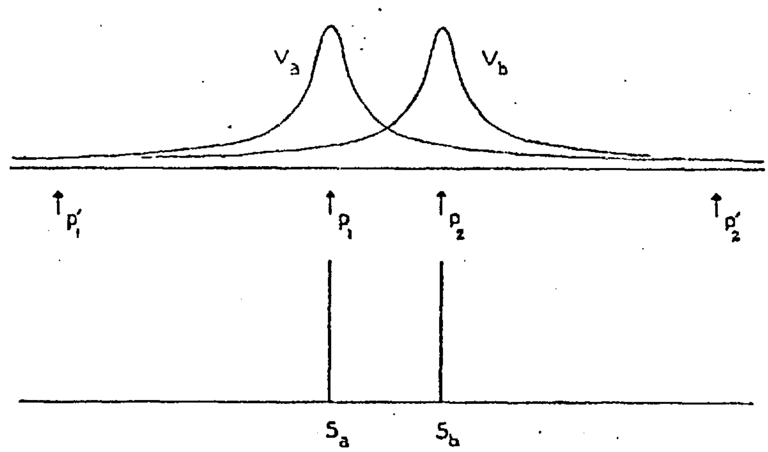

Fig.5.3: Diagram illustrating the system impulse response.

The effect of low-pass filtering is to generate a smoothed version of the epicardial distribution on the body surface. Consider two impulse generators S_a and S_b at locations a and b on the epicardial surface (Fig. 5.3). Each generator will generate a unit response having the general shape V_a and V_b on the body surface. Assuming that these are the only sources, then the optimal body-surface locations for resolving these sources are at P_1 and P_2 respectively. This is clearly illustrated in the following example:

Assuming the contribution to P_1 and P_2 due to unit impulse at a is (0.6,0.1). Similarly, the contribution to these two surface points due to a unit impulse at b is (0.1,0.6). The system equation in this case is,

$$\begin{bmatrix} 0.6 & 0.1 \\ 0.1 & 0.6 \end{bmatrix} \begin{bmatrix} S_1 \\ S_2 \end{bmatrix} = \begin{bmatrix} V_1 \\ V_2 \end{bmatrix} \qquad (5.20)$$

where (S_1,S_2) are the impulse strengths and (V_1,V_2) are the potentials at P_1 and P_2 respectively. For simplicity, assume a source values of (1.0,1.0). The resulting surface values are therefore (0.7,0.7). If in measuring these values an error of say, (+0.01,-0.01) is encountered, then in the inverse calculation the values (1.02,0.98) are obtained for the generators. This represents some $\pm 2\%$ error.

On the other hand, consider the case of two badly selected locations at P_1' and P_2' , the system equation of which is say,

$$\begin{bmatrix} 0.025 & 0.020 \\ 0.020 & 0.025 \end{bmatrix} \begin{bmatrix} S_1 \\ S_2 \end{bmatrix} = \begin{bmatrix} V_1' \\ V_2' \end{bmatrix} \qquad (5.21)$$

Here (V_1', V_2') are the potentials at P_1' and P_2'. For a source values of (1.0,1.0), the surface potentials are (0.045,0.045). Subjecting these observations to the same error (+0.01,-0.01), the error in the inverse solution this time is ±200% , which renders the solution totally useless.

Relation to Condition Number

The same conclusion on the errors in the solutions can be arrived at by considering the system condition number. The eigenvalues in the first example are 0.7 and 0.5. The condition number for this system is therefore 1.4. Consequently, for the ±1.4% error in the observations, the predicted error in the inverse solution is therefore some ±2%, which agrees with the error in the above example.

The eigenvalues in the second example are 0.045 and 0.005. This gives the system a condition number of 9. The percent error in the observation is some ±22%. The predicted error in the solution here is some ±200%, which once again is in agreement with the errors in the example.

Smoothed Errors

If it is assumed that the measurements can be made accurate to 1%, then for a 10% accuracy in the solution, the system condition number must not exceed 10. In practice however, the errors in the observations are of a smooth nature. Typically, the surface potentials are reconstructed from a limited number of sampling electrodes. This usually constitutes the most significant source of errors. On the other hand, errors due to interpolations are of a smooth kind. As a consequence, the system condition number may now be one or even two orders larger, yet giving a solution that is stable. The reason is that the system is less sensitive to low-frequency errors. To illustrate this point, consider once again the ill-conditioned equation (Eqn. 5.21). This time, the observations are subjected to an absolutely smooth error, that is a d.c shift, of (+0.01,+0.01). The resulting inverse solution has a value of (1.22,1.22), which contains only a 22% error. Notice that inspite of a condition number of 9, the percent error in the solution has remained unchanged.

This example demonstrates quite clearly the need to interpret the system condition number more carefully. In actual fact, the system condition number gives the upper bound of the percent error magnification in the inverse solution. With low frequency errors, the magnification can be considerably less. This suggests therefore, that it is always a good practice to smooth out the high frequency fluctuations in the measurements before attempting the inverse calculation. Such a procedure may not increase the accuracy of the solution, but it does however yield a more stable solution.

5.5 Feasibility Studies using a 2-Dimensional Torso Model

In this section, the feasibility of an unconstrained inverse solution is investigated using data obtained from model calculations. A block diagram describing the procedure of the investigation is shown in Fig. 5.4

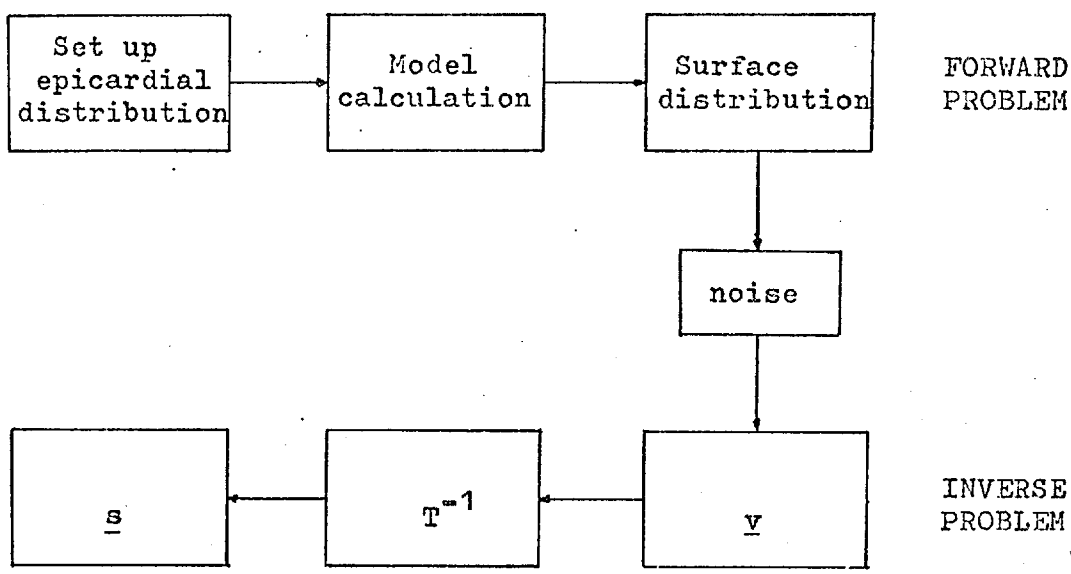

Fig.5.4: Block diagram illustrating the investigation procedure.

Fundamental to the investigation are the questions:

1) The number of epicardial generators that can be unambiguously inferred from surface measurements.
2) The optimal sites for making these observations.
3) The highest spatial harmonic of the epicardial distribution that can be resolved from surface measurements.

Because of the enormous amount of computing resources required for such studies, a practical solution is to limit the investigations to a 2-dimensional model of the human thorax.

Forward Calculations

The 2-dimensional, one-sixth inch grid model of the torso constructed in the preceeding chapter is used in the forward calculations in this section. Sinusoidally varying potentials of various harmonics are applied to the heart-surface as test distributions. Fig. 5.5 shows the model surface distributions for the first four harmonics.

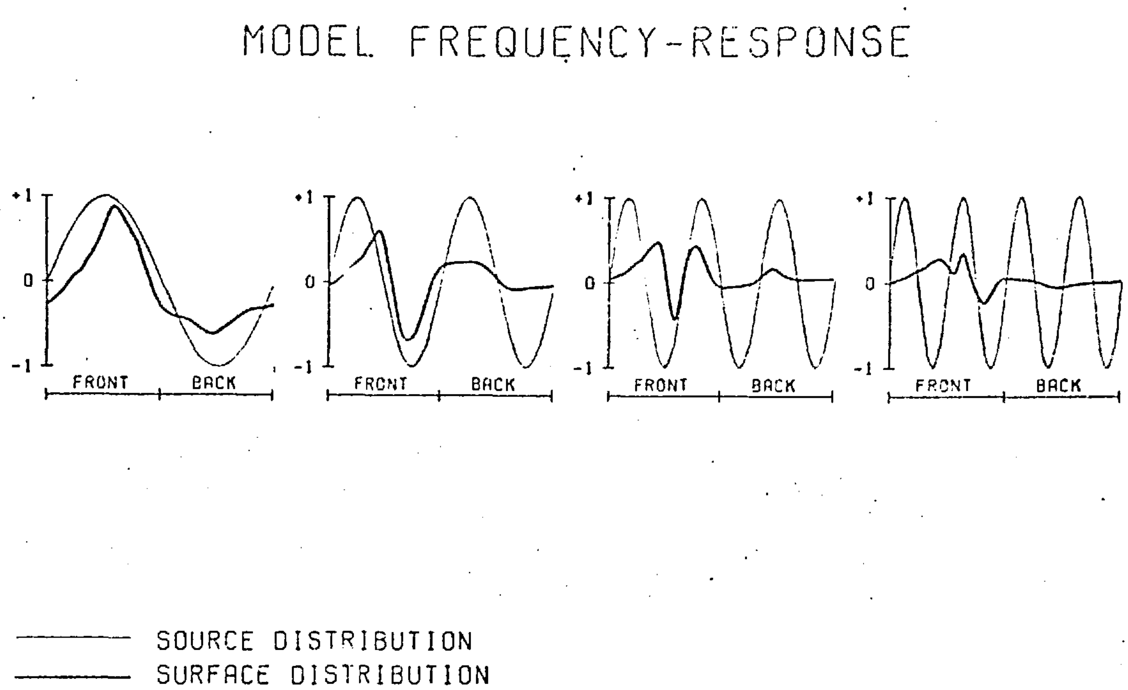

Fig.5.5: Model frequency-response for the first four harmonics.

Notice the 'low-pass' nature of the torso is clearly demonstrated by the rapidly decreasing magnitude of the surface distributions as the harmonic number increases.

A sequence of random numbers scaled to 1% of the peak-to-peak value of the test signals are added to the surface distributions in order to simulate the errors in the real system. These 'noisy' surface potentials provide the data for testing the feasibility of recovering, within some specified accuracy, the original test distributions.

The Equivalent Generator

The equivalent cardiac generators are represented by equal epicardial segments, the potential over each of which is assumed to be constant, having a value equal to the mean of the potentials over that segment. This is the same as approximating the epicardial distribution by a step function as shown in Fig. 5.6.

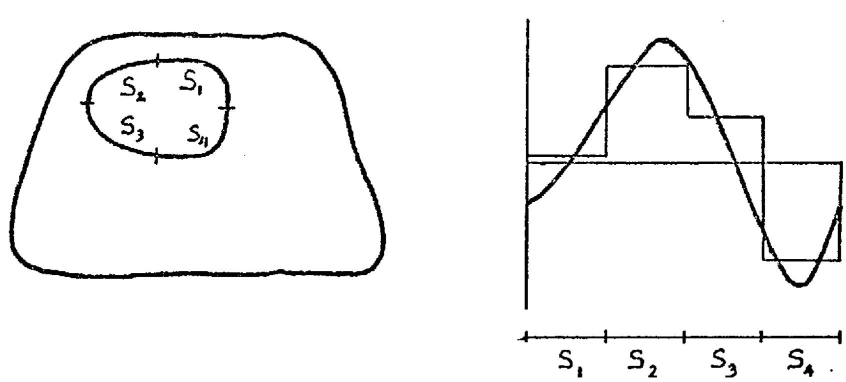

Fig.5.6: Step function approximation of the epicardial potential distribution.

The accuracy of such an approximation clearly depends on the number of segments used and the harmonic content of the epicardial potentials. If the highest harmonic number in the distribution is N, then according to the sampling theorem, 2N segments suffice to represent the distribution. The original analogue function can be recovered from the step function by a smoothing process. A suitable technique is as follows:

1) Decide on the number of points required to represent the smoothed function. Preferably, this should be K such that K/N is an integer, where N is the number of segments in the step function.

2) Set up an array of numbers $(x_1, x_2, \ldots x_K)$ with the first K/N values equal to S_1, the second K/N values equal to S_2 and so on. $S_1, S_2, \ldots S_N$ are the values of the step function at segment 1,2,... N respectively.

3) Smooth the values in the array. For example,

$$\bar{x}_i = (x_{i-1} + 2x_i + x_{i+1})/4$$

where $\bar{x}_i$ is the new value of the ith point.

4) Restore the power in each segment by adding a constant C_1 to all the values in segment 1, C_2 to all the values in segment 2, and so on, where

$$C_1 = S_1 - \frac{N}{K}\sum_{i=1}^{K/N} x_i \qquad , \ldots\ldots \text{ etc.}$$

5) Repeat steps 3 and 4 until the required degree of smoothness is achieved.

A simple example illustrating this process is shown in Fig. 5.7.

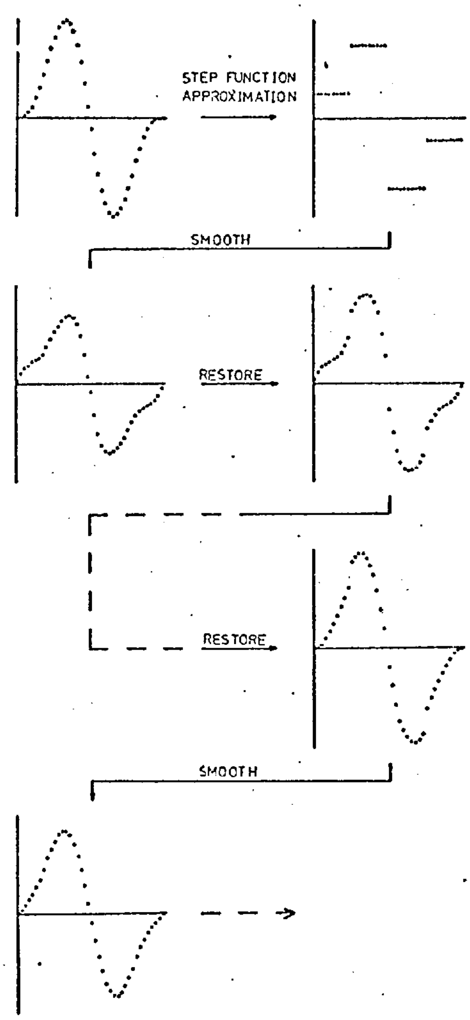

Fig.5.7: Diagram illustrating the process of recovering the analogue function from the step function.

Inverse Solutions for 4 Heart-Segment Model

The feasibility of inferring 4 epicardial generators is presently investigated. Three system matrices were constructed, one for each of the following electrode configurations:

1) Electrodes placed at 4 equally spaced locations.

2) Electrodes placed at locations where the contribution

from each heart generator is the maximum.

3) Overdetermination by a factor of 3. That is, taking three times as many measurements as is theoretically required.

Fig. 5.8 shows these electrode configurations in relation to the surface contribution from each heart generator.

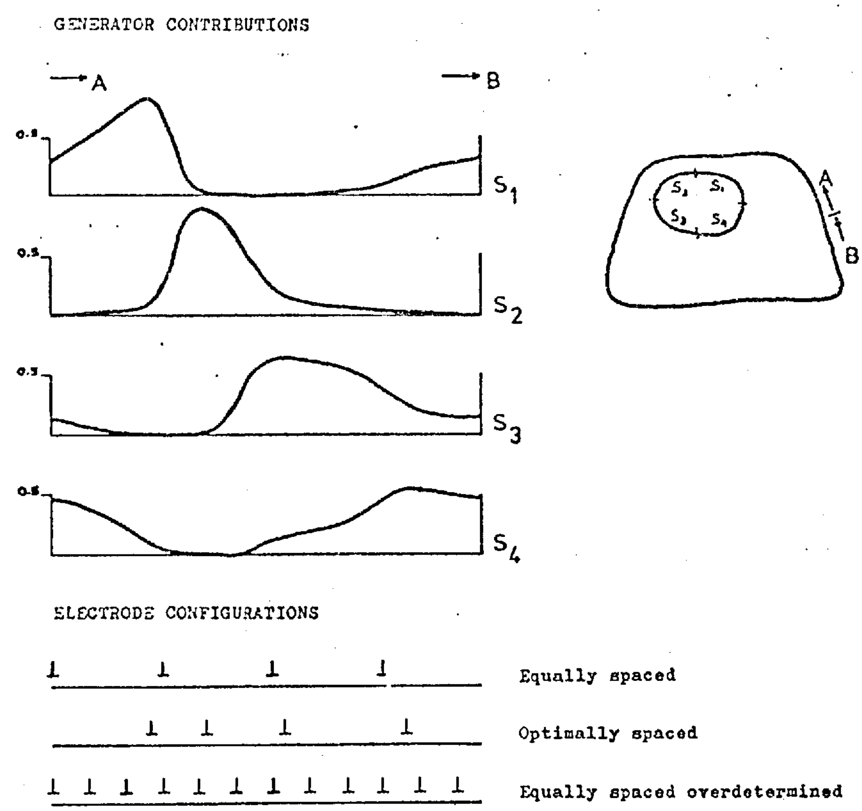

Fig.5.8: Electrode configurations and their relation to the generator contributions.

The inverse solutions for these 3 systems are calculated using the 'noisy' surface distributions from the previous forward calculations as data. These solutions are represented graphically in Fig. 5.9. Since only 4 epicardial segments are used, the highest resolvable harmonic is 2. The solutions from electrode configurations 2 and 3 are stable and it is not difficult to see that a good representation of the original distributions can be recovered by smoothing the step solutions in the manner described previously. On the other hand, the solution from configuration 1 is highly unstable. An investigation of the system eigenvalues revealed that this system has a condition number of 235. The condition numbers for electrode configurations 2 and 3 are 3 and 25 respectively.

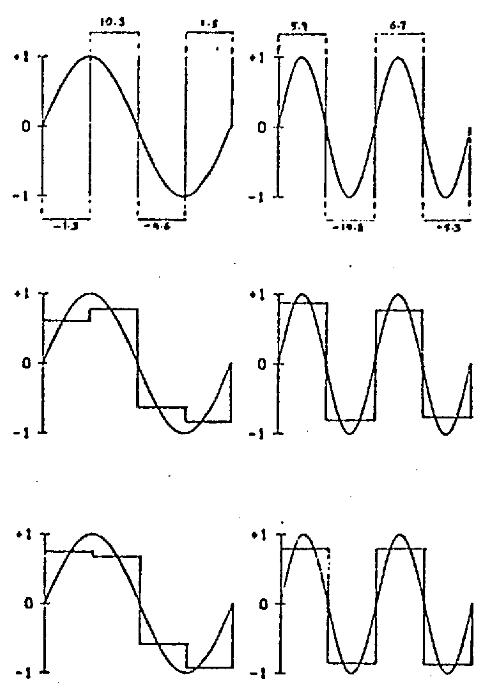

System 1

System 2

System 3

Fig.5.9: Inverse solutions for a 4-segment heart using 3 different system equations.

It is not difficult to see why the system stability is increased by overdetermination since the chances of covering the optimal sites are increased using a large number of electrodes.

Inverse Solution for greater number of Heart Segments

The same inverse calculations were performed for systems with 6,8,10 and 12 epicardial segments. Table 5.1 lists the condition numbers for all the systems investigated.

Table 5.1: System condition numbers.

No. of Heart Segments	Equally Spaced	Optimally Spaced	3X Over-determined
4	235	3	25
6	475	6	80
8	1175	40	364
10	36410	73	540
12	1359610	1117	6480

The sizes of the condition numbers in column 1 of Table.5.1 indicates clearly the unlikely success of an unconstrained solution using evenly-determined systems with arbitrarily selected sampling sites.

Solutions for the 6,8 and 10 heart-segment models are shown in Fig. 5.10, Fig. 5.11 and Fig. 5.12 respectively for electrode configurations 2 and 3. The solutions are stable up to 10 heart segments. Beyond that, the solutions begin to oscillate wildly.

Notice that the condition numbers for the overdetermined systems are one order of magnitude larger than the corresponding

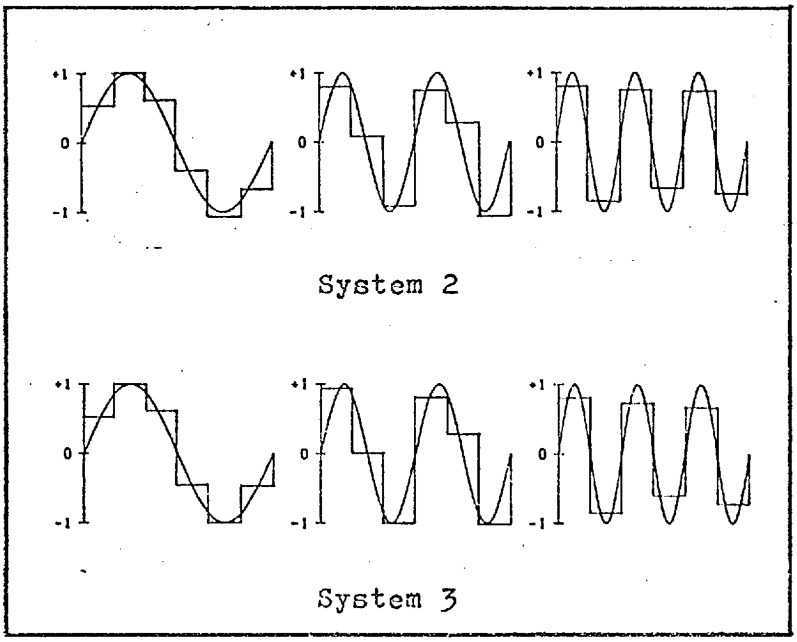

Fig.5.10: Solution for 6-segment heart.

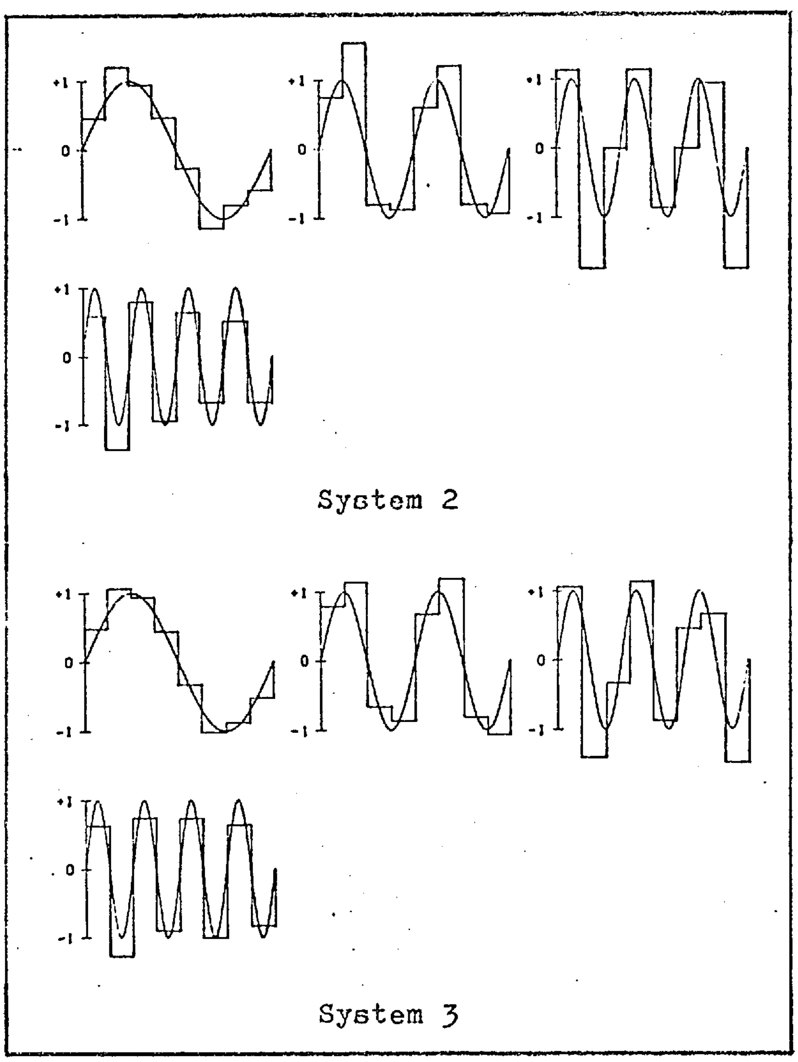

Fig.5.11: Solution for 8-segment heart

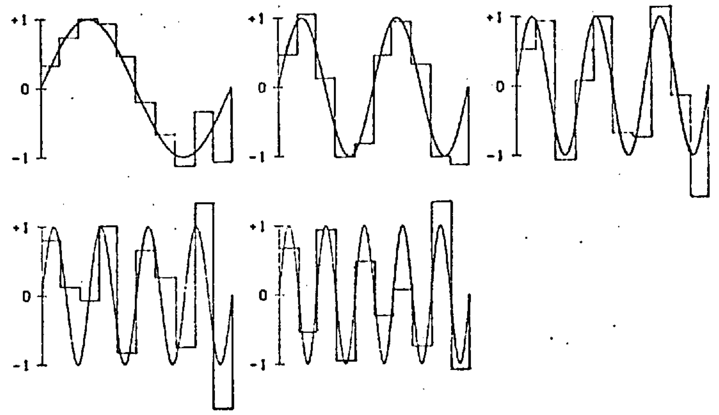

System 2

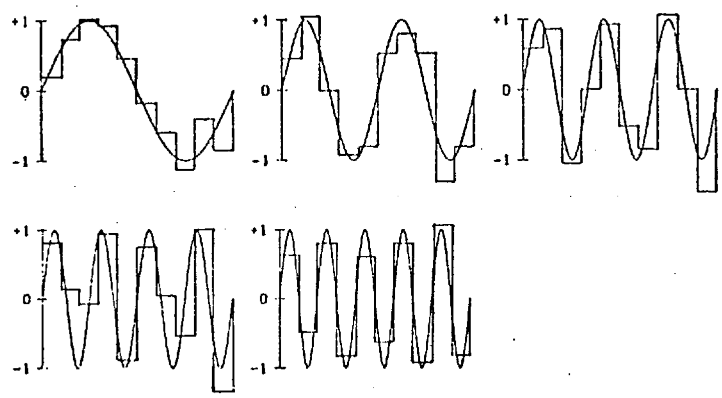

System 3

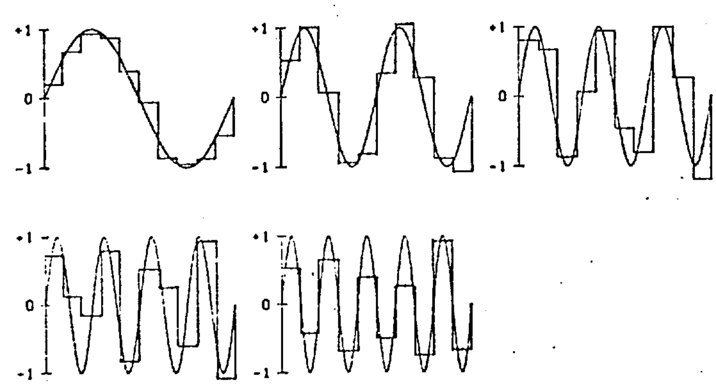

System 2 with smoothed data

Fig.5.12: Solutions for 10 heart-segments

systems using optimally selected electrode sites. In spite of this, the solutions are stable while those for the evenly-determined systems at the same order of condition numbers are unstable. This is because in evenly-determined systems, the solutions are found by the process,

$$\underline{s} = T^{-1}\underline{v} \tag{5.22}$$

which as discussed in Section 5.3, favours high frequency fluctuations. On the other hand, solutions obtained using the method of overdetermination ,

$$\underline{s} = (T^T T)^{-1} T^T \underline{v} \tag{5.23}$$

are such that the errors are minimized in the least-square sense (see Lanczos, 1961).

From the solutions, it is also seen that the first 3 harmonics of the epicardial distributions can be quite accurately recovered using the 6 heart-segment systems. The accuracies of retrieving the higher harmonics using systems with greater number of heart segments are limited by the system stabilities. This problem is somewhat improved by smoothing the data slightly before attempting the inverse calculations (Fig. 5.12).

5.6 Conclusion

The investigations in this chapter have shown that it is feasible to infer up to the 5th harmonic of the epicardial potentials in a 2-dimensional torso model using unconstrained inverse solution. It is not unreasonable to assume that similar results would exist in the 3-dimensional case although the spatial resolution may be poorer. The important achievement in this chapter, nevertheless, is the insight into the inverse problem provided by this investigation. It is also shown that the ability to resolve the epicardial distributions is greatly improved by,

1) carefully selecting the sites of electrode measurements. The optimal sites being those where the contribution from each generator in turn is the maximum.
2) overdetermination of the problem.
3) smoothing the data before inversion.

Although not mentioned in the investigations, clearly, over-determination of the problem is most effective when all the optimal sites are included in the electrode configuration.

CHAPTER 6

CALCULATIONS OF EPICARDIAL POTENTIALS FROM IN-VIVO SURFACE MEASUREMENTS

6.1 Introduction

The investigations in the previous chapter showed that an unconstrained inverse solution is feasible using simulated data on a 2-dimensional model of the human torso. In this chapter this investigation is extended to more realistic 3-dimensional torso model derived in Chapter 4 using surface data measured in-vivo.

For the purpose of the forward calculations, the surface of the heart is divided into 26 approximately equal areal segments. These are configured in three rows of eight segments round the heart and two polar caps. The transfer of the electrical potentials from each segment to the body surface is calculated using the digital model of the torso constructed in Chapter 4.

The system transfer matrix relating the potentials on 26 epicardial segments to 26 body surface locations is then constructed from the forward solutions. These 26 body surface locations are selected from sites where the contribution from each epicardial segment is the maximum. This ensures that the system condition number is kept to a minimum as discussed earlier.

The surface data used in the inverse solutions were obtained from the collection of surface ECG maps acquired by Monro[1]. A

[1] A private communication.

complete description of the data aquisition and mapping procedure of the surface ECG is found in his publication, Monro et al.(1974).

6.2 Forward Calculations

The surface of the heart is segmented into 26 approximately equal areas. These are arranged in three rows of eight segments around the heart and two polar caps, one at the apex and the other, the basal region of the heart (Fig.6.1). The advantage

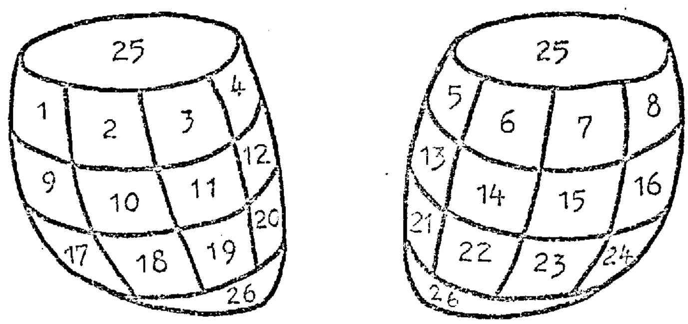

Anterior Posterior

Fig.6.1: Segmentation of the heart-surface into 26 discrete areas.

of using such a configuration is that these segments can be mapped into a regular pattern on a cylindrical surface as shown

25			
1	2	3	4
9	10	11	12
17	18	19	20
26			

Anterior

25			
5	6	7	8
13	14	15	16
21	22	23	24
26			

Posterior

Fig.6.2: Cylindrical projection of the 26 epicardial segments.

in Fig. 6.2. This greatly simplifies the task of reconstructing the epicardial distrubutions in the later stage of the development. Furthermore, as demonstrated by Monro et al (1974), a configuration of this kind can be unfolded into a two dimensional array that repeats along the rows and the columns (Fig. 6.3). The importance is that this array is now directly

	•									
	5									
	25	25	25	25	25	25	25	25		
• • 8	1	2	3	4	5	6	7	8	1	• •
	9	10	11	12	13	14	15	16		
	17	18	19	20	21	22	23	24		
	26	26	26	26	26	26	26	26		
	21	22	23	24	17	18	19	20		
	13	14	15	16	9	10	11	12		
	5	6	7	8	1	2	3	4		
	25									
	1									
	•									

Fig.6.3: A repetitive 2-dimensional array obtained by 'unfolding' the closed heart surface.

amenable to a 2-dimensional discrete Fourier transform, thus opening the possibility of future spectral analysis on the epicardial distribution.

The potential transfer from these segments to the body surface is calculated using the numerical technique developed in Chapter 3 and the anatomical model of the thorax described in Chapter 4. The calculations are made for each segment in turn by applying a unit potential over the segment concerned and zero potential everywhere else on the heart surface. The resulting body surface distribution is listed in Appendix D.

From the forward calculations a system matrix is constructed which relates the potentials on the epicardial segments to the potentials at 26 locations on the body surface. These locations are selected to correspond to the sites where the potential contribution from each segment is the maximum. Fig. 6.4 shows the positions of these locations on two planes which represents

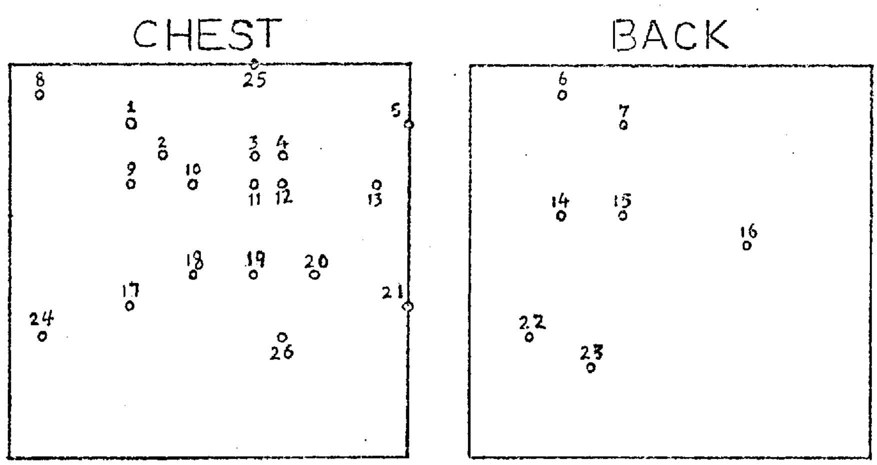

Fig.6.4: Locations on the body-surface where the transfer relationships are computed.

the cylindrical projection of the front and the back of the body surface. The forward transfer matrix for this configuration is given in Table. 6.1.

Table 6.1: The forward transfer matrix.

41	109	80	13	13	39	48	56	44	70	32	21	8	6	14	18	28	43	23	21	16	19	24	34	126	46
35	129	101	13	10	30	35	40	47	109	48	21	6	5	10	13	27	52	29	18	12	15	19	27	103	39
14	58	223	40	17	30	29	23	13	51	111	83	11	5	7	6	10	21	34	40	13	11	12	12	92	27
12	38	140	54	29	42	36	25	9	27	75	129	22	8	11	7	10	16	27	71	24	17	16	15	96	38
15	35	65	32	41	72	60	36	12	20	27	64	32	17	23	13	16	21	20	63	41	35	32	27	112	64
19	39	55	24	34	83	76	46	15	22	22	43	24	17	28	18	19	24	19	46	34	35	36	33	123	62
20	39	46	17	27	80	83	53	17	24	19	32	19	17	34	23	23	28	20	39	32	37	42	41	113	67
33	63	50	12	16	51	64	66	32	40	20	21	11	10	25	29	34	41	23	27	23	30	39	52	117	65
34	107	61	8	8	25	31	37	69	113	34	15	6	5	12	17	45	80	35	18	14	19	25	41	76	55
19	105	124	11	7	17	20	21	35	171	95	22	4	3	6	8	25	77	59	17	9	11	13	20	59	37
8	38	194	31	10	16	15	12	9	57	200	106	8	3	4	4	8	28	87	50	10	8	8	9	45	28
7	24	119	46	22	27	23	15	6	23	108	183	20	6	7	5	7	15	54	121	23	14	12	11	57	39
11	27	58	35	39	53	44	26	9	17	30	92	43	16	18	10	14	20	22	106	55	37	31	24	83	76
13	27	37	17	28	66	62	35	13	18	17	35	27	25	39	20	24	29	23	55	52	58	57	44	79	94
16	31	34	13	22	64	69	42	16	21	15	26	19	22	47	28	29	33	23	43	41	54	62	54	79	90
20	36	32	10	15	48	58	48	23	28	15	19	13	15	38	37	41	45	28	34	34	48	63	75	75	96
16	33	25	7	10	29	35	33	27	33	15	14	9	10	25	29	64	72	41	35	35	52	67	96	52	132
13	34	23	5	6	18	21	21	33	57	22	11	6	6	14	18	85	141	70	29	25	38	50	77	35	135
8	25	23	3	4	10	12	12	22	71	48	13	3	3	8	9	59	205	170	29	17	24	30	41	21	125
3	10	20	4	3	5	6	5	6	26	83	42	3	2	4	3	19	91	331	111	13	15	16	17	11	146
4	9	20	10	11	17	15	9	4	8	19	60	20	7	9	5	12	20	49	352	61	33	25	19	24	171
7	16	24	12	17	31	28	17	9	13	14	37	26	15	19	11	23	33	35	127	89	71	54	39	41	185
9	18	22	9	14	33	33	21	12	16	12	24	19	18	28	16	32	41	35	70	75	89	79	57	42	170
10	21	22	8	13	33	35	25	15	19	12	19	15	16	32	21	40	48	36	53	60	83	87	71	44	157
28	87	129	25	21	50	52	47	23	51	44	38	12	7	13	12	16	26	20	28	17	17	19	22	154	36
5	11	12	4	5	12	13	10	9	16	16	16	7	6	11	9	34	72	108	103	45	51	48	44	19	306

6.3 Inverse Calculations.

Also superimposed on the two body surface planes are the locations where the ECG measurements for surface mapping were taken (Fig. 6.5). The data required for the inverse calculations were recovered from these measurements by means

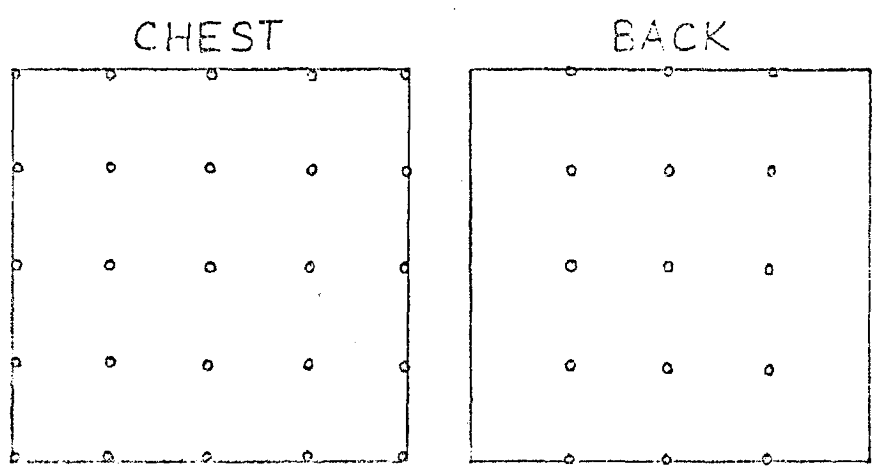

Fig.6.5: Locations on the body surface where surface measurements are taken.

of the 'band-limited' interpolation procedure described by Monro et al.(1974).

Fig. 6.6 shows 20 frames of body surface isopotential maps for a normal subject taken at 2msec. intervals. The corresponding potential values on the 26 epicardial segment for each frame is calculated using the unconstrained solution.

$$\underline{s} = T^{-1}\underline{v} \tag{6.1}$$

where T is the system matrix given in table 6.1, $\underline{V}$ is the surface data on the 26 surface locations shown in Fig. 6.4 and $\underline{s}$, the calculated potential values on the 26 epicardial

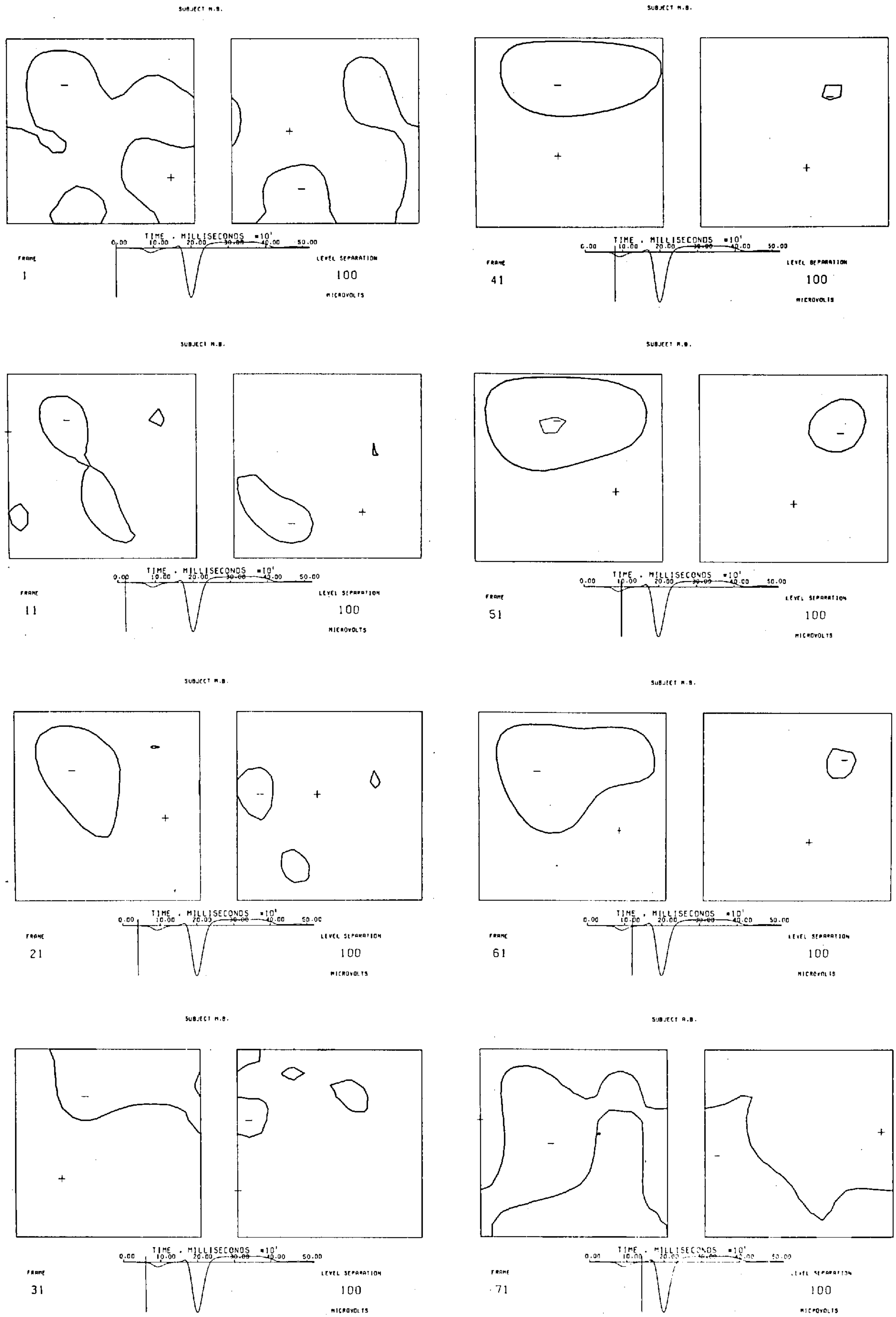

Fig.6.6a: Body-surface maps. Frame 1 - 71.

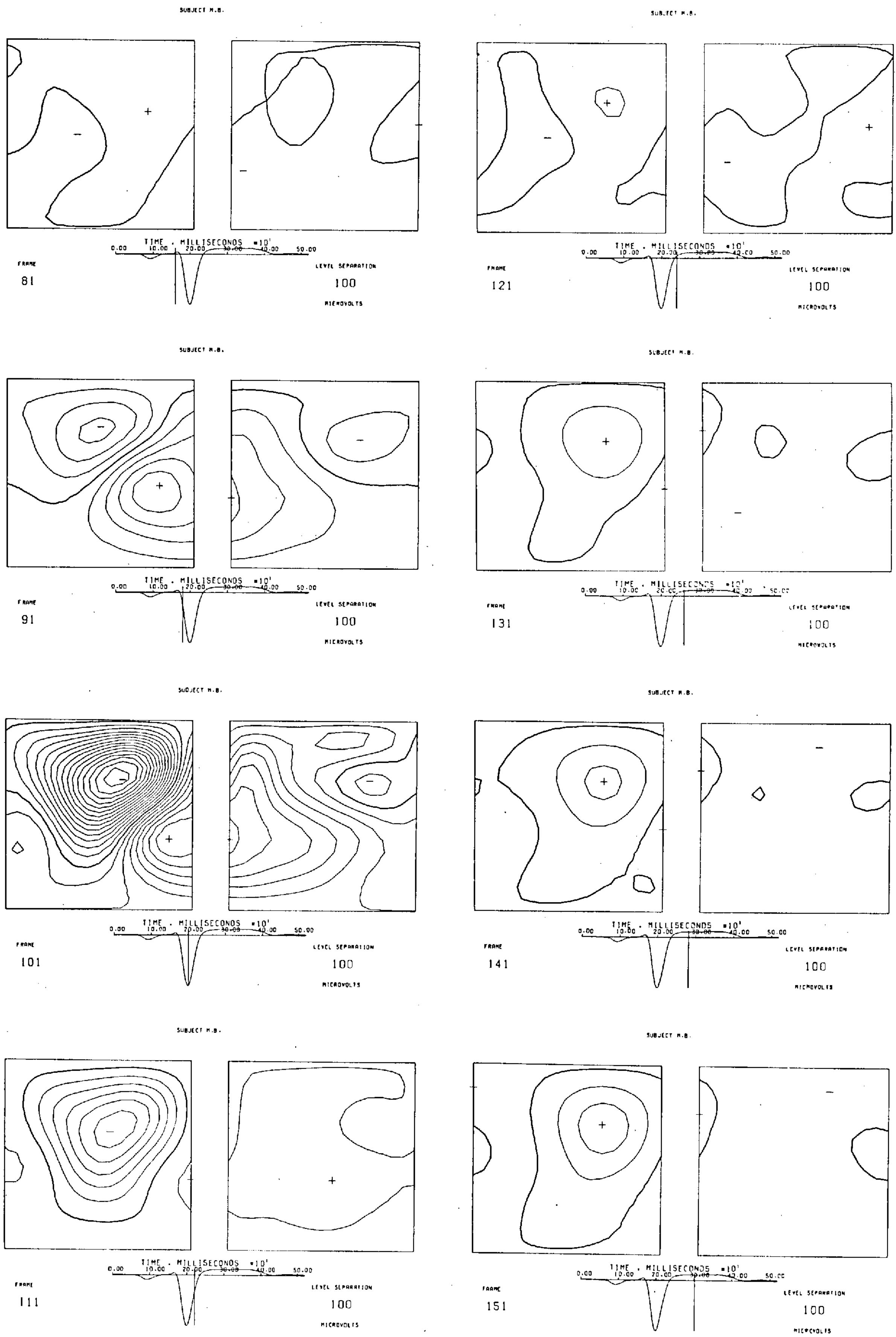

Fig.6.6b: Body-surface maps. Frame 81 - 151.

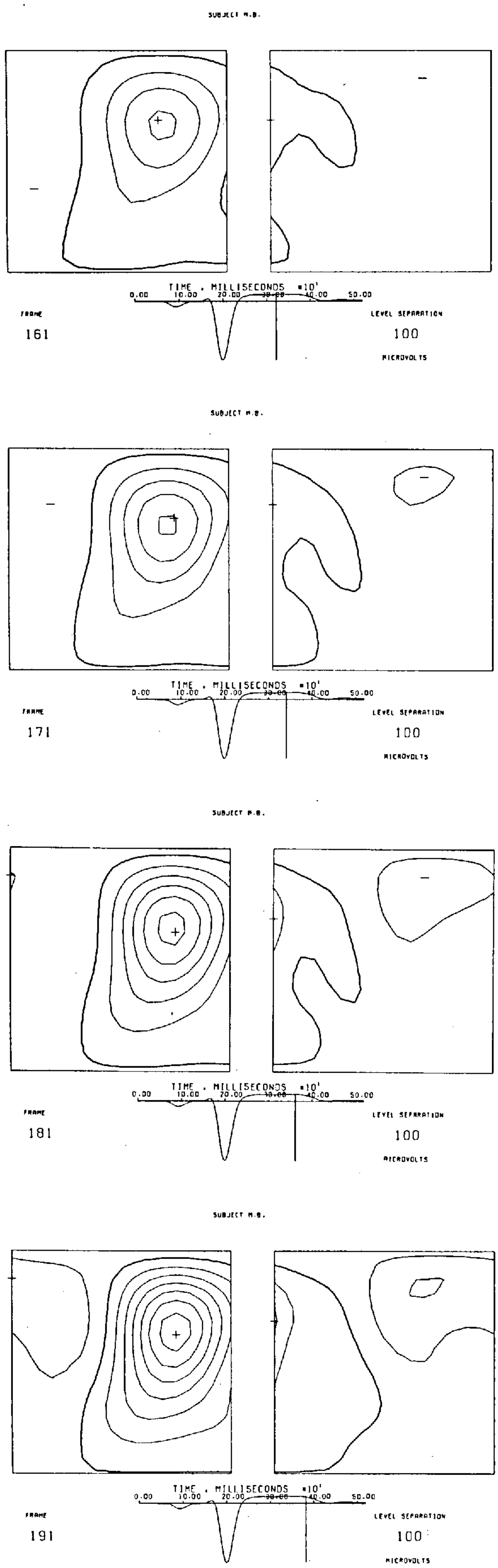

Fig.6.6c: Body-surface maps. Frame 161 - 191.

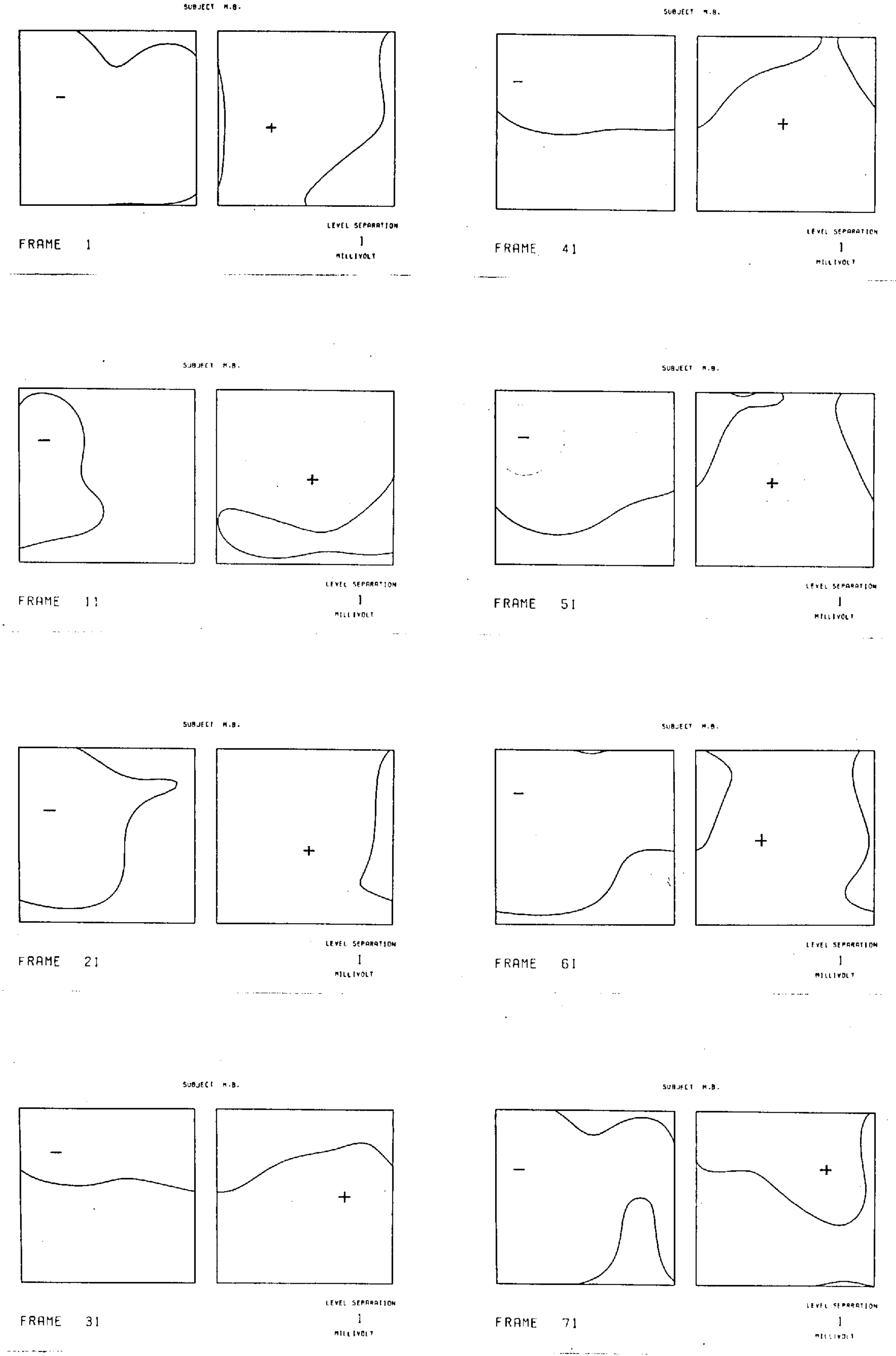

Fig.6.7a: Epicardial maps. Frame 1 - 71.

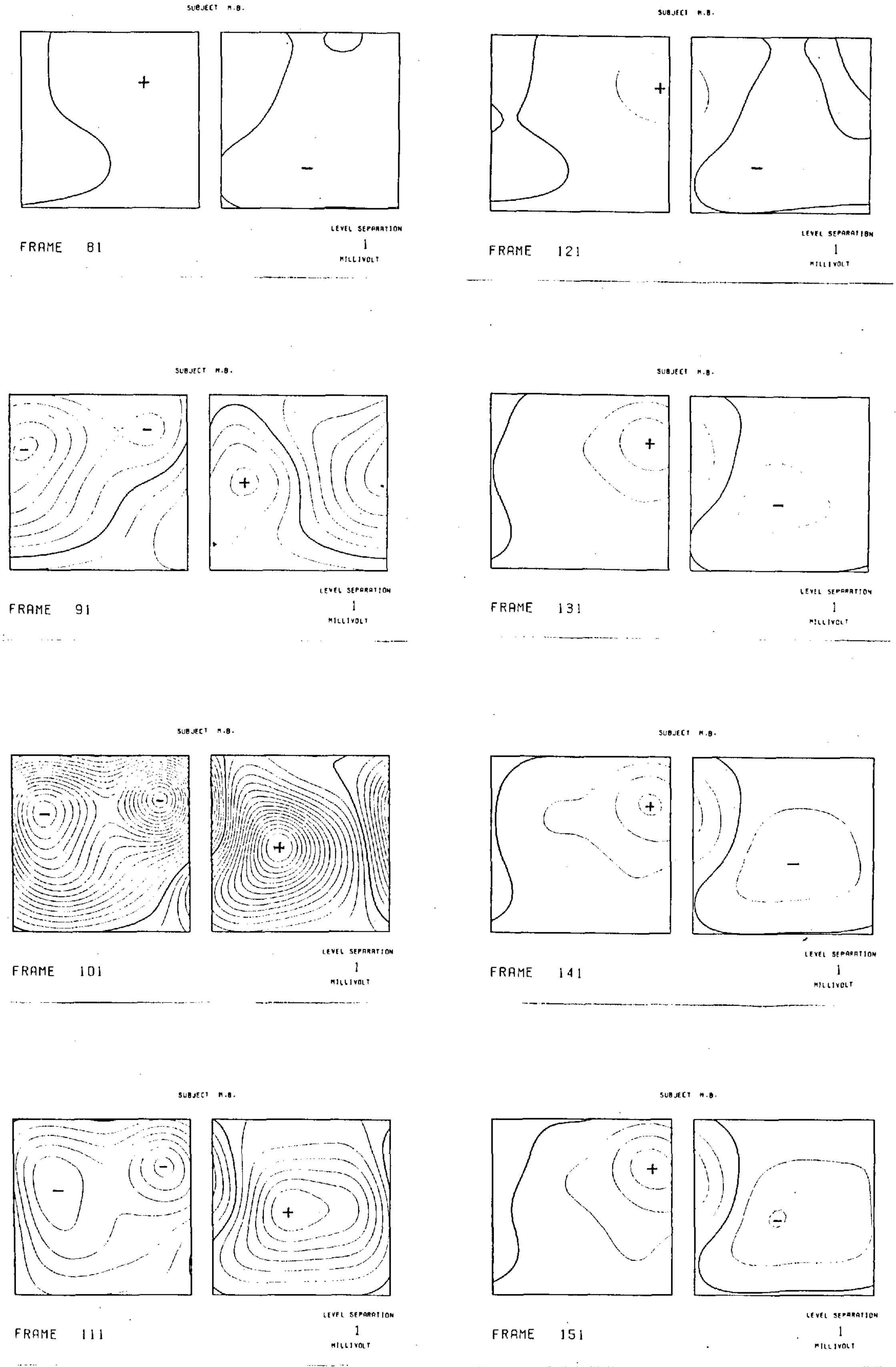

Fig.6.7b: Epicardial maps. Frame 81 - 151.

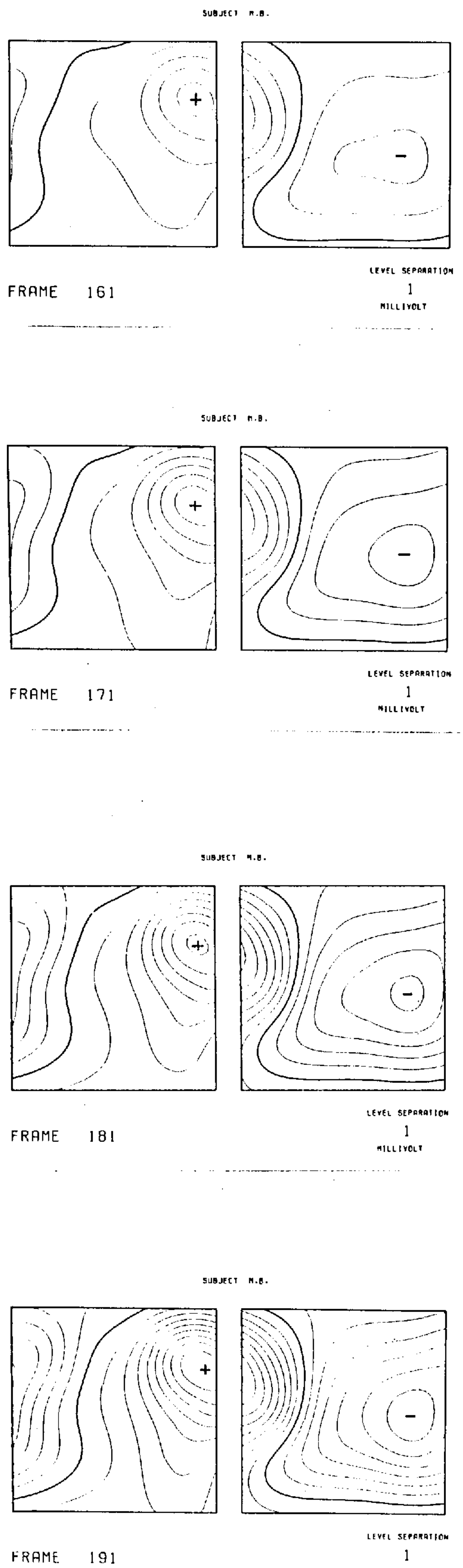

Fig.6.7c: Epicardial maps. Frame 161 - 191.

segments. From the inverse solutions, epicardial isopotential maps were reconstructed using the smoothing technique described in the previous chapter, except that here, the process is in two dimensions. These maps are shown in Fig. 6.7. In order to aid interpretation of the epicardial potential maps, the various regions of the heart surface as projected onto the cylindrical surface is shown in Fig. 6.8.

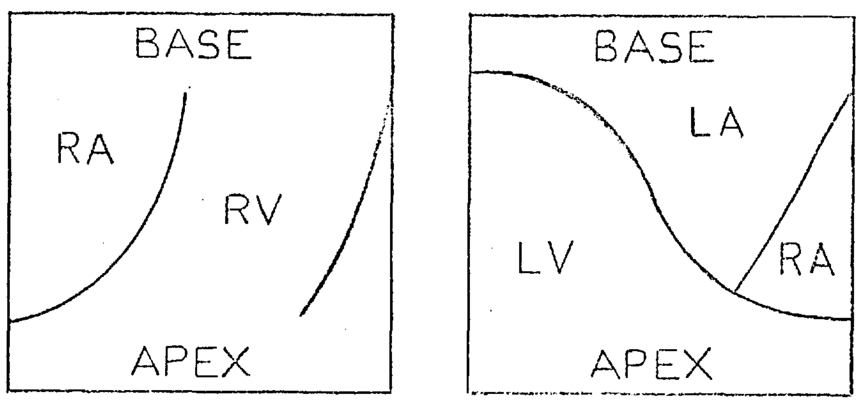

Fig.6.8: Diagram illustrating the cylindrical projection of the heart surface.

6.4 Stability of Inverse Solution

Serious errors were observed in the inverse solution when the validity of Equation 6.1 was first tested. This was later discovered to be due to the limited accuracies in which the exact inverse of the matrix T can be computed. The effect of the errors in the inversion is to cause large oscillating values in the solution. This is clearly seen in the listing of the inverse calculations in Appendix E.1.

This problem was overcome by using an iterative method of solving the system equation. In an iterative scheme, the solution is obtained by successive approximations which in the limit approaches the exact solution. Such a process is relatively unaffected by the machine resolution. Because of the manner in which the system matrix is constructed, the elements along the diagonal are either the largest or of the same order as the largest element in each row. This makes the system equation directly amenable to the Gauss-Seidel iteration previously described in Section 3.5. The solutions obtained using this method is given in Appendix E.2.

There remains however, the question of the magnification of the percentage error expected in the solution. An eigenvalue analysis showed that the system has a condition number of 2104. In the worst case therefore, the percentage error in the solution would be some 2000 x the percentage error in the data. Assuming the magnitude of the surface potentials to be of the order of $\pm$1mV, then for a $\pm$10uV error in the measurements, the error in the solution would therefore be some 2000%. But as discussed in the previous chapter, the magnification of the error in a practical system can be considerably less.

A more useful test of the system stability is to perturb the surface data by some noise and observe if the error in the solution remains within an acceptable limit. The inverse calculations in Appendix E.2 were repeated with 10uV of noise added to the surface data. This is shown in Appendix E.3. An investigation of the inverse solutions showed that the noise level is everywhere of the order of 100uV. Since the values of the inverse solution are an order of magnitude larger than the surface data, the percentage noise level therefore, has remain virtually unchanged. In other words, there is virtually no deterioration in the signal-to-noise ratio in the calculated epicardial potentials in spite of the fact that the system's condition number in some 2000.

6.5 Validity of the Inverse Calculations

The validity of the inverse calculations is somewhat impossible to verify without an accurate and complete picture of the actual epicardial potentials of the same subject to compare with. In-vivo epicardial measurements are beyond the scope of the present study. And even then, it is uncertain whether the epicardial distributions would remain unchanged in an open-chest experiment.

However, several research workers have previously mapped the epicardial potentials for the canine heart (Taccardi and Marchetti, 1965; Spach et al., 1975). Although the excitation of the canine heart is known to differ from the human heart, nevertheless, there exists a large degree of correspondence between them (Durrer et al. 1965). A rough estimate of the validity of the inverse solution can therefore be obtained by comparing the reconstructed epicardial maps with published maps of the canine heart.

One such experiment was conducted by Taccardi and Marchetti (1965) in which an isolated dog's heart was immersed in a Ringer's bath. An exploring electrode was then rotated around the heart, mapping the potentials on a cylindrical surface enclosing the heart. Fig. 6.9 shows the canine maps redrawn from Taccardi at four instances in the QRS cycle corresponding approximately to Frame number 81, 91, 101 and 121 of the calculated human epicardial maps.

It should be noted that the dog's heart in the experiment was suspended in an upright position with both atria superior to the ventricles. Normally, the heart in the body lies on its side.

The map of the various epicardial regions for the inverse calculations is illustrated in Fig. 6.8. The map for the cylindrical projection of the heart surface in the experiment is shown in Fig. 6.10. At the beginning of the QRS cycle, both sets of maps show the presence of a potential maximum directly over the right ventricle and a minimum over the left ventricle. About half-way between the Q-R interval, the potential maximum over the right ventricle is replaced by a minimum in both maps. Another minimum is found over the right atrium and a maximum over the left ventricle. Both sets of maps agree very closely in these features. At the instant of the R-peak, both maps show the right ventricle and the right atrium to be negative while the left ventricle and the left atrium to positive. However, the calculated map shows two minimum, one over the right ventricle and the other over the right atrium. This feature is also observed in the surface map. The canine map on the other hand showed only one minimum over the right ventricle. This difference could be due to several factors ranging from the electrophysiological difference between the human and the canine heart to simply the fact that in the experiment, the epicardial potentials were mapped 'remotely', resulting in the loss of spatial resolution. The two maps agree once more at the end of the QRS complex with a potential maximum appearing over the right ventricle and a minimum over the left ventricle.

These results are also in agreement with the findings of Spach and Barr (1975).

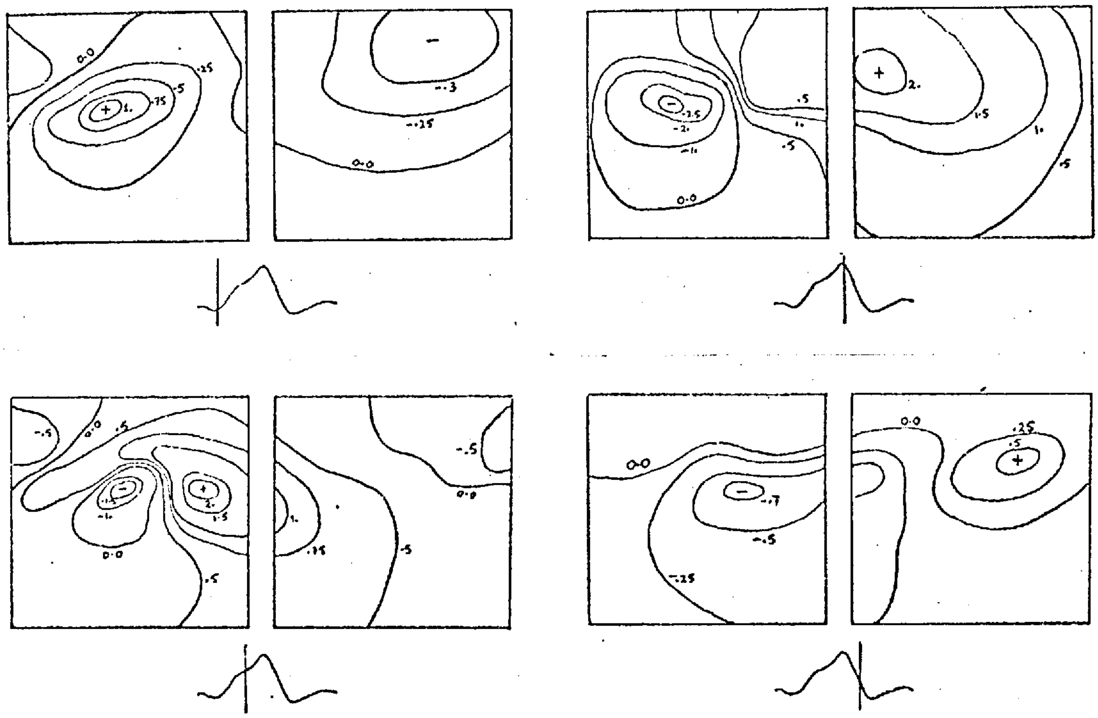

Fig.6.9: Epicardial maps of the canine heart.
(Redrawn from Taccardi and Marchetti).

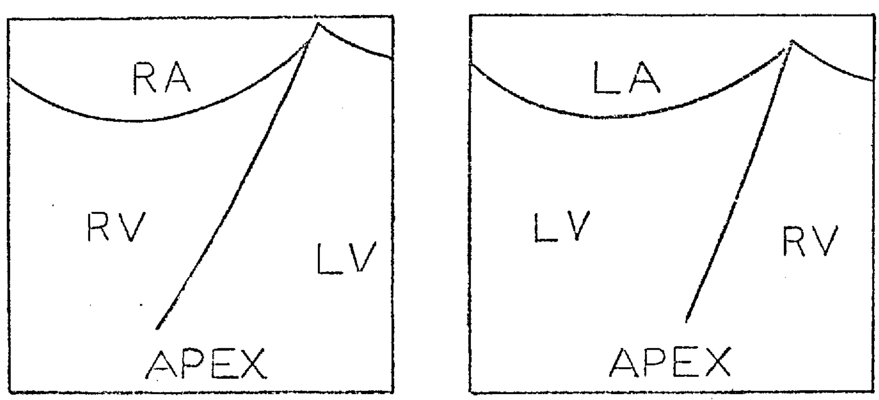

Fig.6.10: Conjectural diagram illustrating the projection of the dog's heart onto the mapping cylinder.

6.6 Conclusion

In this chapter, the transfer function between 26 epicardial segments and 26 body surface locations was calculated. Using this transfer relationship, epicardial potentials were reconstructed from in-vivo surface ECG maps. The validity of the inverse calculations was demonstrated by comparing the reconstructed epicardial maps with published maps of the canine heart.

CHAPTER 7

CONCLUSION

This dissertation is concerned with two fundamental problems in electrocardiography, namely the forward problem and the inverse problem.

Forward Solution

The forward problem was approached using a digital computer model of the human torso based on the numerical-analogue developed in this study. Physically, the model can be thought of as an assembly of discrete blocks of conductors. Each block is assumed to be homogeneous but not necessarily isotropic. In order to represent the torso anatomy on the computer, each discrete block is assigned an alpha-numeric character corresponding to the electrical property of that block. In this way, the entire 3-dimensional torso structure is represented as coded images in the computer. The potential at each node in the model is calculated by the method of finite-differences. A set of linear algebraic equations relating the potential at each node to the potentials at neighbouring nodes is constructed using the general finite-difference equation formula derived in this study. This set of equations is then solved iteratively using the accelerated Gauss-Seidel method. Because of the enormous number of equations involved, the convergence of the solution can be extremely slow indeed. By using a coarser model to obtain an initial estimate of the solution and then improving the accuracy of this solution on the finer model, the amount of computational time required to achieve a solution is greatly reduced.

The validity of this model was demonstrated by comparing simulated body-surface distributions due to a catheter located inside the heart with those actually observed on cardiac-patients with implanted pacemakers.

Inverse Solution

The inverse problem on the other hand, was approached by a careful investigation of the factors that could lead to an unstable solution. It was shown that the torso can be regarded as a kind of spatial filter to the potential transfer from the heart to the body surface. This filter is of a 'low-pass' nature. Consequently, the spatial resolution of the cardiac generators is limited to the 'bandwidth' of this filter. To attempt to resolve cardiac generators outside this bandwith will only lead to instability. A carefully chosen configuration of generators will therefore greatly increase the chances of a successful inverse solution. It was also demonstrated that a well selected body-surface locations for constructing the epicardial to body-surface transfer matrix will enhance the stability of the inversion. The optimum body sites being those where the contribution from each generator is the maximum. The transfer matrix so constructed has amongst the smallest condition number.

Other procedures proposed for improving the stability of the inverse calculations included spatial smoothing of the data before inversion and using an iterative procedure to calculate the inverse solution. Smoothing may be useful because the low-pass characteristic of the torso means that in the inverse transformation the high frequency components are magnified in a much greater proportion than the low frequency ones. Consequently, any high frequency noise in the data could be disproportionally magnified rendering the solution totally useless. The limited resolution of the computer word introduces a similar kind of instability in direct inversion of the system matrix. Here, the noise is a numerical one caused by rounding off during the computation. This problem is overcome by using an iterative process to obtain the inverse solution where the stability of the solution is relatively unaffected by the machine resolution.

Epicardial potential distributions at 2msec. intervals were calculated from in-vivo body surface measurements. The reconstructed epicardial maps were shown to be grossly consistent with those found in the literature. The stability of the inverse solutions was tested by adding random noise to the surface data. The solutions showed virtually no deterioration in their signal-to-noise ratios.

In conclusion, this study has demonstrated the feasibility of an unconstrained inverse solution based on recovering the epicardial potentials.

APPENDIX A

PROGRAM DESCRIPTION

A computer program for calculating volume-conductor fields based on the numerical-analogue developed in Chapter 3 is described. The Program is organized into four phases as follows:

PHASE1 - Unpacks the input data into coded cross-sectional images.

PHASE2 - Generates the finite-difference nodes.

PHASE3 - Constructs the set of finite-difference equations.

PHASE4 - Solves the set of equations iteratively using the Gauss-Seidel method.

A.1 Program Flow Diagrams

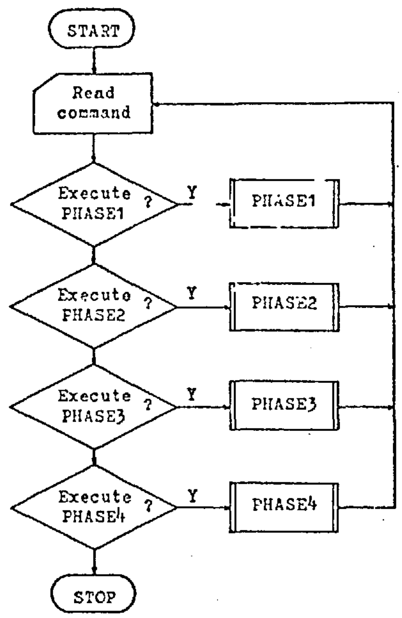

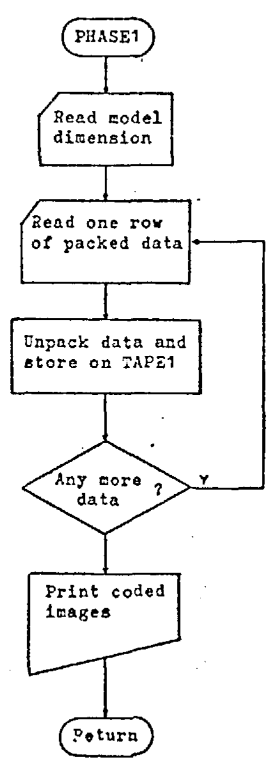

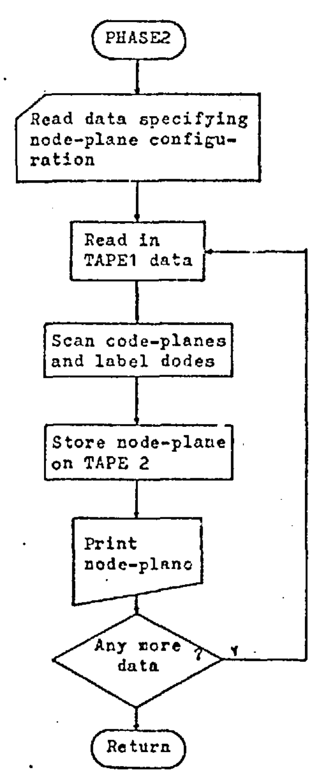

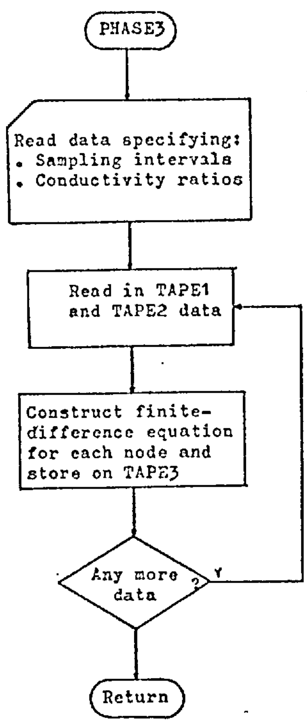
PHASE3
Read data specifying:
• Sampling intervals
• Conductivity ratios
Read in TAPE1 and TAPE2 data
Construct finite-difference equation for each node and store on TAPE3
Any more data ?
Y
Return

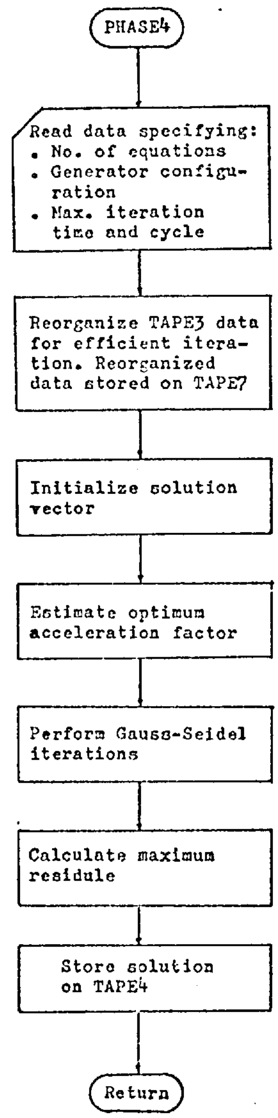
PHASE4
Read data specifying:
• No. of equations
• Generator configuration
• Max. iteration time and cycle
Reorganize TAPE3 data for efficient iteration. Reorganized data stored on TAPE7
Initialize solution vector
Estimate optimum acceleration factor
Perform Gauss-Seidel iterations
Calculate maximum residule
Store solution on TAPE4
Return

A.2 Program Listings

```
      PROGRAM FINITE(INPUT,OUTPUT,TAPE1,TAPE2,TAPE3,TAPE4,TAPE5,TAPE6)
C
C
C  PROGRAM FINITE COMPUTEDS THE ELECTRICAL POTENTIAL DISTRIBUTION
C  IN A VOLUME-CONDUCTOR USING THE METHOD OF FINITE-DIFFERENCES.
C  THE PROGRAM IS ORGANIZED INTO 5 PHASES OF OPERATIONS:
C
C  PHASE1  READS AND UNPACK THE COMPRESSED INPUT DATA INTO CODED
C          CROSS-SECTION IMAGES OF THE DISCRETE CONDUCTOR.
C  PHASE2  SCANS THE DATA ON TAPE1 AND GENERATES THE FINITE-
C          DIFFERENCE NODES FOR THE CONDUCTOR
C  PHASE3  GENERATES THE SET OF FINITE-DIFFERENCE EQUATIONS
C          FROM THE DATA ON TAPE1 AND TAPE2.
C  PHASE4  CALCULATES THE POTENTIAL DISTRIBUTIONS BY SOLVING
C          THE SET OF EQUATIONS ITERATIVELY USING THE GAUSS-
C          SEIDEL METHOD. THE SOLUTIONS ARE STORED ON TAPE6.
C
C  THE EXECUTION SEQUENCE OF THE PROGRAM IS DEFINED BY A
C  DATA CARD.
C  EXAMPLE:
C          TO EXECUTE PHASE1 AND PHASE2 ONLY, THEN
C  PHASE1,PHASE2
C          IF TAPE1 AND TAPE2 DATA ARE ALREADY AVAILABLE
C  PHASE3,PHASE4
C
C  INPUT FORMAT OF THE COMMAND CARD IS  10(I6,1X)
C
C
      DIMENSION KOMAND(10),NAME(5)
      DATA NAME/'PHASE1','PHASE2','PHASE3','PHASE4','      '/
C
C  FORMAT STATEMENTS
C
 1000 FORMAT(10(A6,1X))
 3000 FORMAT('   ILLEGAL COMMAND IN COLUMN ',I2)
 3010 FORMAT(///'      *****  RUN COMPLETED  *****'//)
C
C
      READ(5,1000) (KOMAND(I),I=1,10)
      IND=0
    1 IND=IND+1
      DO 2 I=1,5
      K=I
      IF(KOMAND(IND).EQ.NAME(I))GO TO 3
    2 CONTINUE
      PRINT 3000,IND
      GO TO 1
    3 GO TO (10,20,30,40,50),K
   10 CALL PHASE1
      GO TO 1
   20 CALL PHASE2
      GO TO 1
   30 CALL PHASE3
      GO TO 1
   40 CALL PHASE4
      GO TO 1
   50 PRINT3010
      STOP
      END
```

```
      SUBROUTINE PHASE1
C
C   PHASE1 READS AND UNPACKS THE COMPRESSED FORM OF CODED IMAGES
C   AND STORES THE DATA ON TAPE1
C     NSLAB  SPECIFIES THE NUMBER OF SLABS
C     IBIT   SPECIFIES THE Y-DIMENSION OF THE GRID
C     JBIT   SPECIFIES THE X -DIMENSION OF THE GRID
C     NUM    ARRAY CONTAINING THE NUMBER OF CODINGS IN EACH SEQUENCE
C     KODE   ARRAY CONTAINING THE CODINGS IN EACH OF THE SEQUENCE
C     IP     SUPPESS LISTING OF TAPE1 DATA IF IP=0
C
C   ARRAY DIMENSIONS
C          ARRAY NAME                  DIMENSION
C            IC                 NO. OF CARD COLUMNS
C            IB                 NO. OF CARD COLUMNS
C            NUM                MAX. NO. OF CODE SEQUENCES IN A ROW
C            KODE               MAX. NO. OF CODE SEQUENCES IN A ROW
C
      COMMON IC(80),IB(80),NUM(20),KODE(20)
      DATA IB/80*' '/
C
C   FORMAT STATEMENTS
C
 1000 FORMAT(3I5)
 1010 FORMAT(20(I2,A1))
 1020 FORMAT(80A1)
 1030 FORMAT(///'      SLAB NUMBER  ',I5/)
 1050 FORMAT(///'  NSLAB =',I5,'   IBIT =',I5,'   JBIT =',I5)
 3000 FORMAT(///'      *****  EXECUTE PHASE1  *****'//)
 3010 FORMAT(' NSLAB =',I3,'  IBIT =',I3,'  JBIT =',I3)
 3020 FORMAT(///'      *****  END PHASE1  *****'//)
C
C   READ IN PARAMETERS SPECIFYING THE NO. OF SLABS AND THE GRID
C   DIMENSIONS
C
      PRINT 3000
      REWIND 1
      READ(5,1000)NSLAB,IBIT,JBIT
      WRITE(1,1000)NSLAB,IBIT,JBIT
      PRINT 3010,NSLAB,IBIT,JBIT
C
C   BEGIN LOOP TO READ IN CODED DATA
C
      DO 30 NS=1,NSLAB
      DO 30 I=1,IBIT
      DO 5 J=1,JBIT
    5 IC(J)=IB(J)
      READ(5,1010) (NUM(J),KODE(J),J=1,20)
C
C   UNPACK DATA
C
      KK=0
      DO 10 K=1,20
      L=NUM(K)
      IF(L.LE.0)GO TO 20
      DO 10 KL=1,L
      KK=KK+1
      IC(KK)=KODE(K)
   10 CONTINUE
C
C   WRITE UNPACKED DATA ONTO TAPE1
C
   20 WRITE(1,1020) (IC(J),J=1,JBIT)
   30 CONTINUE
C
C   LIST TAPE1 DATA
C
      READ(5,1000)IP
      IF(IP.EQ.0)GO TO 50
      REWIND 1
      READ(1,1000)NSLAB,IBIT,JBIT
      DO 40 NS=1,NSLAB
      PRINT 1030,NS
      DO 40 I=1,IBIT
      READ(1,1020) (IC(J),J=1,JBIT)
      PRINT 1020,(IC(J),J=1,JBIT)
   40 CONTINUE
   50 PRINT 3020
      RETURN
      END
```

```
      SUBROUTINE PHASE2
C
C
C   PHASE2 SCANS THROUGH THE CODED IMAGE OF THE TORSO AND NUMBER
C   THOSE NODES THAT BELONG IN THE FIELD.
C   THE INPUT DATA ARE ON TAPE1.
C   THE NODE NUMBERS AND THEIR POSITION IN THE FIELD ARE STORED
C   ON TAPE2.
C     NONO     NO. OF CODINGS FOR WHICH NO NODES ARE TO BE GENERATED
C     NENO     NO. OF CODINGS FOR WHICH NODES ARE PREFIXED BY -VE SIGN
C     NO       ARRAY CONTAINING THE CODINGS FOR NO NODE GENERATION
C     NE       ARRAY CONTAINING THE CODINGS FOR -VE NODES
C     IP       SUPPRESS LISTING OF NODE PLANES IF IP=0
C   ARRAY DIMENSIONS
C          ARRAY NAME                    DIMENSION
C            IC1                         (IBIT,JBIT)
C            IC2                         (IBIT,JBIT)
C            N                         (IBIT-1,JBIT-1)
C            M                             (IBIT-1)
C            MM                            (IBIT-1)
C            NO                             (NONO)
C            NE                             (NENO)
C
C
C
C
      COMMON IC1(22,34),IC2(22,34),N(21,33),M(21),MM(21),NO(4),NE(4)
      DATA IB/' '/
C
C   FORMAT STATEMENTS
C
 1000 FORMAT(16I5)
 1010 FORMAT(40(A1,1X))
 1020 FORMAT(80A1)
 2000 FORMAT(20I4)
 2010 FORMAT('  TOTAL NO. OF NODES = ',I5)
 2020 FORMAT(//)
 3000 FORMAT(///'       *****  EXECUTE PHASE2  *****'//)
 3010 FORMAT('  NONO =',I3,'  NENO =',I3)
 3020 FORMAT('  NO(I) =',4(1X,A1))
 3030 FORMAT('  NE(I) =',4(1X,A1))
 3040 FORMAT(///'       *****  END PHASE2  *****'//)
C
C   READ IN DATA
C
      PRINT 3000
      REWIND 1
      REWIND 2
      REWIND 7
      READ(1,1000)NSLAB,IBIT,JBIT
      READ(5,1000)NONO,NENO
      PRINT 3010,NONO,NENO
      IF(NONO.EQ.0)GO TO 1
      READ(5,1010) (NO(I),I=1,NONO)
      PRINT 3020,(NO(I),I=1,NONO)
    1 IF(NENO.EQ.0)GO TO 2
      READ(5,1010) (NE(I),I=1,NENO)
      PRINT 3030,(NE(I),I=1,NENO)
    2 READ(5,1000)IP
C
C   INITIALIZE VALUES
C
      II=IBIT-1
      JJ=JBIT-1
      NOW=0
      NSL=NSLAB+1
      DO 10 I=1,IBIT
      DO 10 J=1,JBIT
   10 IC2(I,J)=IB
C
C   BEGIN LOOP TO GENERATE NODE PLANE
C
      DO 180 NS=1,NSL
      DO 20 I=1,IBIT
      DO 20 J=1,JBIT
   20 IC1(I,J)=IC2(I,J)
      IF(NS.NE.NSL)GO TO 40
      DO 30 I=1,IBIT
      DO 30 J=1,JBIT
   30 IC2(I,J)=IB
      GO TO 60
C
C   READ IN ONE SLAB OF CODED SECTION
C
   40 DO 50 I=1,IBIT
   50 READ(1,1020) (IC2(I,J),J=1,JBIT)
   60 DO 130 I=1,II
      DO 130 J=1,JJ
      M(1)=IC1(I,J)
      M(2)=IC1(I,J+1)
      M(3)=IC1(I+1,J)
      M(4)=IC1(I+1,J+1)
      M(5)=IC2(I,J)
      M(6)=IC2(I,J+1)
      M(7)=IC2(I+1,J)
      M(8)=IC2(I+1,J+1)
C
C   CHECK IF NODE TO BE GENERATED
C
      IF(NONO.EQ.0)GO TO 90
      DO 80 K=1,8
      DO 70 KK=1,NONO
      IF(M(K).EQ.NO(KK))GO TO 80
   70 CONTINUE
      GO TO 90
   80 CONTINUE
      N(I,J)=0
      GO TO 130
   90 NOW=NOW+1
```

```
C
C  CHECK IF NODE TO BE ASSIGNED -VE
C
      IF(NEND.EQ.0)GO TO 110
      DO 100 K=1,8
      DO 100 KK=1,NEND
      IF(M(K).EQ.NE(KK))GO TO 120
  100 CONTINUE
  110 N(I,J)=NOW
      GO TO 130
  120 N(I,J)=-NOW
  130 CONTINUE
C
C  WRITE NODE-PLANE ONTO TAPE2
C
      WRITE(2,1000)((N(I,J),J=1,JJ),I=1,II)
C
C  LIST NODE PLANES
C
      IF(IP.EQ.0)GO TO 180
      PRINT 2020
      DO 170 J=1,JJ
      DO 140 I=1,II
  140 M(I)=N(IBIT-I,J)
      DO 150 I=1,II
  150 MM(I)=M(I)/1000
      PRINT 2000,(MM(I),I=1,II)
      DO 160 I=1,II
      M(I)=IABS(M(I))
  160 MM(I)=MOD(M(I),1000)
      PRINT 2000,(MM(I),I=1,II)
  170 CONTINUE
  180 CONTINUE
      PRINT 2010,NOW
      PRINT 3040
      RETURN
      END
```

```
      SUBROUTINE PHASE3
C
C  PHASE4 COMPUTES THE MATRIX OF FINITE-DIFFERENCE COEFFICIENTS
C  AND STORES THE COEFFICIENTS ON TAPE4.
C
C    STN     ARRAY CONTAINING THE RATIOS OF SLAB THICKNESSES
C    STI     ARRAY CONTAINING THE RATIOS OF GRID INTERVALIN
C              THE Y-DIRECTION
C    STJ     ARRAY CONTAINING THE RATIOS OF GRID INTERVAL IN
C              THE X-DIRECTION
C    NCODE   NO.OF CODINGS USED IN THE DIGITIZATION
C    ICODE   ARRAY CONTAINING ALL CODINGS USED IN THE DISCRETE
C              CONDUCTOR
C    SEG     ARRAY CONTAINING THE CONDUCTIVITY RATIOS OF THE CODINGS
C  ARRAY DIMENSIONS
C          ARRAY NAME               DIMENSION
C             STN                   (NSLAB+2)
C             STI                   (IBIT)
C             STJ                   (JBIT)
C             SEG                   (NCODE+1,5)
C             ICODE                 (NCODE)
C             IC1,IC2               (IBIT,JBIT)
C             N1,N2,N3              (IBIT-1,JBIT-1)
C             ACOEF,ICOEF           (6)
C
      COMMON STN(19),STI(22),STJ(34),SEG(15,5),ICODE(15)
      COMMON IC1(22,34),IC2(22,34),N1(21,33),N2(21,33),N3(21,33)
      COMMON ACOEF(6),ICOEF(6)
C
C  FORMAT STATEMENTS
C
 1000 FORMAT(16I5)
 1010 FORMAT(20F4.1)
 1020 FORMAT(A1,4X,5F5.2)
 1030 FORMAT(80A1)
 1040 FORMAT(I5,6(I5,F7.3))
 3000 FORMAT(///'        ***** EXECUTE PHASE3  *****'//)
 3010 FORMAT('  RATIO OF STEP SIZES IN Z-DIRECTION')
 3020 FORMAT('  RATIO OF STEP SIZES IN Y-DIRECTION')
 3030 FORMAT('  RATIO OF STEP SIZES IN X-DIRECTION')
 3040 FORMAT('  NCODE =',I3)
 3050 FORMAT('  CODINGS      CONDUCTIVITY RATIOS')
 3060 FORMAT(5X,A1,5X,5(1X,F5.2))
 3070 FORMAT(///'        ***** END PHASE3  *****'//)
C
      PRINT 3000
      REWIND 1
      REWIND 2
      REWIND 3
C
C  READ IN DATA
C
      READ(1,1000)NSLAB,IBIT,JBIT
      NSL=NSLAB+1
```

```
      IIB=IBIT-1
      JJB=JBIT-1
      READ(5,1010) (STN(I),I=2,NSL)
      PRINT 3010
      PRINT 1010,(STN(I),I=2,NSL)
      READ(5,1010) (STI(I),I=1,IBIT)
      PRINT 3020
      PRINT 1010,(STI(I),I=1,IBIT)
      READ(5,1010) (STJ(I),I=1,JBIT)
      PRINT 3030
      PRINT 1010,(STJ(I),I=1,JBIT)
      STN(1)=1.
      STN(NSL+1)=1.
      READ(5,1000)NCODE
      PRINT 3040,NCODE
      PRINT 3050
      DO 20 K=1,NCODE
      READ(5,1020) ICODE(K),(SEG(K+1,I),I=1,5)
      IF(SEG(K+1,2).GT.0.)GO TO 20
      DO 10 I=2,5
   10 SEG(K+1,I)=SEG(K+1,1)
      PRINT 3060,ICODE(K),(SEG(K+1,I),I=1,5)
   20 CONTINUE
      DO 30 I=1,5
   30 SEG(1,I)=0.
      DO 40 I=1,IBIT
      DO 40 J=1,JBIT
   40 IC2(I,J)=1
      DO 50 I=1,IIB
      DO 50 J=1,JJB
   50 N2(I,J)=0
      READ(2,1000) ((N3(I,J),J=1,JJB),I=1,IIB)
C
C  BEGIN LOOP TO SCAN FOR NODES
C
      DO 190 IS=1,NSL
      DO 60 I=1,IBIT
      DO 60 J=1,JBIT
   60 IC1(I,J)=IC2(I,J)
      DO 70 I=1,IIB
      DO 70 J=1,JJB
      N1(I,J)=N2(I,J)
   70 N2(I,J)=N3(I,J)
      IF(IS.NE.NSL)GO TO 100
      DO 80 I=1,IIB
      DO 80 J=1,JJB
   80 N3(I,J)=0
      DO 90 I=1,IBIT
      DO 90 J=1,JBIT
   90 IC2(I,J)=1
      GO TO 140
C
C  READ IN TAPE1 AND TAPE2 DATA
C
  100 READ(2,1000) ((N3(I,J),J=1,JJB),I=1,IIB)
      DO 110 I=1,IBIT
  110 READ(1,1030) (IC2(I,J),J=1,JBIT)
C
C  CONVERT CODINGS INTO CONDUCTIVITY ADDRESSES
C
      DO 130 I=1,IBIT
      DO 130 J=1,JBIT
      DO 120 K=1,NCODE
      IF(IC2(I,J).NE.ICODE(K))GO TO 120
      IC2(I,J)=K+1
      GO TO 130
  120 CONTINUE
  130 CONTINUE
  140 DO 180 I=1,IIB
      DO 180 J=1,JJB
      IF(N2(I,J).EQ.0)GO TO 180
      N2(I,J)=IABS(N2(I,J))
      KOUNT=0
      INODE=N2(I,J)
C
C  COMPUTE THE FINITE-DIFFERENCE COEFFICIENTS
C
      CALL EQ(I,J,IS,KOUNT,IIB,JJB)
      WRITE(3,1040) INODE,(ICOEF(K),ACOEF(K),K=1,KOUNT)
  180 CONTINUE
  190 CONTINUE
      PRINT 3070
      RETURN
      END
      SUBROUTINE EQ(I,J,L,KOUNT,IIB,JJB)
C
C  THIS SUB ROUTINE COMPUTES THE FINITE DIFFERENCE COEFFICIENTS
C
      COMMON STN(19),STI(22),STJ(34),SEG(15,5),ICODE(15)
      COMMON IC1(22,34),IC2(22,34),N1(21,33),N2(21,33),N3(21,33)
      COMMON ACOEF(6),ICOEF(6)
      DO 80 K=1,6
      GO TO (10,20,30,40,50,60),K
   10 N=N1(I,J)
      IF(N.EQ.0)GO TO 80
      II=IC1(I,J)
      JJ=IC1(I,J+1)
      KK=IC1(I+1,J+1)
      LL=IC1(I+1,J)
      SGMA=((SEG(II,5)*STJ(J)+SEG(JJ,5)*STJ(J+1))*STI(I)+
     +(SEG(KK,5)*STJ(J+1)+SEG(LL,5)*STJ(J))*STI(I+1))/STN(L)
      GO TO 70
   20 IF(I-1.LE.0)GO TO 80
      N=N2(I-1,J)
      IF(N.EQ.0)GO TO 80
      II=IC1(I,J)
      JJ=IC1(I,J+1)
      KK=IC2(I,J+1)
```

```
      LL=IC2(I,J)
      SGMA=((SEG(II,2)*STJ(J)+SEG(JJ,4)*STJ(J+1))*STN(L)+
     +(SEG(KK,4)*STJ(J+1)+SEG(LL,2)*STJ(J))*STN(L+1))/STI(I)
      GO TO 70
   30 IF(J-1.LE.0)GO TO 80
      N=N2(I,J-1)
      IF(N.EQ.0)GO TO 80
      II=IC1(I+1,J)
      JJ=IC1(I,J)
      KK=IC2(I,J)
      LL=IC2(I+1,J)
      SGMA=((SEG(II,1)*STI(I+1)+SEG(JJ,3)*STI(I))*STN(L)+
     +(SEG(KK,3)*STI(I)+SEG(LL,1)*STI(I+1))*STN(L+1))/STJ(J)
      GO TO 70
   40 IF(J+1.GT.JJB)GO TO 80
      N=N2(I,J+1)
      IF(N.EQ.0)GO TO 80
      II=IC1(I+1,J+1)
      JJ=IC1(I,J+1)
      KK=IC2(I,J+1)
      LL=IC2(I+1,J+1)
      SGMA=((SEG(II,1)*STI(I+1)+SEG(JJ,3)*STI(I))*STN(L)+
     +(SEG(KK,3)*STI(I)+SEG(LL,1)*STI(I+1))*STN(L+1))/STJ(J+1)
      GO TO 70
   50 IF(I+1.GT.IIB)GO TO 80
      N=N2(I+1,J)
      IF(N.EQ.0)GO TO 80
      II=IC1(I+1,J)
      JJ=IC1(I+1,J+1)
      KK=IC2(I+1,J+1)
      LL=IC2(I+1,J)
      SGMA=((SEG(II,2)*STJ(J)+SEG(JJ,4)*STJ(J+1))*STN(L)+
     +(SEG(KK,4)*STJ(J+1)+SEG(LL,2)*STJ(J))*STN(L+1))/STI(I+1)
      GO TO 70
   60 N=N3(I,J)
      IF(N.EQ.0)GO TO 80
      II=IC2(I,J)
      JJ=IC2(I,J+1)
      KK=IC2(I+1,J+1)
      LL=IC2(I+1,J)
      SGMA=((SEG(II,5)*STJ(J)+SEG(JJ,5)*STJ(J+1))*STI(I)+
     +(SEG(KK,5)*STJ(J+1)+SEG(LL,5)*STJ(J))*STI(I+1))/STN(L+1)
   70 KOUNT=KOUNT+1
      ACOEF(KOUNT)=SGMA
      ICOEF(KOUNT)=IABS(N)
   80 CONTINUE
      RETURN
      END
```

```
      SUBROUTINE PHASE4
C
C  PHASE4 COMPUTES THE POTENTIAL DISTRIBUTIONS BY SOLVING
C  THE FINITE-DIFFERENCE EQUATIONS ON TAPE3 ITERATIVELY
C  USING THE GAUSS-SEIDEL METHOD.
C    NEQN     NO. OF EQUATIONS IN TAPE3
C    NGEN     NO. OF GENERATORS
C    NOD      ARRAY CONTAINING THE NO. OF NODES IN THE GENERATORS
C    NODE     ARRAY CONTAINING THE NODE NUMBERS OF GENERATORS
C    ISOCE    ARRAY CONTAINING THE MAGNITUDES OF THE GENERATORS
C    ITIME    MAXIMUM ITERATION TIME IN SECONDS
C    ITMAX    MAXIMUM NO. OF ITERATIONS
C    IFILE    READ INITIAL SOLUTION VECTOR FROM TAPE4 IF IFILE=1
C  ARRAY DIMENSIONS
C         ARRAY NAME             DIMENSION
C         ACOEF,ICOEF             (6,MBUFF)
C         INODE,ICONT             (MBUFF)
C         ACO,ICO                 (6)
C         NOD,ISOCE               (NGEN)
C         X                       (NEQN)
C
      COMMON ACOEF(6,100),ICOEF(6,100),INODE(100),ICONT(100)
      COMMON ACO(6),ICO(6),NOD(26),ISOCE(26),NODE(200)
      COMMON X(10000)
C
C  FORMAT STATEMENTS
C
 1000 FORMAT(16I5)
 1010 FORMAT(I5,6(I5,F7.3))
 1030 FORMAT(10F8.3)
 3000 FORMAT(///'      *****  EXECUTE PHASE4  *****'//)
 3010 FORMAT('  NEQN =',I3)
 3020 FORMAT('  NGEN =',I3)
 3030 FORMAT('  MAGNITUDES OF GENERATORS:')
 3040 FORMAT('  ITIME =',I5,'  ITMAX =',I5)
 3050 FORMAT('  MAXIMUM RESIDULE =',E10.3)
 3060 FORMAT('  NODE NUMBERS OF GENERATORS:')
 3070 FORMAT(///'      *****  END PHASE4  *****'//)
C
      PRINT 3000
      CALL SECOND(T1)
      REWIND 3
      REWIND 4
      REWIND 7
C
C INITIALIZE VALUES
C
      MBUFF=100
      NUM=0
      M=0
      KF=1
C
C  READ IN DATA SPECIFYING GENERATOR CONFIGURATION
C
```

```
      READ(5,1000)NEQN
      PRINT 3010,NEQN
      READ(5,1000)NGEN
      PRINT 3020,NGEN
      PRINT 3060
      DO 1 N=1,NGEN
      READ(5,1000)NOD(N)
      PRINT 1000,NOD(N)
      KL=NOD(N)+KF-1
      READ(5,1000)(NODE(I),I=KF,KL)
      PRINT 1000,(NODE(I),I=KF,KL)
      KF=KL+1
    1 CONTINUE
      READ(5,1000)(ISOCE(I),I=1,NGEN)
      PRINT 3030
      PRINT 1000,(ISOCE(I),I=1,NGEN)
C
C  READ IN DATA SPECIFYING MAX. ITERATION TIME AND CYCLE
C
      READ(5,1000)ITIME,ITMAX
      PRINT 3040,ITIME,ITMAX
C
C  REORGANIZE EQUATIONS ON TAPE3 FOR EFFICIENT ITERATION
C
      DO 100 NE=1,NEQN
      READ(3,1010)IND,(ICO(I),ACO(I),I=1,6)
C
C  REMOVE EQUATIONS FOR NODES BELONGING TO GENERATORS
C
      DO 10 K=1,KL
   10 IF(IND.EQ.NODE(K))GO TO 100
C
C  COMPUTE NO. OF COEFFICIENTS IN EQUATION
C
      KOUNT=0
      DO 20 I=1,6
   20 IF(ICO(I).NE.0)KOUNT=KOUNT+1
      M=M+1
      INODE(M)=IND
      ICONT(M)=KOUNT
C
C  NORMALIZE COEFFICIENTS
C
      SUM=0.
      DO 30 I=1,KOUNT
   30 SUM=SUM+ACO(I)
      IF(ABS(SUM).LT.1.E-20)GO TO 50
      DO 40 I=1,KOUNT
   40 ACO(I)=ACO(I)/SUM
   50 DO 60 I=1,KOUNT
      ICOEF(I,M)=ICO(I)
   60 ACOEF(I,M)=ACO(I)
C
C  WRITE INTO A BUFFER ARRAY
C  IF BUFFER FULL DUMP INTO TAPE7
C
      IF(M.NE.MBUFF)GO TO 100
      WRITE(7)INODE,ICONT,ICOEF,ACOEF
      NUM=NUM+M
      M=0
  100 CONTINUE
      WRITE(7)INODE,ICONT,ICOEF,ACOEF
      NUM=NUM+M
C
C  INITIALIZE SOLUTION VECTOR
C
      IF(IFILE.NE.1)GO TO 105
      READ(4,1000)NEQM
      READ(4,1030)(X(I),I=1,NEQM)
      GO TO 115
  105 DO 110 I=1,NEQN
  110 X(I)=0.
      K=0
  115 DO 120 N=1,NGEN
      KK=NOD(N)
      DO 120 N1=1,KK
      K=K+1
  120 X(NODE(K))=FLOAT(ISOCE(N))
C
C  BEGIN ITERATIONS
C  COMPUTE OPTIMUM ACCELERATION FACTOR
C
      IT=ITMAX/10
      DO 200 ITER=1,IT
  150 REWIND 7
      XXX=0.
      NT=0
      MB=MBUFF
  160 READ(7)INODE,ICONT,ICOEF,ACOEF
      NT=NT+MBUFF
      IF(NT.GT.NUM)MB=NUM+MBUFF-NT
      DO 180 JK=1,MB
      IFL=INODE(JK)
      KKK=ICONT(JK)
      XX=X(IFL)
      X(IFL)=0.
      DO 170 K=1,KKK
      J=ICOEF(K,JK)
      X(IFL)=X(IFL)+ACOEF(K,JK)*X(J)
  170 CONTINUE
      IF(ABS(XX-X(IFL)).GT.XXX)XXX=ABS(XX-X(IFL))
  180 CONTINUE
      IF(NT.LT.NUM)GO TO 160
      IF(ITER.NE.IT)GO TO 200
      R=XXX/XX1
      IF(R.LT.1.)GO TO 190
      ACC=1.
      GO TO 200
```

```
  190 ACC=2./(1.+SQRT(1.-R))
  200 XX1=XXX
C
C  ACCELERATED GAUSS-SEIDEL ITERATIONS
C
      ITMAX=ITMAX-IT
      DO 250 ITER=1,ITMAX
      PRINT,ITER
  210 REWIND 7
      NT=0
      MB=MBUFF
  220 READ(7)INODE,ICONT,ICOEF,ACOEF
      NT=NT+MBUFF
      IF(NT.GT.NUM)MB=NUM+MBUFF-NT
      DO 240 JK=1,MB
      IFL=INODE(JK)
      KKK=ICONT(JK)
      XX=X(IFL)
      X(IFL)=0.
      DO 230 K=1,KKK
      J=ICOEF(K,JK)
      X(IFL)=X(IFL)+ACOEF(K,JK)*X(J)
  230 CONTINUE
      X(IFL)=XX+ACC*(X(IFL)-XX)
  240 CONTINUE
      IF(NT.LT.NUM)GO TO 220
      CALL SECOND(T2)
      IF(T2-T1.GE.FLOAT(ITIME))GO TO 260
  250 CONTINUE
C
C  COMPUTE MAXIMUM RESIDULE
C
  260 REWIND 7
      XXX=0.
      NT=0
      MB=MBUFF
  270 READ(7)INODE,ICONT,ICOEF,ACOEF
      NT=NT+MBUFF
      IF(NT.GT.NUM)MB=NUM+MBUFF-NT
      DO 290 JK=1,MB
      IFL=INODE(JK)
      KKK=ICONT(JK)
      XX=0.
      A=0.
      DO 280 K=1,KKK
      A=A+ACOEF(K,JK)
      J=ICOEF(K,JK)
      XX=XX+ACOEF(K,JK)*X(J)
  280 CONTINUE
      XX=X(IFL)*A-XX
      IF(XXX.LT.ABS(XX))XXX=ABS(XX)
  290 CONTINUE
      IF(NT.LT.NUM)GO TO 270
C
```

```
C  END OF ITERATIONS
      PRINT 3050,XXX
C  STORE SOLUTION VECTOR ON TAPE4
C
      WRITE(4,1000)NEQN
      WRITE(4,1030)(X(I),I=1,NEQN)
  300 PRINT 3000
      RETURN
      END
```

A.3 Variable Name List

	VARIABLE NAME	DESCRIPTION
Program control	KOMAND	Array containing execution sequence.
PHASE1	NSLAB	Number of slabs.
	IBIT	Y-dimension of sampling grid.
	JBIT	X-dimension of sampling grid.
	NUM	Array of number of times a coding is repeated.
	KODE	Array containing the coding sequence.
	IP	Output listings suppression indicator.
PHASE2	NONO	No. of codings for which no equations are generated.
	NENO	No. of codings for which the nodes are labelled with a negative sign to facilitate identification of specific regions.
	NO	Array containing codings for no equations.
	NE	Array containing codings for -ve nodes.
	IP	Output listings suppression indicator
PHASE3	STN	Array of sampling ratios in the Z-direction.
	STI	Array of sampling ratios in the Y-direction.
	STJ	Array of sampling ratios in the X-direction.
	NCODE	Number of codings used.
	ICODE	Array containing the codings used.
	SEG	Array of conductivity ratios of the codings.
PHASE4	NEQN	Number of equations generated. This is specified from the output of PHASE2.
	NGEN	Number of generators. Each generator is made up of one or more nodes.
	NOD	Array containing the number of nodes for each generator.
	NODE	Array containing the node numbers which constitute the generators.

	ISOCE	Array containing the generator strengths.
	ITIME	Maximum iteration time in seconds.
PHASE4	ITMAX	Maximum iteration cycle.
	IFILE	Indicator to read in the initial solution vector from previous TAPE4.

A.4 Data Format

	CARD STRUCTURE	FORMAT
Program control	KOMAND(1),KOMAND(2),..... KOMAND(10)	10(A6,1X)
PHASE1	NSLAB,IBIT,JBIT	3I5
	NUM(1),KODE(1),..... NUM(20),KODE(20)	20(I2,A1)
	⋮ (NSLAB x IBIT) sets	⋮
	NUM(1),KODE(1),..... NUM(20),KODE(20)	
	IP	I5
PHASE2	NONO,NENO	2I5
	NO(1),NO(2),..... NO(NONO)	40(A1,1X)
	NE(1),NE(2),..... NE(NENO)	40(A1,1X)
	IP	I5
PHASE3	STN(1),STN(2),..... STN(NSLAB)	20F4.1
	STI(1),STI(2),..... STI(IBIT)	20F4.1
	STJ(1),STJ(2),..... STJ(JBIT)	20F4.1
	NCODE	I5
	ICODE,SEG(1),SEG(2),..... SEG(5)	A1,4X,5F5.2
	⋮ NCODE sets	⋮
	ICODE,SEG(1),SEG(2),..... SEG(5)	
PHASE4	NEQN	I5
	NGEN	I5
	NOD	I5
	NODE(1),NODE(2),..... NODE(NOD)	16I5
	⋮ NGEN sets	⋮
	NOD	
	NODE(1),NODE(2),..... NODE(NOD)	
	ISOCE(1),ISOCE(2),..... ISOCE(NGEN)	16I5
	ITIME,ITMAX	2I5
	IFILE	I5

A.5 Sample Problem

The following example illustrates the application of the computer program for calculating the potential distribution due to a dipole source located in the centre of a conducting sphere which is embedded inside a solid cylinder. The conductivity of the sphere is three times greater than that of the cylinder. Fig. A.1 shows the manner in which the conductor is digitized.

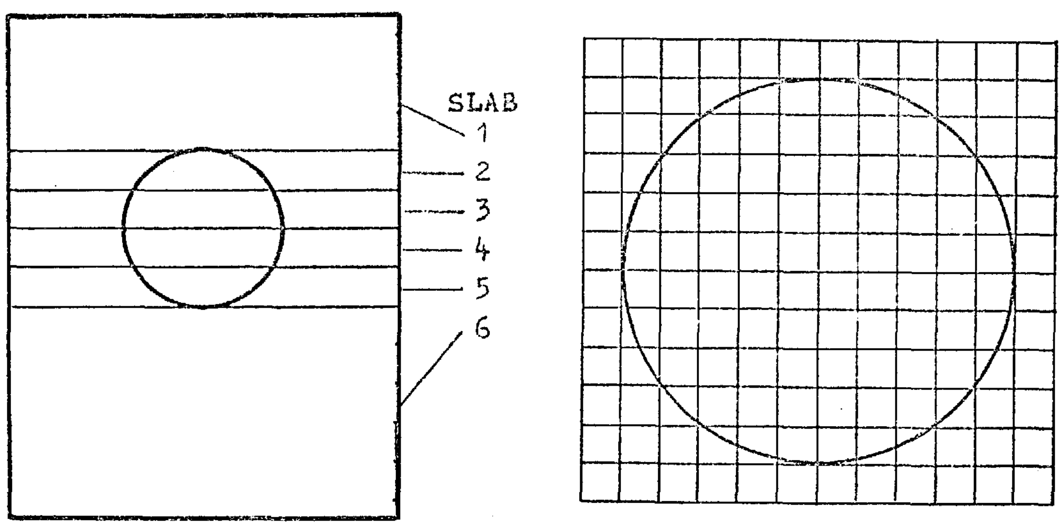

Fig.A.1: Discretization of the volume-conductor.

What follows illustrates the input data structure and outputs from the program.

```
CARD  1      PHASE1,PHASE2
CARD  2          6    12    12
CARD  3      12
CARD  4       4   4S  4
CARD  5       2   8S  2
CARD  6       2   8S  2
CARD  7       1  10S  1
CARD  8       1  10S  1
CARD  9       1  10S  1
CARD 10       1  10S  1
CARD 11       2   8S  2
CARD 12       2   8S  2
CARD 13       4   4S  4
CARD 14      12
CARD 15      12
CARD 16       4   4S  4
CARD 17       2   8S  2
CARD 18       2   8S  2
CARD 19       1  10S  1
CARD 20       1   4S  2M  4S  1
CARD 21       1   4S  2M  4S  1
CARD 22       1  10S  1
CARD 23       2   8S  2
CARD 24       2   8S  2
CARD 25       4   4S  4
CARD 26      12
CARD 27      12
CARD 28       4   4S  4
CARD 29       2   8S  2
CARD 30       2   8S  2
CARD 31       1   4S  2M  4S  1
CARD 32       1   3S  4M  3S  1
CARD 33       1   3S  4M  3S  1
CARD 34       1   4S  2M  4S  1
CARD 35       2   8S  2
CARD 36       2   8S  2
CARD 37       4   4S  4
CARD 38      12
CARD 39      12
CARD 40       4   4S  4
CARD 41       2   8S  2
CARD 42       2   8S  2
CARD 43       1   4S  2M  4S  1
CARD 44       1   3S  4M  3S  1
CARD 45       1   3S  4M  3S  1
CARD 46       1   4S  2M  4S  1
CARD 47       2   8S  2
CARD 48       2   8S  2
CARD 49       4   4S  4
CARD 50      12
CARD 51      12
CARD 52       4   4S  4
CARD 53       2   8S  2
CARD 54       2   8S  2
CARD 55       1  10S  1
CARD 56       1   4S  2M  4S  1
CARD 57       1   4S  2M  4S  1
CARD 58       1  10S  1
CARD 59       2   8S  2
CARD 60       2   8S  2
CARD 61       4   4S  4
CARD 62      12
CARD 63      12
CARD 64       4   4S  4
CARD 65       2   8S  2
CARD 66       2   8S  2
CARD 67       1  10S  1
CARD 68       1  10S  1
CARD 69       1  10S  1
CARD 70       1  10S  1
CARD 71       2   8S  2
CARD 72       2   8S  2
CARD 73       4   4S  4
CARD 74      12
CARD 75           1
CARD 76           1       1
CARD 77
CARD 78      M
CARD 79           1
```

```
          *****  EXECUTE PHASE1  *****

NSLAB =  6  IBIT = 12  JBIT = 12

      SLAB NUMBER        1

   SSSS
 SSSSSSSS
 SSSSSSSS
SSSSSSSSSS
SSSSSSSSSS
SSSSSSSSSS
SSSSSSSSSS
 SSSSSSSS
 SSSSSSSS
   SSSS

      SLAB NUMBER        2

   SSSS
 SSSSSSSS
 SSSSSSSS
SSSSSSSSSS
SSSSMMSSSS
SSSSMMSSSS
SSSSSSSSSS
 SSSSSSSS
 SSSSSSSS
   SSSS

      SLAB NUMBER        3

   SSSS
 SSSSSSSS
 SSSSSSSS
SSSSMMSSSS
SSSMMMMSSS
SSSMMMMSSS
SSSSMMSSSS
 SSSSSSSS
 SSSSSSSS
   SSSS

      SLAB NUMBER        4

   SSSS
 SSSSSSSS
 SSSSSSSS
SSSSMMSSSS
SSSMMMMSSS
SSSMMMMSSS
SSSSMMSSSS
 SSSSSSSS
 SSSSSSSS
   SSSS

      SLAB NUMBER        5

   SSSS
 SSSSSSSS
 SSSSSSSS
SSSSSSSSSS
SSSSMMSSSS
SSSSMMSSSS
SSSSSSSSSS
 SSSSSSSS
 SSSSSSSS
   SSSS
```

SLAB NUMBER 6

```
  SSSS
 SSSSSSSS
 SSSSSSSS
SSSSSSSSSS
SSSSSSSSSS
SSSSSSSSSS
SSSSSSSSSS
 SSSSSSSS
 SSSSSSSS
  SSSS
```

***** END PHASE1 *****

***** EXECUTE PHASE2 *****

NONO = 1 NENO = 1
NO(I) =
NE(I) = M

0	0	0	0	0	0	0	0	0	0	0
0	0	0	68	57	46	35	24	0	0	0
0	0	0	0	0	0	0	0	0	0	0
0	88	79	69	58	47	36	25	15	6	0
0	0	0	0	0	0	0	0	0	0	0
0	89	80	70	59	48	37	26	16	7	0
0	0	0	0	0	0	0	0	0	0	0
97	90	81	71	60	49	38	27	17	8	1
0	0	0	0	0	0	0	0	0	0	0
98	91	82	72	61	50	39	28	18	9	2
0	0	0	0	0	0	0	0	0	0	0
99	92	83	73	62	51	40	29	19	10	3
0	0	0	0	0	0	0	0	0	0	0
100	93	84	74	63	52	41	30	20	11	4
0	0	0	0	0	0	0	0	0	0	0
101	94	85	75	64	53	42	31	21	12	5
0	0	0	0	0	0	0	0	0	0	0
0	95	86	76	65	54	43	32	22	13	0
0	0	0	0	0	0	0	0	0	0	0
0	96	87	77	66	55	44	33	23	14	0
0	0	0	0	0	0	0	0	0	0	0
0	0	0	78	67	56	45	34	0	0	0

0	0	0	0	0	0	0	0	0	0	0
0	0	0	169	158	147	136	125	0	0	0
0	0	0	0	0	0	0	0	0	0	0
0	189	180	170	159	148	137	126	116	107	0
0	0	0	0	0	0	0	0	0	0	0
0	190	181	171	160	149	138	127	117	108	0
0	0	0	0	0	0	0	0	0	0	0
198	191	182	172	161	150	139	128	118	109	102
0	0	0	0	-0	-0	-0	0	0	0	0
199	192	183	173	162	151	140	129	119	110	103
0	0	0	0	-0	-0	-0	0	0	0	0
200	193	184	174	163	152	141	130	120	111	104
0	0	0	0	-0	-0	-0	0	0	0	0
201	194	185	175	164	153	142	131	121	112	105
0	0	0	0	0	0	0	0	0	0	0
202	195	186	176	165	154	143	132	122	113	106
0	0	0	0	0	0	0	0	0	0	0
0	196	187	177	166	155	144	133	123	114	0
0	0	0	0	0	0	0	0	0	0	0
0	197	188	178	167	156	145	134	124	115	0
0	0	0	0	0	0	0	0	0	0	0
0	0	0	179	168	157	146	135	0	0	0

0	0	0	0	0	0	0	0	0	0	0
0	0	0	270	259	248	237	226	0	0	0
0	0	0	0	0	0	0	0	0	0	0
0	290	281	271	260	249	238	227	217	208	0
0	0	0	0	0	0	0	0	0	0	0
0	291	282	272	261	250	239	228	218	209	0
0	0	0	0	-0	-0	-0	0	0	0	0
299	292	283	273	262	251	240	229	219	210	203
0	0	0	-0	-0	-0	-0	-0	0	0	0
300	293	284	274	263	252	241	230	220	211	204
0	0	0	-0	-0	-0	-0	-0	0	0	0
301	294	285	275	264	253	242	231	221	212	205
0	0	0	-0	-0	-0	-0	-0	0	0	0
302	295	286	276	265	254	243	232	222	213	206
0	0	0	0	-0	-0	-0	0	0	0	0
303	296	287	277	266	255	244	233	223	214	207
0	0	0	0	0	0	0	0	0	0	0
0	297	288	278	267	256	245	234	224	215	0
0	0	0	0	0	0	0	0	0	0	0
0	298	289	279	268	257	246	235	225	216	0
0	0	0	0	0	0	0	0	0	0	0
0	0	0	280	269	258	247	236	0	0	0

0	0	0	0	0	0	0	0	0	0	0
0	0	0	371	360	349	338	327	0	0	0
0	0	0	0	0	0	0	0	0	0	0
0	391	382	372	361	350	339	328	318	309	0
0	0	0	0	0	0	0	0	0	0	0
0	392	383	373	362	351	340	329	319	310	0
0	0	0	0	-0	-0	-0	0	0	0	0
400	393	384	374	363	352	341	330	320	311	304
0	0	0	-0	-0	-0	-0	-0	0	0	0
401	394	385	375	364	353	342	331	321	312	305
0	0	0	-0	-0	-0	-0	-0	0	0	0
402	395	386	376	365	354	343	332	322	313	306
0	0	0	-0	-0	-0	-0	-0	0	0	0
403	396	387	377	366	355	344	333	323	314	307
0	0	0	0	-0	-0	-0	0	0	0	0
404	397	388	378	367	356	345	334	324	315	308
0	0	0	0	0	0	0	0	0	0	0
0	398	389	379	368	357	346	335	325	316	0
0	0	0	0	0	0	0	0	0	0	0
0	399	390	380	369	358	347	336	326	317	0
0	0	0	0	0	0	0	0	0	0	0
0	0	0	381	370	359	348	337	0	0	0

0	0	0	0	0	0	0	0	0	0	0
0	0	0	472	461	450	439	428	0	0	0
0	0	0	0	0	0	0	0	0	0	0
0	492	483	473	462	451	440	429	419	410	0
0	0	0	0	0	0	0	0	0	0	0
0	493	484	474	463	452	441	430	420	411	0
0	0	0	0	-0	-0	-0	0	0	0	0
501	494	485	475	464	453	442	431	421	412	405
0	0	0	-0	-0	-0	-0	-0	0	0	0
502	495	486	476	465	454	443	432	422	413	406
0	0	0	-0	-0	-0	-0	-0	0	0	0
503	496	487	477	466	455	444	433	423	414	407
0	0	0	-0	-0	-0	-0	-0	0	0	0
504	497	488	478	467	456	445	434	424	415	408
0	0	0	0	-0	-0	-0	0	0	0	0
505	498	489	479	468	457	446	435	425	416	409
0	0	0	0	0	0	0	0	0	0	0
0	499	490	480	469	458	447	436	426	417	0
0	0	0	0	0	0	0	0	0	0	0
0	500	491	481	470	459	448	437	427	418	0
0	0	0	0	0	0	0	0	0	0	0
0	0	0	482	471	460	449	438	0	0	0

```
  0   0   0   0   0   0   0   0   0   0   0
  0   0   0 573 562 551 540 529   0   0   0
  0   0   0   0   0   0   0   0   0   0   0
  0 593 584 574 563 552 541 530 520 511   0
  0   0   0   0   0   0   0   0   0   0   0
  0 594 585 575 564 553 542 531 521 512   0
  0   0   0   0   0   0   0   0   0   0   0
602 595 586 576 565 554 543 532 522 513 506
  0   0   0   0  -0  -0  -0   0   0   0   0
603 596 587 577 566 555 544 533 523 514 507
  0   0   0   0  -0  -0  -0   0   0   0   0
604 597 588 578 567 556 545 534 524 515 508
  0   0   0   0  -0  -0  -0   0   0   0   0
605 598 589 579 568 557 546 535 525 516 509
  0   0   0   0   0   0   0   0   0   0   0
606 599 590 580 569 558 547 536 526 517 510
  0   0   0   0   0   0   0   0   0   0   0
  0 600 591 581 570 559 548 537 527 518   0
  0   0   0   0   0   0   0   0   0   0   0
  0 601 592 582 571 560 549 538 528 519   0
  0   0   0   0   0   0   0   0   0   0   0
  0   0   0 583 572 561 550 539   0   0   0


  0   0   0   0   0   0   0   0   0   0   0
  0   0   0 674 663 652 641 630   0   0   0
  0   0   0   0   0   0   0   0   0   0   0
  0 694 685 675 664 653 642 631 621 612   0
  0   0   0   0   0   0   0   0   0   0   0
  0 695 686 676 665 654 643 632 622 613   0
  0   0   0   0   0   0   0   0   0   0   0
703 696 687 677 666 655 644 633 623 614 607
  0   0   0   0   0   0   0   0   0   0   0
704 697 688 678 667 656 645 634 624 615 608
  0   0   0   0   0   0   0   0   0   0   0
705 698 689 679 668 657 646 635 625 616 609
  0   0   0   0   0   0   0   0   0   0   0
706 699 690 680 669 658 647 636 626 617 610
  0   0   0   0   0   0   0   0   0   0   0
707 700 691 681 670 659 648 637 627 618 611
  0   0   0   0   0   0   0   0   0   0   0
  0 701 692 682 671 660 649 638 628 619   0
  0   0   0   0   0   0   0   0   0   0   0
  0 702 693 683 672 661 650 639 629 620   0
  0   0   0   0   0   0   0   0   0   0   0
  0   0   0 684 673 662 651 640   0   0   0
 TOTAL NO. OF NODES =    707

      *****  END PHASE2  *****
```

```
CARD  1      PHASE3,PHASE4
CARD  2       3.5 1.0 1.0 1.0 1.0 5.5
CARD  3       1.0 1.0 1.0 1.0 1.0 1.0 1.0 1.0 1.0 1.0 1.0 1.0
CARD  4       1.0 1.0 1.0 1.0 1.0 1.0 1.0 1.0 1.0 1.0 1.0 1.0
CARD  5         3
CARD  6           0.0
CARD  7      S    1.0
CARD  8      M    3.0
CARD  9        707
CARD 10          2
CARD 11          1
CARD 12        353
CARD 13          1
CARD 14        355
CARD 15        100 -100
CARD 16         20  200
```

0	0	0	6	6	6	6	6	0	0	0
0	4	4	5	6	6	6	5	4	4	0
0	4	4	4	5	5	5	4	4	4	0
2	2	3	3	4	4	4	3	3	2	2
1	1	1	2	2	2	2	2	1	1	1
0	0	0	0	0	0	0	0	0	0	0
-1	-1	-1	-1	-2	-2	-2	-1	-1	-1	-1
-1	-2	-3	-3	-4	-4	-4	-3	-3	-2	-1
0	-3	-4	-4	-5	-5	-5	-4	-4	-3	0
0	-4	-4	-5	-5	-5	-5	-5	-4	-4	0
0	0	0	-5	-6	-6	-6	-5	0	0	0

0	0	0	10	10	11	10	10	0	0	0
0	7	8	9	11	12	11	9	8	7	0
0	6	7	10	13	15	13	10	7	6	0
3	4	6	10	17	25	17	10	6	4	3
2	2	4	9	16	29	16	9	4	2	2
0	0	0	0	0	0	0	0	0	0	0
-2	-2	-4	-9	-16	-29	-16	-9	-4	-2	-2
-3	-4	-6	-10	-17	-25	-17	-10	-6	-4	-3
0	-6	-7	-9	-13	-15	-13	-9	-7	-6	0
0	-7	-7	-9	-11	-11	-11	-9	-7	-7	0
0	0	0	-10	-10	-11	-10	-10	0	0	0

0	0	0	9	9	10	9	9	0	0	0
0	6	7	8	9	10	9	8	7	6	0
0	6	6	8	10	10	10	8	6	6	0
3	4	5	7	9	11	9	7	5	4	3
2	2	3	4	7	9	7	4	3	2	2
0	0	0	0	0	0	0	0	0	0	0
-1	-2	-3	-4	-7	-9	-7	-4	-3	-2	-1
-2	-4	-5	-7	-9	-11	-9	-7	-5	-4	-3
0	-6	-6	-8	-9	-10	-9	-8	-6	-6	0
0	-6	-7	-8	-9	-10	-9	-8	-7	-6	0
0	0	0	-9	-9	-9	-9	-9	0	0	0

0	0	0	8	9	9	9	8	0	0	0
0	6	6	8	8	9	8	8	6	6	0
0	5	6	7	8	9	8	7	6	5	0
2	3	5	6	8	9	8	6	5	3	2
1	2	2	4	6	8	6	4	2	2	1
0	0	0	0	0	0	0	0	0	0	0
-1	-2	-2	-4	-6	-7	-6	-4	-2	-2	-1
-2	-3	-4	-6	-8	-9	-9	-6	-4	-3	-2
0	-5	-6	-7	-8	-9	-8	-7	-6	-5	0
0	-6	-6	-8	-8	-9	-8	-8	-6	-6	0
0	0	0	-8	-8	-9	-8	-8	0	0	0

0	0	0	10	11	11	11	10	0	0	0
0	7	8	10	11	12	11	10	8	7	0
0	7	8	10	13	16	13	10	8	7	0
3	4	6	10	18	25	18	10	6	4	3
2	2	4	8	16	30	16	8	4	2	2
0	0	0	0	0	0	0	0	0	0	0
-2	-2	-4	-8	-16	-30	-16	-8	-4	-2	-2
-3	-4	-6	-10	-18	-25	-18	-10	-6	-4	-3
0	-6	-7	-10	-13	-16	-13	-10	-7	-6	0
0	-7	-8	-10	-11	-12	-11	-10	-8	-7	0
0	0	0	-10	-11	-11	-11	-10	0	0	0

0	0	0	3	3	3	3	3	0	0	0
0	2	2	3	3	3	3	3	2	2	0
0	2	2	2	2	3	2	2	2	2	0
1	1	1	2	2	2	2	2	1	1	1
0	0	1	1	1	1	1	1	1	0	0
0	0	0	0	0	0	0	0	0	0	0
-0	-0	-0	-0	-1	-1	-1	-0	-0	-0	-0
-0	-1	-1	-1	-2	-2	-2	-1	-1	-1	-0
0	-2	-2	-2	-2	-2	-2	-2	-2	-2	0
0	-2	-2	-2	-3	-3	-3	-2	-2	-2	0
0	0	0	-3	-3	-3	-3	-3	0	0	0

0	0	0	11	11	12	11	11	0	0	0
0	7	8	10	12	13	12	10	8	7	0
0	7	8	11	16	20	16	11	8	7	0
3	5	7	12	25	43	25	12	7	5	3
2	3	5	11	30	100	30	11	5	3	2
0	0	0	0	0	0	0	0	0	0	0
-2	-2	-5	-11	-30	-100	-30	-11	-5	-2	-2
-3	-5	-7	-12	-25	-43	-25	-12	-7	-5	-3
0	-7	-8	-11	-16	-20	-16	-11	-8	-7	0
0	-7	-8	-10	-12	-13	-12	-10	-8	-7	0
0	0	0	-10	-11	-12	-11	-10	0	0	0

APPENDIX B

TABLE OF BODY TISSUE RESISTIVITIES*

Mean resistivity in Ohm-Cm.

TISSUE	Kaufman and Johnston	Burger and van Milaan	Schwan and Kay	Burger and van Dongen	Rush Abildskov and McFee
Blood	208	160	100	160	162
Liver	506		840		700
Lung	744		1120		2100
Fat	2060	1500-5000			2500
Heart	216	965			563high 252low
Skeletal muscle		470high 230low		675high 245low	2300high 150low
Human trunk		415			463

* Table taken from Rush et al. (1963).

APPENDIX C

COMPUTER DATA OF THE DISCRETE TORSO MODELS

C.1 Data for the Irregularly Digitized Torso

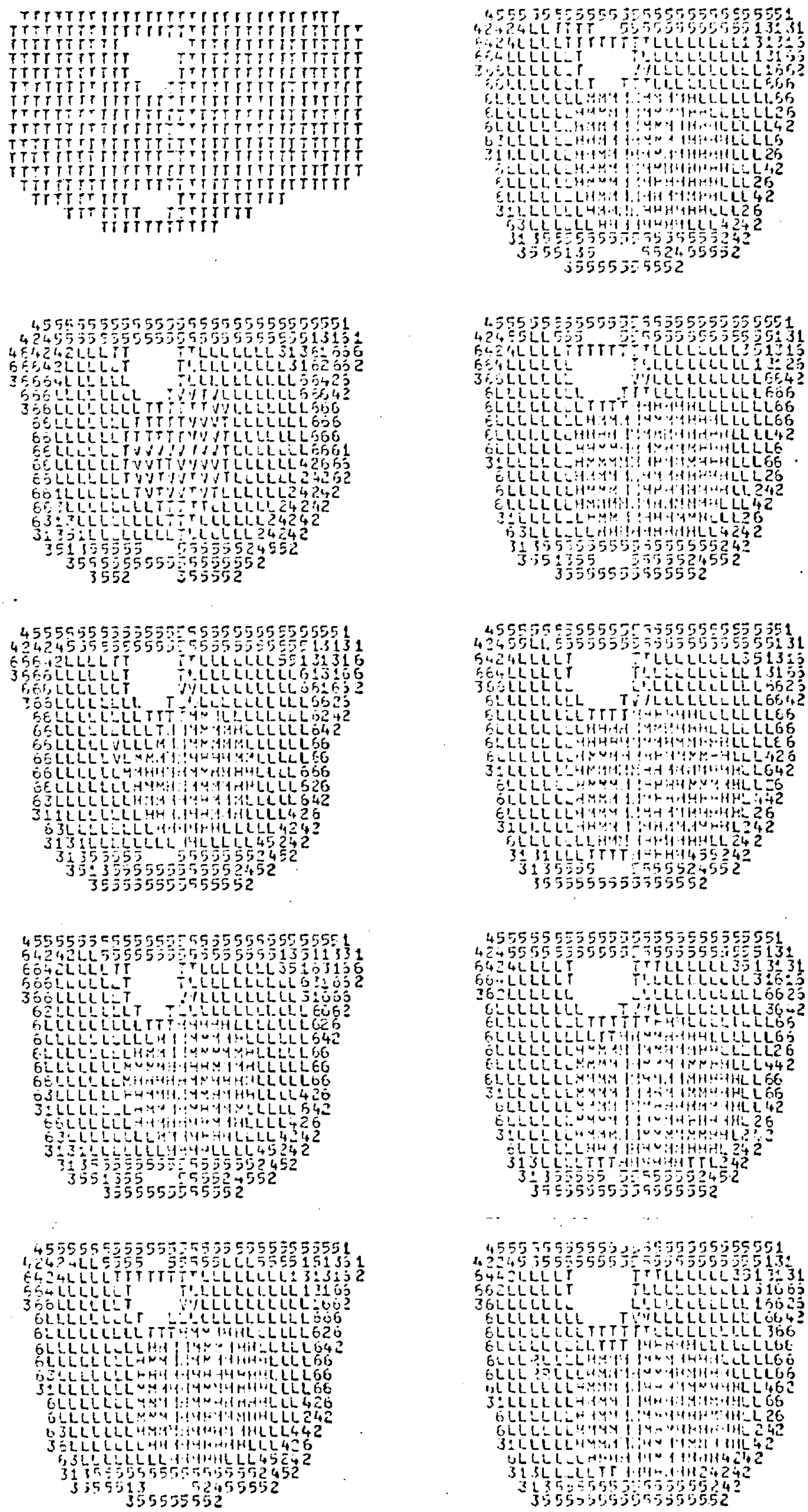

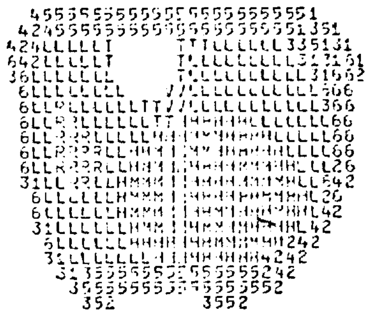

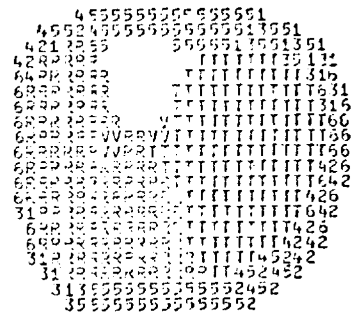

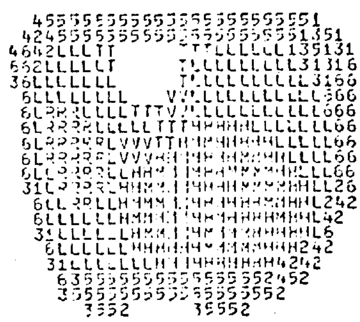

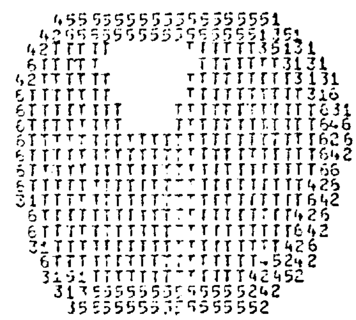

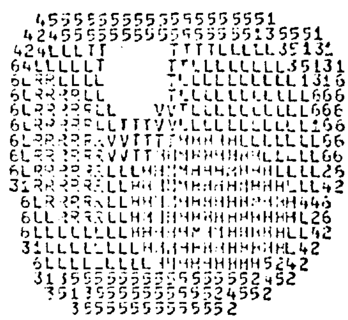

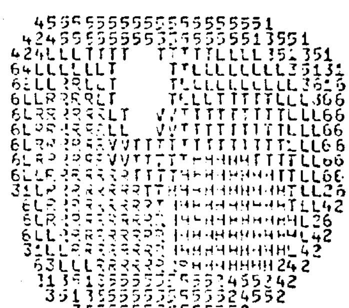

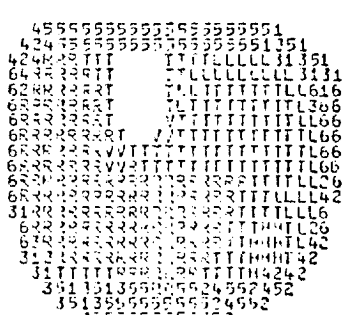

C.2 Data for Torso Digitized at One-Half Inch Grid

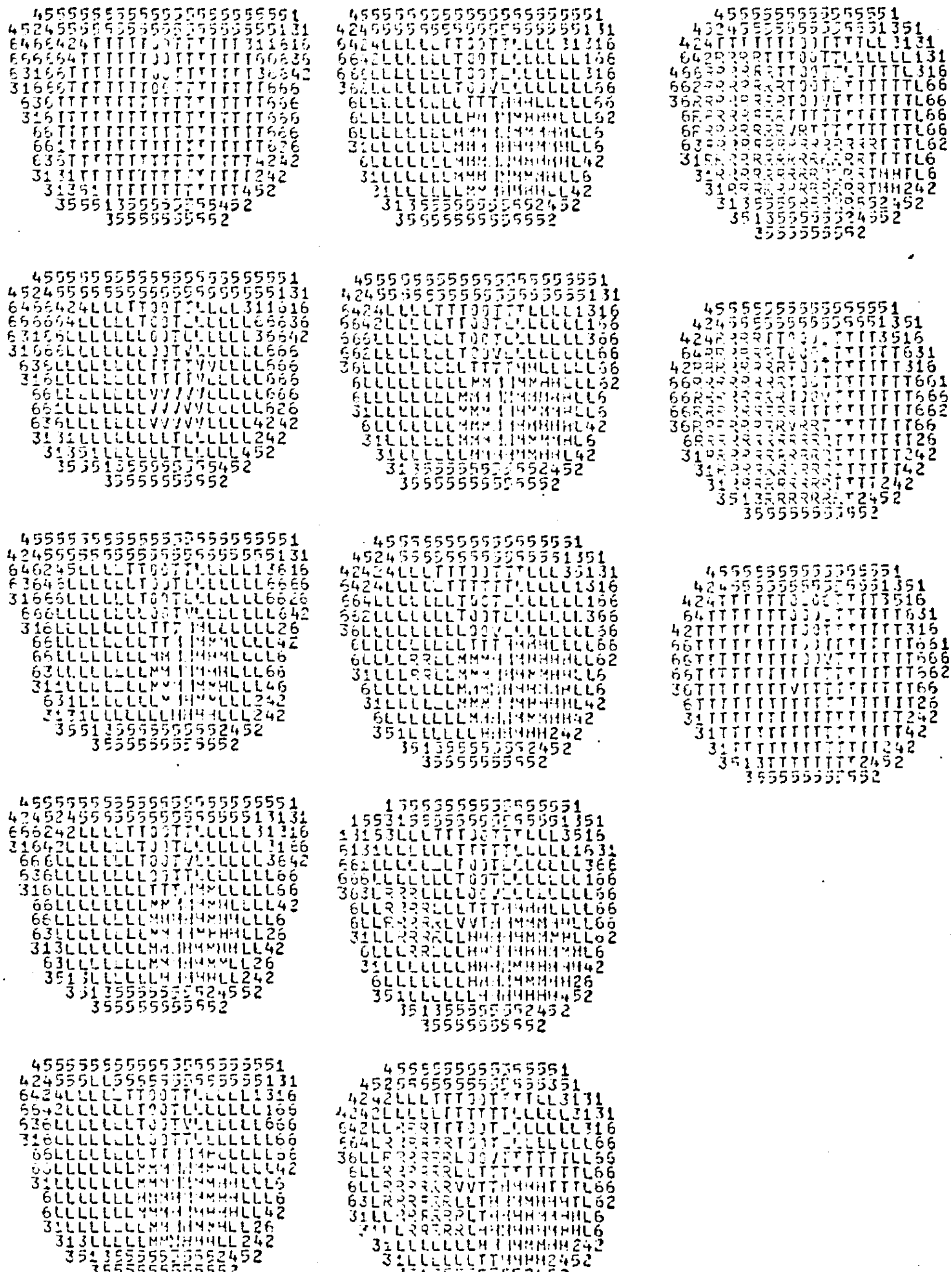

APPENDIX D

POTENTIAL CONTRIBUTIONS FROM EACH EPICARDIAL SEGMENT TO THE BODY SURFACE

SEGMENT 1

FRONT													BACK												
33	36	38	39	39	37	33	29	25	21	18	17	17	17	17	18	19	21	23	25	27	28	30	31	32	33
32	36	38	40	40	36	33	28	23	19	17	16	16	16	17	17	18	20	22	24	26	28	29	30	31	32
32	36	39	41	42	38	32	26	21	17	16	15	16	16	16	17	18	19	21	23	25	27	29	30	31	32
31	35	38	41	41	35	27	20	15	13	13	14	14	14	15	16	17	18	20	22	24	26	27	29	30	31
29	33	36	37	35	28	20	13	8	8	10	12	13	13	14	15	15	16	18	20	22	24	26	27	29	29
26	28	30	28	24	17	11	7	4	4	6	9	11	11	12	13	14	15	16	18	20	22	24	25	26	26
23	23	23	21	16	12	8	5	3	3	4	7	9	9	11	12	13	14	15	17	19	20	21	23	23	23
19	19	18	16	14	11	8	6	5	4	5	7	8	8	9	10	12	13	14	15	17	18	19	20	20	19
17	17	16	14	13	11	9	7	6	5	6	7	7	7	8	9	10	11	12	13	15	16	16	17	18	17
17	16	15	14	12	11	9	8	7	6	6	7	8	8	8	9	10	11	12	13	14	15	16	16	17	17
16	15	14	13	12	11	10	8	7	7	7	7	8	8	9	9	10	11	12	13	14	14	15	16	16	16
15	15	14	13	12	11	10	9	8	8	7	8	8	8	9	9	10	11	11	12	13	14	14	15	15	15
15	14	13	13	12	11	10	9	9	8	8	8	8	8	9	9	10	11	11	12	13	13	14	14	15	15

SEGMENT 2

FRONT													BACK												
62	70	77	86	95	100	98	88	72	56	45	41	38	38	38	38	39	41	43	46	49	52	55	57	59	62
61	69	78	89	102	109	107	93	73	53	43	39	37	37	36	37	38	39	42	45	48	51	53	56	58	61
60	69	79	93	109	119	116	97	72	50	40	37	35	35	35	35	36	37	40	43	46	49	52	55	57	60
59	68	79	97	117	129	122	91	58	39	35	33	32	32	33	33	33	35	37	40	43	47	50	53	55	59
55	63	75	91	108	116	105	70	38	25	25	27	29	29	30	30	31	32	34	37	40	44	47	50	53	55
49	55	63	72	72	64	51	33	18	12	15	20	23	23	26	27	28	29	31	34	37	40	43	46	48	49
43	46	51	51	44	35	25	17	10	7	10	16	19	19	22	24	26	27	29	32	34	37	39	42	43	43
38	38	39	38	34	29	22	16	11	8	10	14	16	16	19	21	23	25	27	29	32	34	35	37	38	38
35	35	34	32	29	26	21	17	14	12	12	14	15	15	17	19	20	22	24	26	28	30	32	33	34	35
33	33	32	30	28	25	21	18	15	13	13	15	16	16	17	19	20	22	23	25	27	29	30	32	33	33
32	31	30	29	27	24	21	19	16	15	15	15	16	16	18	19	20	21	23	25	26	28	29	31	31	32
30	30	29	27	26	24	21	19	18	16	16	16	17	17	18	19	20	21	23	24	26	27	28	29	30	30
29	29	28	27	25	23	21	20	18	17	17	17	17	17	18	19	20	21	22	24	25	27	28	28	29	29

SEGMENT 3

FRONT													BACK												
49	54	59	67	80	96	114	129	130	110	89	77	67	67	61	58	56	53	51	49	48	48	48	48	48	49
48	53	57	66	80	100	125	149	152	122	91	76	65	65	59	56	53	51	49	47	46	46	46	46	47	48
47	51	56	64	80	104	137	172	177	134	93	76	63	63	57	54	51	48	46	45	45	44	45	45	46	47
45	49	53	60	75	102	149	213	223	141	92	72	58	58	54	51	48	45	43	42	42	42	42	43	44	45
42	45	48	52	62	82	124	186	194	119	76	59	52	52	50	46	43	40	39	38	38	39	40	41	42	42
37	38	40	41	42	45	55	68	69	53	41	40	41	41	42	40	38	36	35	34	35	36	37	38	38	37
33	32	32	31	29	26	23	21	20	18	20	27	32	32	35	34	33	32	32	32	32	33	33	34	34	33
29	28	27	25	24	22	19	16	13	12	15	21	25	25	28	27	28	28	28	29	29	30	30	30	30	29
27	26	25	23	21	20	18	15	14	13	14	18	20	20	21	22	23	23	24	24	25	26	26	27	27	27
26	25	24	22	21	19	18	16	15	14	15	17	19	19	20	21	22	22	23	23	24	25	25	26	26	26
25	24	23	22	21	19	18	16	15	15	16	17	19	19	20	20	21	21	22	23	23	24	25	25	25	25
24	24	23	21	20	19	18	17	16	16	16	17	18	18	19	20	20	21	21	22	23	23	24	24	24	24
23	23	22	21	20	19	18	17	17	16	17	17	18	18	19	19	20	20	21	22	22	23	23	23	24	23

SEGMENT 4

FRONT

13	13	13	14	16	18	21	25	32	38	38	35	31
12	12	13	13	15	17	20	25	34	42	41	37	31
12	12	12	12	14	16	19	26	37	47	44	38	32
12	11	11	11	11	13	16	24	41	54	49	39	31
11	11	10	9	9	9	11	17	31	47	45	35	28
10	9	9	8	7	6	6	7	11	20	24	24	22
9	8	7	6	5	5	4	4	4	6	11	15	17
8	7	7	6	5	5	4	4	4	4	7	11	12
7	7	6	6	5	5	4	4	4	4	6	8	9
7	7	6	6	5	5	5	5	4	5	6	8	9
7	7	6	6	6	5	5	5	5	5	6	7	8
7	7	6	6	6	6	5	5	5	5	6	7	8
7	7	6	6	6	6	6	5	5	6	6	7	7

BACK

31	28	26	24	22	19	17	16	14	14	13	13	13
31	28	26	23	21	19	17	15	14	13	13	12	12
32	28	25	23	20	18	16	15	14	13	12	12	12
31	27	24	22	19	17	15	14	13	12	12	12	12
28	25	22	20	17	15	14	13	12	12	11	11	11
22	21	20	17	15	14	13	12	11	11	11	10	10
17	18	16	15	14	12	12	11	10	10	10	9	9
12	14	13	12	12	11	10	10	9	9	9	8	8
9	10	10	9	9	9	9	8	8	8	8	8	7
9	9	9	9	8	8	8	8	8	8	8	7	7
8	8	8	8	8	8	8	8	8	8	7	7	7
8	8	8	8	8	8	8	7	7	7	7	7	7
7	7	7	7	7	7	7	7	7	7	7	7	7

SEGMENT 5

FRONT

16	16	16	16	16	17	19	21	26	33	38	40	39
16	15	15	15	15	15	17	19	25	33	39	41	40
16	15	14	14	14	14	15	17	23	33	40	42	40
15	14	13	12	11	11	11	13	18	30	39	42	40
14	13	12	10	9	8	7	7	10	22	34	39	39
13	12	11	9	7	6	5	4	5	10	21	29	32
12	11	9	8	6	5	4	3	3	5	11	20	24
11	10	9	7	6	6	5	4	4	5	9	14	18
10	10	9	8	7	6	6	5	5	6	8	11	14
10	10	9	8	7	7	6	6	6	6	8	11	13
10	9	9	8	8	7	7	7	7	7	9	11	12
10	9	9	8	8	8	7	7	7	8	9	10	11
10	9	9	8	8	8	8	8	8	8	9	10	11

BACK

39	38	37	35	32	28	25	22	20	19	17	17	16
40	39	37	35	32	28	25	22	20	18	17	16	16
40	39	37	35	31	28	24	21	19	18	17	16	16
40	39	37	34	30	26	23	20	18	17	16	16	15
39	37	35	32	28	24	21	19	17	16	16	15	14
32	33	32	28	25	22	20	18	16	15	15	14	13
24	28	27	24	22	20	18	17	15	14	13	13	12
18	21	20	20	19	17	16	15	14	13	12	12	11
14	15	15	15	14	14	13	12	12	12	11	11	10
13	13	14	13	13	13	12	12	12	11	11	10	10
12	12	13	13	12	12	12	11	11	11	11	10	10
11	12	12	12	12	11	11	11	11	11	10	10	10
11	11	11	11	11	11	11	11	11	10	10	10	10

SEGMENT 6

FRONT

51	50	49	47	47	47	48	50	56	63	69	73	76
50	49	47	45	43	43	43	45	50	58	66	71	75
49	47	45	42	40	38	37	39	44	54	63	68	73
48	45	42	37	33	30	28	28	31	43	55	64	70
45	42	38	32	26	21	18	15	16	27	42	54	65
41	37	32	26	20	15	11	9	8	13	26	41	53
36	32	27	22	17	14	10	8	6	8	17	31	41
32	29	25	21	18	15	13	10	9	9	16	25	32
30	28	25	22	19	17	15	14	13	13	17	22	26
29	28	25	22	20	18	17	15	14	15	18	22	25
29	27	25	22	21	19	18	17	16	16	19	22	25
28	27	25	23	21	20	19	18	18	18	20	22	24
27	26	25	23	22	21	20	19	19	19	21	22	23

BACK

76	79	81	83	83	80	75	69	63	59	55	53	51
75	78	81	83	83	80	75	68	62	58	54	53	50
73	77	80	83	84	81	75	68	61	57	54	52	49
70	74	77	80	81	78	72	65	59	55	52	50	48
65	70	73	74	75	72	67	61	56	52	50	48	45
53	61	66	66	66	64	60	56	52	49	47	44	41
41	50	55	56	58	57	55	51	48	45	42	40	36
32	40	43	47	49	48	47	45	43	40	37	35	32
26	30	33	35	36	36	36	36	35	35	33	32	30
25	28	31	33	33	34	34	34	33	33	32	31	29
25	27	29	31	31	32	32	32	32	31	31	30	29
24	26	28	29	29	30	30	30	30	30	29	29	28
23	25	26	27	28	29	29	29	29	29	29	28	27

SEGMENT 7

FRONT													BACK												
64	63	61	59	56	54	53	52	54	56	59	62	65	65	69	72	76	80	81	81	78	74	71	68	66	64
63	61	59	56	53	50	48	47	48	52	56	59	63	63	67	71	76	80	82	81	78	74	70	67	65	63
62	60	57	53	49	45	42	41	42	47	52	57	62	62	66	71	76	81	83	82	78	74	70	66	64	62
60	57	53	47	41	36	32	29	29	36	46	52	59	59	64	68	73	79	82	81	76	72	68	65	63	60
57	53	48	40	32	26	20	16	15	23	35	44	54	54	60	64	69	74	77	76	72	68	64	62	61	57
51	46	40	32	25	18	13	9	7	11	22	35	45	45	53	59	63	67	70	69	66	63	61	58	55	51
45	40	34	27	21	16	12	9	6	7	15	27	36	36	44	51	56	60	63	63	61	58	55	52	49	45
39	36	31	26	22	18	15	12	10	9	15	23	29	29	36	41	47	51	53	54	53	51	48	45	43	39
37	34	30	26	23	20	17	15	14	14	17	22	25	25	30	33	36	39	40	42	42	42	41	40	39	37
35	33	30	26	24	21	19	17	16	16	18	22	25	25	28	31	34	36	38	39	39	39	39	38	37	35
34	32	29	26	24	22	20	19	18	18	20	22	25	25	28	30	32	34	35	37	37	37	37	37	36	34
33	32	29	27	25	23	22	21	20	20	21	23	24	24	27	29	31	32	33	34	35	35	35	35	34	33
32	31	29	27	25	24	23	22	21	21	22	23	24	24	26	28	30	31	32	33	34	34	34	34	33	32

SEGMENT 8

FRONT													BACK												
67	67	66	65	61	56	51	47	44	41	39	39	39	39	41	44	47	51	55	60	63	65	66	66	66	67
66	66	65	63	59	53	47	43	39	37	36	37	38	38	40	42	45	49	54	59	63	65	66	66	66	66
65	65	64	61	56	50	43	38	34	33	34	35	36	36	38	41	44	48	53	58	62	64	65	65	65	65
63	63	61	56	48	41	33	27	24	25	29	32	34	34	36	38	41	45	50	56	60	62	63	63	63	63
60	59	56	48	38	30	22	16	13	16	22	26	31	31	34	36	38	42	47	52	56	58	59	60	61	60
53	51	46	37	28	20	14	9	6	8	14	21	26	26	30	33	35	38	43	47	51	53	55	56	55	53
45	42	37	30	22	17	12	8	5	5	10	16	21	21	25	29	32	35	39	43	47	49	49	50	48	45
38	36	31	26	21	18	14	10	8	7	10	15	18	18	22	24	28	31	35	38	41	43	43	43	42	38
35	33	29	25	22	19	16	13	12	11	12	14	16	16	19	21	24	26	29	31	34	35	36	37	36	35
33	32	28	25	22	20	17	15	13	12	13	15	17	17	19	21	23	25	27	30	32	33	34	35	34	33
32	30	28	25	22	20	18	16	15	14	14	16	17	17	19	21	23	24	26	28	30	32	32	33	33	32
31	29	27	24	22	21	19	17	16	15	16	17	17	17	19	21	22	24	25	27	29	30	31	31	31	31
29	28	26	24	23	21	20	18	17	17	17	17	18	18	19	20	22	23	25	26	28	29	30	30	30	29

SEGMENT 9

FRONT													BACK												
32	35	37	38	36	33	28	23	19	15	13	13	13	13	14	14	15	17	19	21	23	26	28	30	31	32
32	36	39	41	40	36	29	23	18	14	13	12	13	13	13	14	15	16	18	21	23	26	28	30	31	32
33	[illegible]	41	45	45	40	31	23	17	[illegible]	12	12	12	12	13	14	14	16	18	20	23	26	28	30	31	33
34	39	46	55	57	47	33	21	13	10	10	11	12	12	12	13	14	15	17	20	23	25	28	30	31	34
34	41	51	65	70	58	36	18	9	7	8	10	11	11	12	13	14	15	17	19	22	25	27	29	31	34
33	41	52	64	63	49	29	15	7	4	[illegible]	8	10	10	11	12	13	15	17	19	22	24	27	29	31	33
32	38	47	51	45	34	22	13	[illegible]	4	5	8	9	9	11	12	13	15	17	19	21	24	26	29	30	32
30	33	36	37	34	28	20	14	9	6	6	8	9	9	10	12	13	15	17	19	21	23	25	27	29	30
28	30	31	30	28	24	20	15	12	9	8	9	10	10	11	12	13	15	16	18	20	22	24	26	27	28
27	28	29	28	26	23	19	16	13	11	10	10	10	10	11	13	14	15	17	18	20	22	23	25	27	27
26	27	27	27	25	22	19	16	14	12	11	11	11	11	12	13	14	15	17	18	20	22	23	24	26	26
25	26	26	25	23	21	19	17	15	13	12	12	12	12	13	14	15	16	17	18	20	21	22	24	25	25
25	25	24	23	22	21	19	17	15	14	13	13	13	13	13	14	15	16	17	18	20	21	22	23	24	25

SEGMENT 10

FRONT

39	44	47	52	56	59	58	52	42	31	26	24	22
39	44	49	56	63	68	67	59	45	31	25	23	21
40	45	51	60	71	79	78	67	48	30	24	22	21
40	46	55	70	92	109	111	86	51	27	21	20	20
39	46	57	80	114	153	171	122	58	23	17	17	18
38	45	58	82	107	138	152	102	44	16	12	14	16
37	43	55	69	78	80	71	50	26	11	9	12	14
35	39	45	53	57	56	49	36	22	12	10	12	14
34	36	40	43	43	41	36	30	23	17	14	14	14
33	35	37	39	40	38	33	28	23	18	15	15	15
32	34	35	37	36	35	31	27	23	19	17	16	16
31	32	33	34	33	32	29	26	23	20	18	17	17
31	31	32	32	31	30	28	25	23	21	19	18	18

BACK

22	22	22	23	24	26	28	30	32	34	36	38	39
21	21	22	22	23	25	27	30	32	34	36	38	39
21	21	21	22	23	24	27	29	32	34	36	37	40
20	20	20	21	22	23	26	28	31	33	35	37	40
18	19	19	20	21	22	25	27	30	32	35	36	39
16	17	18	19	20	22	24	26	29	31	34	35	38
14	16	17	18	20	21	23	26	28	30	33	35	37
14	15	17	18	19	21	23	25	27	29	32	34	35
14	16	17	18	19	21	23	25	27	29	31	33	34
15	16	17	19	20	21	23	25	27	28	30	32	33
16	17	18	19	20	22	23	25	27	28	30	31	32
17	18	19	20	21	22	24	25	27	28	29	31	31
18	19	19	20	21	22	24	25	27	28	29	30	31

SEGMENT 11

FRONT

20	22	24	26	30	35	41	45	45	41	35	31	27
20	22	23	26	31	38	46	53	55	47	37	32	27
20	22	23	27	33	41	53	64	67	55	40	33	27
19	21	23	27	35	49	73	103	112	75	45	33	26
19	20	22	26	35	53	95	171	200	108	48	30	24
18	19	21	25	31	44	79	157	196	100	34	23	20
17	18	20	22	27	35	48	70	83	46	20	17	18
16	17	18	20	22	26	31	34	32	22	14	14	15
16	16	17	18	19	20	21	21	20	16	13	13	13
15	16	16	17	18	18	19	19	18	15	13	13	13
15	15	16	16	17	17	17	17	16	15	13	13	13
15	15	15	16	16	16	16	16	15	14	13	13	13
15	15	15	15	15	15	15	15	15	14	13	13	13

BACK

27	25	24	23	21	20	20	20	19	20	20	20	20
27	25	23	22	21	20	19	19	19	19	19	20	20
27	24	23	21	20	19	19	18	19	19	19	19	20
26	23	22	20	19	18	18	18	18	18	19	19	19
24	22	20	19	18	17	17	17	17	18	18	19	19
20	20	19	17	16	16	16	16	16	17	17	18	18
18	18	17	16	15	15	15	15	16	16	17	17	17
15	15	14	14	14	14	14	15	15	15	16	16	16
13	13	13	13	13	13	14	14	14	15	15	16	16
13	13	13	13	13	13	13	14	14	15	15	15	15
13	13	13	13	13	13	13	14	14	14	15	15	15
13	13	13	13	13	13	13	14	14	14	15	15	15
13	13	13	13	13	13	13	14	14	14	15	15	15

SEGMENT 12

FRONT

21	21	21	22	24	27	32	39	50	64	68	65	58
21	21	21	21	23	26	31	39	55	74	75	70	60
20	20	20	20	21	24	30	40	61	87	90	79	62
20	19	19	18	19	21	28	42	83	130	111	83	63
19	18	17	16	15	17	23	41	107	183	145	92	62
18	17	15	14	13	13	16	30	95	170	128	79	57
16	15	14	13	12	12	13	19	43	65	61	55	49
15	15	13	12	12	12	12	14	19	26	32	37	38
15	14	14	13	12	12	12	12	14	16	21	26	28
15	14	14	13	13	12	12	13	14	16	19	23	25
15	14	14	13	13	13	13	13	14	16	19	22	23
15	14	14	14	13	13	13	14	14	16	18	20	21
15	14	14	14	14	14	14	14	15	16	17	19	20

BACK

58	53	48	43	38	34	30	27	25	23	22	22	21
60	53	48	43	38	33	29	26	24	23	22	21	21
62	54	48	43	37	32	28	26	24	22	21	21	20
63	54	47	42	36	31	27	24	23	22	21	20	20
62	52	45	39	34	29	26	23	22	21	20	20	19
57	49	42	36	31	27	24	22	21	20	19	19	18
49	44	37	32	28	25	23	21	20	19	18	17	16
38	36	30	27	25	23	21	20	19	18	17	16	15
28	26	24	22	21	19	18	18	17	16	16	15	15
25	24	22	21	20	19	18	17	17	16	16	15	15
23	22	21	20	19	18	17	17	16	16	16	15	15
21	21	20	19	18	18	17	16	16	16	15	15	15
20	19	19	18	18	17	17	16	16	16	15	15	15

SEGMENT 13

FRONT													BACK												
11	11	10	10	10	10	11	12	15	21	26	28	29	29	28	27	25	22	19	17	15	14	13	12	12	11
11	11	10	10	9	9	10	11	15	21	27	30	31	31	30	28	25	22	20	17	15	14	13	12	12	11
11	10	10	9	8	8	9	10	14	21	29	32	32	32	31	29	26	23	20	17	15	14	13	12	12	11
11	10	9	8	7	7	7	8	12	22	31	36	35	35	33	30	27	24	20	17	15	14	13	12	11	11
11	10	9	7	6	5	5	5	8	20	36	43	39	39	35	32	28	24	20	17	15	13	12	12	11	11
10	9	8	7	6	5	4	3	4	13	33	43	40	40	36	32	28	23	20	17	15	13	12	12	11	10
10	9	8	7	6	5	4	3	4	8	20	32	35	35	35	31	26	22	19	16	14	13	12	11	10	10
9	9	8	7	6	6	5	5	5	7	14	23	27	27	29	26	22	20	17	15	14	12	11	11	10	9
9	9	8	8	7	7	6	6	7	8	12	17	20	20	21	20	18	16	15	13	12	12	11	10	10	9
9	9	8	8	7	7	7	7	7	9	12	16	18	18	19	18	17	15	14	13	12	11	11	10	10	9
10	9	9	8	8	8	8	8	8	9	12	15	17	17	17	16	15	14	14	13	12	11	11	10	10	10
10	9	9	9	8	8	8	8	9	10	12	14	15	15	15	15	14	14	13	12	12	11	11	10	10	10
10	9	9	9	9	9	9	9	9	10	12	13	14	14	14	14	14	13	13	12	11	11	11	10	10	10

SEGMENT 14

FRONT													BACK												
11	10	9	8	8	7	7	7	8	10	13	15	16	16	17	17	17	17	16	15	14	13	12	12	11	11
11	10	9	8	7	7	6	7	8	10	13	15	17	17	18	18	18	18	17	16	14	13	12	12	11	11
11	10	9	8	7	6	6	6	7	9	13	15	17	17	19	19	19	19	18	16	15	14	13	12	11	11
11	10	9	7	6	5	5	4	5	8	12	16	18	18	20	21	21	21	19	17	16	14	13	12	12	11
11	10	8	7	5	4	3	3	3	6	11	16	19	19	21	23	23	23	21	19	17	15	13	12	12	11
11	10	8	7	5	4	3	2	2	4	9	16	20	20	23	25	25	24	22	20	17	15	14	12	12	11
10	9	8	7	6	5	4	3	2	3	8	14	19	19	23	25	25	24	22	20	17	15	14	12	11	10
10	10	8	7	6	6	5	4	4	5	8	13	16	16	20	22	23	22	20	18	16	15	13	12	11	10
10	10	9	8	7	7	6	6	6	7	9	12	14	14	17	18	19	18	17	16	15	14	13	12	11	10
10	10	9	8	8	7	7	7	7	7	9	12	13	13	15	17	17	17	16	15	14	13	12	12	11	10
10	10	9	9	8	8	8	8	8	8	10	12	13	13	15	16	16	16	15	14	14	13	12	11	11	10
10	10	10	9	9	9	8	8	8	9	10	12	13	13	14	14	15	15	14	14	13	12	12	11	11	10
11	10	10	9	9	9	9	9	9	9	10	12	12	12	13	14	14	14	14	13	13	12	12	11	11	11

SEGMENT 15

FRONT													BACK												
25	23	21	19	16	15	14	13	14	16	18	21	23	23	25	27	28	29	30	31	30	29	28	27	27	25
25	23	21	18	16	14	12	12	12	15	18	20	23	23	26	28	29	31	32	33	32	31	29	28	27	25
26	23	21	18	15	12	11	10	11	13	17	20	23	23	26	29	31	33	35	35	34	32	30	29	28	26
26	23	20	17	13	11	9	8	8	11	16	20	24	24	27	30	33	37	39	39	36	34	31	30	28	26
26	24	20	16	12	9	7	5	5	8	13	19	24	24	28	32	37	41	44	43	40	36	33	30	29	26
27	24	20	16	12	9	7	5	3	5	11	18	23	23	28	34	39	45	47	46	42	38	34	31	29	27
26	23	20	16	13	10	8	6	4	4	9	16	21	21	27	33	40	45	47	46	43	39	35	31	28	26
26	24	20	17	15	13	11	9	8	7	11	16	20	20	25	31	37	41	43	43	40	37	34	30	28	26
25	24	21	19	17	15	14	12	11	11	14	17	19	19	24	28	32	35	37	37	35	33	31	29	27	25
25	24	21	19	18	16	15	14	13	13	15	18	20	20	23	27	30	33	34	34	33	32	30	28	27	25
25	24	22	20	19	17	16	15	15	15	16	18	20	20	23	26	29	31	32	32	31	30	29	28	26	25
25	24	22	20	19	19	18	17	16	16	18	19	20	20	23	25	27	29	30	30	30	29	28	27	26	25
25	24	22	21	20	19	19	18	18	16	19	20	21	21	23	24	26	27	28	28	28	28	27	26	25	25

SEGMENT 16

FRONT													BACK													
29	27	25	23	19	16	14	12	12	11	12	13	14	14	15	17	18	20	22	25	27	29	30	30	30	29
30	28	26	23	19	16	13	11	10	10	12	13	14	14	15	17	18	20	23	26	28	30	30	31	31	30
31	29	27	23	19	15	12	10	9	9	11	12	14	14	15	17	19	21	24	27	29	31	32	32	31	31
32	30	27	23	18	14	10	8	6	8	10	12	13	13	15	17	19	22	25	29	32	33	33	33	32	32
33	32	29	24	18	12	8	5	4	5	8	11	13	13	15	17	20	23	27	31	34	35	35	34	33	33
34	33	29	24	18	13	8	5	3	3	6	10	12	12	15	17	20	24	28	33	36	37	36	35	35	34
33	32	28	23	17	13	10	6	4	3	6	9	12	12	14	17	21	24	29	33	36	37	37	36	35	33
32	30	27	23	19	15	12	9	7	6	7	10	12	12	14	17	20	24	28	31	34	35	35	34	33	32
31	29	26	23	20	17	14	12	10	9	10	11	12	12	14	17	20	22	25	29	31	32	33	32	32	31
30	28	26	23	20	18	16	13	12	11	11	12	13	13	15	17	20	22	25	27	29	31	31	31	30	30
29	27	25	23	20	19	16	15	13	12	12	13	14	14	16	17	19	22	24	26	28	29	30	30	29	29
28	27	25	23	21	19	17	16	15	14	14	14	14	14	16	18	19	21	23	25	27	28	28	28	28	28
27	26	24	23	21	20	18	17	16	15	15	15	15	15	16	18	19	21	23	24	26	27	27	28	27	27

SEGMENT 17

FRONT													BACK													
34	33	32	29	26	23	20	17	15	14	15	15	16	16	18	18	20	21	23	25	28	30	32	33	34	34
35	35	33	31	27	23	19	16	14	13	14	15	16	16	18	19	20	21	23	26	28	31	33	34	35	35
36	36	35	33	29	24	19	16	13	12	14	15	16	16	18	19	20	22	24	26	29	32	34	35	36	36
38	39	39	38	34	28	20	14	10	10	12	15	17	17	18	19	21	23	25	28	31	33	35	37	38	38
41	44	45	48	46	37	25	15	9	8	11	15	17	17	19	20	22	24	27	30	33	36	38	39	40	41
48	53	58	64	67	61	44	27	13	7	10	16	18	18	20	22	24	26	29	32	36	39	41	43	45	48
56	63	71	79	82	76	60	38	20	10	12	18	20	20	22	24	26	29	31	35	38	41	45	48	51	56
61	67	76	84	85	81	68	50	34	21	19	22	24	24	25	28	30	32	35	39	42	46	50	53	57	61
63	68	75	80	82	79	70	58	46	35	29	28	28	28	30	33	35	38	41	44	48	51	54	57	61	63
63	67	73	77	78	75	68	58	48	39	33	31	31	31	33	35	38	40	43	46	50	53	55	58	61	63
63	67	71	74	74	71	66	58	50	42	36	35	34	34	36	38	40	42	45	48	51	54	56	59	61	63
63	66	69	70	70	68	63	57	51	45	40	38	37	37	38	40	42	44	46	49	52	55	57	59	61	63
63	65	67	68	67	65	61	57	52	47	42	40	39	39	40	42	43	45	48	50	53	55	57	59	62	63

SEGMENT 18

FRONT													BACK													
41	41	41	39	37	34	30	27	23	21	20	21	22	22	23	24	25	26	28	31	33	36	38	40	41	41
42	43	43	42	40	37	32	27	23	20	20	21	22	22	23	24	25	26	28	31	34	36	39	41	42	42
43	44	45	45	43	40	35	28	22	19	19	20	22	22	23	24	25	27	29	31	34	37	40	41	43	43
45	47	49	53	55	53	45	33	22	16	18	20	22	22	23	25	26	27	30	33	36	39	41	43	44	45
48	52	57	69	81	86	78	55	29	15	16	20	23	23	24	26	27	29	31	34	38	41	43	45	46	48
55	61	72	94	126	155	163	127	63	30	16	22	25	25	26	27	29	31	34	37	40	43	45	48	51	55
62	71	87	115	155	190	206	173	91	31	21	26	28	28	28	30	32	34	36	39	42	46	49	53	57	62
68	76	92	116	141	164	178	162	109	52	33	33	34	34	33	36	37	38	41	44	47	50	54	59	63	68
71	78	90	106	120	130	136	129	106	73	49	42	40	40	41	42	43	45	48	50	54	57	59	63	67	71
71	78	88	101	111	118	121	116	100	74	53	47	44	44	45	45	47	48	51	53	56	59	61	65	68	71
72	77	86	96	103	108	110	105	93	73	57	50	48	48	48	49	50	51	53	56	58	61	63	66	70	72
73	77	84	90	95	98	98	95	86	72	60	54	52	52	52	52	53	54	56	58	61	63	65	68	71	73
73	77	82	87	90	91	90	87	82	72	62	57	54	54	54	54	55	56	58	60	62	64	66	69	71	73

SEGMENT 19

FRONT													BACK												
24	23	23	22	21	21	21	21	20	19	19	19	19	19	19	19	19	19	20	20	21	22	23	23	24	24
24	24	24	23	22	22	22	22	21	20	20	20	20	20	20	20	20	20	20	21	22	22	23	24	24	24
25	25	24	24	24	24	24	25	24	22	20	20	20	20	20	20	20	20	20	21	22	23	24	24	25	25
26	26	26	26	27	30	34	37	35	28	22	21	21	21	21	21	21	21	21	22	23	24	25	25	25	26
27	28	29	31	35	43	59	82	88	54	27	23	22	22	21	22	22	22	22	23	24	25	26	26	27	27
30	32	35	41	55	79	128	209	248	132	36	26	25	25	24	23	23	24	24	25	26	27	27	28	29	30
34	37	41	51	72	106	171	279	332	168	49	32	28	28	26	26	25	25	26	26	27	28	30	31	32	34
38	41	47	56	71	93	134	194	224	137	57	39	34	34	31	30	29	29	29	29	30	31	33	34	36	38
40	43	49	56	66	79	98	121	133	108	64	47	40	40	37	35	34	34	34	34	35	35	36	38	39	40
41	44	49	56	64	73	88	104	112	96	63	48	42	42	40	38	37	36	36	36	37	37	38	39	40	41
43	45	49	55	61	69	80	91	97	85	61	49	44	44	42	40	39	39	38	38	39	39	40	41	42	43
44	46	50	54	59	64	71	79	82	75	59	50	46	46	44	42	41	41	40	40	40	41	41	42	43	44
45	47	50	54	58	61	66	70	72	67	57	51	48	48	46	44	43	42	42	42	42	42	42	43	44	45

SEGMENT 20

FRONT													BACK												
28	26	25	24	24	24	25	28	35	45	54	56	56	56	54	51	47	43	39	36	33	31	30	29	29	28
28	26	25	24	23	22	24	27	35	49	58	60	59	59	56	52	48	43	39	36	33	31	30	29	29	28
28	26	25	23	21	21	22	26	35	53	64	65	62	62	59	54	49	44	40	36	33	32	30	29	29	28
28	26	24	22	20	19	20	24	40	72	80	75	68	68	63	57	52	46	40	37	34	32	31	30	29	28
28	27	24	22	19	17	17	23	51	121	135	106	79	79	68	61	54	47	42	38	35	33	31	30	30	28
30	28	26	23	21	20	21	30	78	255	277	158	102	102	78	64	56	49	43	39	36	34	32	31	30	30
31	30	27	26	25	26	29	40	111	334	353	197	124	124	90	69	57	50	44	40	37	35	33	32	31	31
33	32	31	30	29	31	34	43	84	212	251	170	122	122	93	71	58	51	46	41	38	36	35	34	33	33
34	33	33	33	34	35	39	47	63	104	136	124	107	107	86	70	60	53	48	44	40	38	37	35	34	34
35	35	35	35	36	38	42	48	60	88	114	109	98	98	81	68	59	53	49	45	42	39	38	37	36	35
36	36	36	37	38	40	44	49	59	80	99	97	90	90	77	66	59	54	49	46	43	41	39	38	37	36
37	38	38	39	40	42	46	50	58	72	85	86	82	82	72	65	58	54	50	47	44	42	40	39	38	37
38	38	39	40	42	44	47	51	57	66	75	77	76	76	69	63	58	54	51	47	45	42	41	40	39	38

SEGMENT 21

FRONT													BACK												
24	22	21	19	18	17	16	17	20	25	31	35	37	37	38	37	35	33	31	29	28	27	26	25	25	24
24	22	21	19	17	16	15	16	18	25	32	36	39	39	40	39	37	34	32	30	28	27	26	26	25	24
24	23	21	18	16	14	13	14	17	24	33	38	41	41	42	41	38	36	33	31	29	28	27	26	26	24
25	23	21	18	15	13	11	11	14	24	35	43	47	47	46	44	42	38	35	32	30	29	28	27	26	25
26	24	21	18	15	12	9	8	10	23	42	55	55	55	51	50	47	43	38	35	32	30	29	28	27	26
28	26	23	20	17	15	12	10	9	22	57	76	70	70	63	57	52	47	42	36	35	33	31	29	29	28
30	28	26	23	21	19	17	15	14	25	61	87	84	84	76	67	57	51	45	40	37	35	33	31	30	30
32	31	29	27	26	25	24	24	26	34	63	86	88	88	82	74	63	55	49	44	40	37	35	34	33	32
34	33	32	31	31	31	32	33	37	46	66	81	86	86	83	76	67	60	54	48	44	40	38	36	35	34
35	35	34	33	33	34	35	37	40	49	65	77	81	81	79	73	66	60	54	49	45	42	40	37	36	35
37	36	36	36	36	37	38	40	44	51	64	74	77	77	75	70	65	59	54	50	46	43	41	39	37	37
38	38	37	38	38	40	41	44	47	53	63	70	73	73	71	68	63	59	54	50	47	44	42	40	39	38
39	39	39	39	40	42	44	46	49	54	62	67	70	70	69	66	62	58	55	51	47	45	43	41	39	39

SEGMENT 22

FRONT													BACK													
31	29	27	24	21	19	16	18	19	22	27	30	33	33	35	35	35	35	34	34	33	33	33	33	32	31
32	29	27	24	21	18	16	16	17	21	27	31	34	34	37	37	37	36	36	35	35	34	34	34	33	32
32	30	27	24	20	17	15	14	15	20	27	31	36	36	38	39	39	38	37	37	36	35	35	34	34	32
33	31	28	24	19	16	13	11	12	18	26	33	39	39	42	43	43	42	41	40	39	38	37	36	35	33
36	33	29	25	20	15	11	9	8	14	26	38	44	44	46	49	50	49	47	45	43	41	40	38	37	36
39	37	33	28	25	21	17	12	9	12	28	46	54	54	56	57	59	57	54	51	48	45	43	41	40	39
43	41	37	34	31	28	25	20	15	17	34	54	63	63	66	69	68	64	60	56	52	49	47	44	44	43
48	46	44	41	39	37	35	33	32	33	47	63	72	72	77	82	79	73	68	62	57	54	52	49	48	48
50	49	48	46	46	46	46	47	48	52	62	73	79	79	86	89	88	84	78	71	65	60	57	53	51	50
52	51	50	50	49	50	51	52	53	57	66	75	80	80	86	88	87	83	78	72	66	62	58	55	53	52
54	53	53	52	53	53	55	56	57	61	69	76	80	80	85	86	85	82	77	72	67	63	60	57	55	54
56	55	55	55	56	57	58	60	62	65	72	77	80	80	83	84	83	81	77	72	68	64	61	59	57	56
57	57	57	57	58	59	61	63	65	68	74	78	80	80	82	83	82	80	76	72	68	65	62	60	58	57

SEGMENT 23

FRONT													BACK													
39	37	34	30	26	23	21	19	20	22	26	28	31	31	34	35	36	37	38	39	40	41	41	41	41	39
40	37	34	30	25	22	19	18	18	21	25	29	32	32	35	37	38	39	40	41	42	42	43	42	42	40
41	38	35	30	25	20	17	16	16	19	25	29	33	33	36	38	40	41	42	43	44	44	44	44	43	41
43	40	36	30	24	19	15	12	12	17	23	29	35	35	38	41	43	45	47	48	48	47	47	46	45	43
46	43	38	32	26	19	14	10	8	13	22	31	38	38	42	46	50	53	54	55	54	52	51	49	48	46
52	49	44	38	32	27	21	15	10	10	22	36	43	43	47	52	58	61	63	62	60	58	56	53	53	52
58	56	50	45	41	36	30	23	16	15	25	40	48	48	53	60	66	69	70	69	66	63	61	59	58	58
63	62	59	54	51	47	43	38	33	30	37	48	55	55	61	71	76	78	78	76	72	69	67	65	63	63
66	65	63	61	59	58	56	53	50	48	52	58	63	63	72	79	85	88	87	84	80	76	73	70	67	66
68	67	65	64	62	61	60	58	56	55	58	62	66	66	74	80	85	87	87	84	80	77	74	71	69	68
69	68	67	66	65	65	64	62	61	60	62	66	69	69	75	80	84	86	86	83	80	77	75	72	70	69
70	70	69	68	68	68	67	66	66	65	67	70	71	71	77	80	83	84	84	82	80	78	75	73	72	70
71	71	70	70	70	70	70	69	69	69	70	72	73	73	77	81	83	84	83	82	80	78	76	74	72	71

SEGMENT 24

FRONT													BACK													
53	50	46	41	35	29	26	23	21	22	24	25	27	27	30	32	33	36	39	42	46	49	52	53	54	53
54	51	47	42	35	29	24	21	19	20	23	25	28	28	30	32	34	37	40	44	48	51	54	55	56	54
56	53	49	43	35	28	23	19	17	18	22	25	28	28	31	33	35	38	41	46	50	53	56	57	58	56
60	57	52	45	36	28	20	15	13	15	20	25	29	29	32	34	37	40	44	49	53	57	59	61	61	60
66	64	59	52	41	30	20	13	9	11	18	25	30	30	33	36	40	44	49	54	59	63	65	65	65	66
76	77	73	64	54	43	30	19	11	9	17	27	32	32	36	39	44	49	55	60	66	69	71	72	74	76
87	89	85	76	66	55	42	29	18	13	19	30	35	35	38	44	49	54	59	65	71	75	79	81	83	87
94	96	94	87	77	68	56	45	35	27	29	36	40	40	44	50	56	60	66	73	78	82	87	90	92	94
97	98	96	92	86	79	70	61	52	44	42	44	47	47	52	58	64	69	75	82	87	91	93	95	96	97
97	97	96	92	87	81	73	65	58	51	48	49	51	51	56	61	66	71	77	83	88	91	93	95	96	97
96	96	95	91	87	82	76	69	63	57	54	54	55	55	59	64	68	73	78	83	86	91	93	95	96	96
96	96	94	91	87	83	78	73	67	62	59	59	59	59	63	66	71	75	79	83	87	90	92	94	95	96
95	95	93	91	88	84	80	75	71	66	63	62	62	62	65	68	72	76	80	84	87	90	92	94	95	95

SEGMENT 25

FRONT

116	122	127	134	142	148	152	154	153	146	135	129	123
113	118	122	128	135	140	143	145	144	138	128	123	118
110	114	117	122	127	130	132	133	133	128	120	116	112
105	107	109	107	104	103	100	96	92	97	104	105	103
97	97	95	86	76	69	59	50	45	57	75	84	91
83	80	75	64	52	40	31	23	18	25	42	60	72
70	65	59	50	39	30	22	15	11	13	25	43	55
60	56	49	42	36	30	24	18	15	14	22	34	43
54	51	46	40	36	31	27	23	20	19	24	30	35
52	49	45	40	36	32	28	25	23	22	26	31	34
50	48	44	40	36	33	30	27	25	25	27	31	34
48	46	43	39	37	34	31	29	28	27	29	32	34
47	45	42	39	37	35	33	31	30	29	30	32	33

BACK

123	121	122	123	124	124	123	121	119	117	115	115	116
118	116	117	118	119	119	118	116	115	113	112	112	113
112	111	112	113	114	114	113	112	110	109	108	109	110
103	104	104	104	104	104	104	104	103	103	103	104	105
91	95	93	92	91	91	92	93	94	95	97	98	97
72	79	82	80	79	80	81	82	84	87	88	67	83
55	64	67	69	71	72	73	75	76	76	77	75	70
43	51	53	57	60	62	64	66	67	66	66	64	60
35	40	43	45	47	49	52	54	55	56	57	56	54
34	38	41	43	45	47	49	51	52	53	54	54	52
34	37	39	41	43	45	47	49	50	51	51	51	50
34	36	38	40	41	43	45	46	48	49	49	49	48
33	35	37	39	40	42	43	45	46	47	47	47	47

SEGMENT 26

FRONT

66	62	58	53	47	42	39	37	38	43	50	56	60
68	64	59	53	46	41	37	34	35	42	51	57	63
70	66	61	54	46	39	34	32	32	40	51	59	66
73	69	64	56	48	40	33	28	28	38	52	63	71
79	76	70	64	56	46	37	30	28	39	58	76	81
91	89	85	81	81	79	76	70	62	67	90	109	107
103	105	103	104	110	117	125	130	147	178	172	157	140
117	120	124	129	136	147	167	195	246	296	261	211	180
126	129	135	144	155	172	196	228	267	307	290	245	211
131	135	142	151	162	177	199	227	258	290	278	242	214
137	141	148	157	167	180	199	222	247	271	263	236	214
143	147	153	162	172	184	200	218	236	253	248	230	215
146	151	158	166	176	186	200	214	228	240	237	226	216

BACK

60	63	63	63	63	63	64	65	65	67	68	68	66
63	65	66	65	65	65	66	67	68	69	70	70	68
66	68	69	68	67	67	68	69	70	71	72	72	70
71	73	74	74	73	72	73	73	74	75	75	75	73
81	81	82	83	62	80	80	80	81	81	80	79	79
107	99	94	94	92	90	89	89	89	88	87	89	91
140	122	114	108	103	99	97	96	96	97	98	100	103
180	154	143	130	122	116	112	110	109	110	111	113	117
211	188	171	157	149	141	134	129	126	125	124	124	126
214	194	178	166	157	149	143	137	134	131	130	131	131
214	198	183	172	164	156	149	144	140	138	136	136	137
215	201	189	178	171	163	156	151	146	144	142	142	143
216	204	192	183	175	168	161	155	151	148	147	146	146

APPENDIX E

EPICARDIAL POTENTIALS CALCULATED FROM IN-VIVO BODY-SURFACE MEASUREMENTS

E.1 Solutions by Direct Matrix Inversion

FRAME 1

BODY-SURFACE POTENTIALS (MICROVOLTS)

6	6	6	6	6	6	6	6
13	-24	0	-4	4	4	13	-12
-2	0	-8	-4	-6	36	24	4
-12	-6	-4	12	16	-6	-0	33
0	0	0	0	0	0	0	0

EPICARDIAL POTENTIALS (10 MICROVOLTS)

-0	-0	-0	-0	-0	-0	-0	-0
-1311	215	-11	-18	101	-153	-92	676
214	-85	13	3	-168	776	59	-402
-71	23	-7	0	-3	-6	-179	142
10	10	10	10	10	10	10	10

FRAME 21

BODY-SURFACE POTENTIALS (MICROVOLTS)

12	12	12	12	12	12	12	12
20	-25	-6	2	6	10	25	4
24	4	-12	40	4	10	32	8
13	20	6	22	32	0	18	32
8	8	8	8	8	8	8	8

EPICARDIAL POTENTIALS (10 MICROVOLTS)

-22	-22	-22	-22	-22	-22	-22	-22
-1500	218	-0	-171	298	-173	-81	893
320	-102	7	33	-36	-577	654	-1045
-214	47	2	-4	34	52	-195	293
6	6	6	6	6	6	6	6

FRAME 11

BODY-SURFACE POTENTIALS (MICROVOLTS)

12	12	12	12	12	12	12	12
25	-10	8	0	10	18	25	12
16	10	2	16	2	20	38	6
0	10	-6	18	6	-8	16	48
8	8	8	8	8	8	8	8

EPICARDIAL POTENTIALS (10 MICROVOLTS)

-51	-51	-51	-51	-51	-51	-51	-51
-1178	189	4	-106	189	21	-294	871
225	-79	7	11	50	-700	959	-1076
-115	36	-3	3	-102	365	-550	335
6	6	6	6	6	6	6	6

FRAME 31

BODY-SURFACE POTENTIALS (MICROVOLTS)

0	0	0	0	0	0	0	0
38	-4	-13	-8	0	2	2	4
51	51	48	64	12	30	50	30
57	103	59	64	88	30	57	62
27	27	27	27	27	27	27	27

EPICARDIAL POTENTIALS (10 MICROVOLTS)

47	47	47	47	47	47	47	47
-485	-54	-1	-178	-77	228	-597	641
225	16	9	45	45	-640	1956	-1227
-217	25	4	-11	156	-126	-175	425
11	11	11	11	11	11	11	11

FRAME 41

BODY-SURFACE POTENTIALS (MICROVOLTS)

10	10	10	10	10	10	10	10
44	-51	-117	-53	4	10	22	0
88	94	90	85	51	60	74	60
111	110	116	92	83	62	107	101
53	53	53	53	53	53	53	53

EPICARDIAL POTENTIALS (10 MICROVOLTS)

430	430	430	430	430	430	430	430
-386	-432	-35	-616	166	-665	269	-123
435	146	43	111	13	326	289	-584
-201	-3	-4	-9	92	-324	253	210
21	21	21	21	21	21	21	21

FRAME 51

BODY-SURFACE POTENTIALS (MICROVOLTS)

12	12	12	12	12	12	12	12
16	-111	-146	-66	18	20	25	-30
55	0	10	57	55	69	76	41
66	67	74	92	76	72	100	80
50	50	50	50	50	50	50	50

EPICARDIAL POTENTIALS (10 MICROVOLTS)

447	447	447	447	447	447	447	447
-1935	-169	-49	-739	554	-749	2	659
628	27	53	118	-133	63	936	-918
-278	31	-16	1	-113	461	-677	419
25	25	25	25	25	25	25	25

FRAME 61

BODY-SURFACE POTENTIALS (MICROVOLTS)

13	13	13	13	13	13	13	13
25	-53	-33	-32	8	8	30	-8
38	-18	-27	44	12	33	41	33
10	18	27	44	40	13	44	27
22	22	22	22	22	22	22	22

EPICARDIAL POTENTIALS (10 MICROVOLTS)

104	104	104	104	104	104	104	104
-1908	226	0	-461	484	-444	71	755
376	-113	11	79	-100	33	405	-372
-216	55	-5	0	-125	412	-537	232
20	20	20	20	20	20	20	20

FRAME 71

BODY-SURFACE POTENTIALS (MICROVOLTS)

8	8	8	8	8	8	8	8
20	-25	-2	-6	8	0	18	0
22	-32	-36	22	-30	2	12	13
0	-8	2	8	-16	-27	2	0
0	0	0	0	0	0	0	0

EPICARDIAL POTENTIALS (10 MICROVOLTS)

-35	-35	-35	-35	-35	-35	-35	-35
-1332	257	14	-283	723	-477	299	546
205	-118	-3	49	-316	315	-220	-89
-119	39	0	-8	6	-165	227	-52
12	12	12	12	12	12	12	12

FRAME 81

BODY-SURFACE POTENTIALS (MICROVOLTS)

4	4	4	4	4	4	4	4
8	0	53	76	32	0	10	-38
27	-30	-10	74	-13	0	-10	-2
-27	-13	20	8	-33	-33	-6	-6
-2	-2	-2	-2	-2	-2	-2	-2

EPICARDIAL POTENTIALS (10 MICROVOLTS)

-223	-223	-223	-223	-223	-223	-223	-223
-1082	406	18	108	651	-412	382	514
37	-158	-16	7	-117	262	-234	-80
-98	54	15	1	-244	334	-307	114
18	16	18	18	18	18	18	18

FRAME 91

BODY-SURFACE POTENTIALS (MICROVOLTS)

-62	-62	-62	-62	-62	-62	-62	-62
-130	-278	-431	-148	257	130	-124	-223
-27	-146	-4	598	441	271	50	-50
38	38	221	481	447	274	178	36
88	88	88	88	88	88	88	88

EPICARDIAL POTENTIALS (10 MICROVOLTS)

1212	1212	1212	1212	1212	1212	1212	1212
-216	-1320	57	-3827	4327	-1882	-1004	-1
871	306	9	726	-1562	3119	1931	-878
-950	137	16	-13	-342	1442	-2871	1280
243	243	243	243	243	243	243	243

FRAME 101

BODY-SURFACE POTENTIALS (MICROVOLTS)

66	66	66	66	66	66	66	66
-67	-776	-1831	-1689	521	484	132	-110
139	-270	-1250	164	1024	793	484	171
278	125	-12	687	943	771	602	324
300	300	300	300	300	300	300	300

EPICARDIAL POTENTIALS (10 MICROVOLTS)

5119	5119	5119	5119	5119	5119	5119	5119
995	-5143	538	-17499	22154	-13779	6713	-6039
3952	811	-28	2382	-11499	12031	-290	2980
-4526	471	-257	27	1654	614	-2683	1646
274	274	274	274	274	274	274	274

FRAME 111

BODY-SURFACE POTENTIALS (MICROVOLTS)

106	106	106	106	106	106	106	106
115	-276	-608	-630	55	167	214	92
153	-85	-655	-301	139	209	235	182
125	24	-139	0	157	167	209	167
103	103	103	103	103	103	103	103

EPICARDIAL POTENTIALS (10 MICROVOLTS)

1836	1636	1836	1836	1836	1836	1836	1836
-2299	-1238	79	-5034	6071	-5275	3904	-1969
1799	57	22	596	-3718	4184	-2044	2522
-1693	169	-130	15	822	-667	915	-302
-15	-15	-15	-15	-15	-15	-15	-15

FRAME 121

BODY-SURFACE POTENTIALS (MICROVOLTS)

4	4	4	4	4	4	4	4
25	-18	35	150	41	13	8	-16
30	-24	0	94	-18	-8	-12	30
-2	-8	30	0	-8	-36	12	0
6	6	6	6	6	6	6	6

EPICARDIAL POTENTIALS (10 MICROVOLTS)

-348	-348	-348	-348	-348	-348	-348	-348
-2396	744	-12	629	48	215	-298	1316
140	-266	-7	-54	87	115	-408	156
-54	69	25	2	-183	77	109	-111
11	11	11	11	11	11	11	11

FRAME 131

BODY-SURFACE POTENTIALS (MICROVOLTS)

-8	-8	-8	-8	-8	-8	-8	-8
0	2	135	260	38	-4	-16	-33
-2	-16	83	135	-46	-33	-33	-10
-38	-18	36	-16	-32	-72	-24	-30
-12	-12	-12	-12	-12	-12	-12	-12

EPICARDIAL POTENTIALS (10 MICROVOLTS)

-705	-705	-705	-705	-705	-705	-705	-705
-3310	1186	-33	1495	-834	1201	-1298	2503
73	-377	-2	-164	700	-1095	717	-1185
79	77	43	5	-374	520	-561	266
8	8	8	8	8	8	8	8

FRAME 141

BODY-SURFACE POTENTIALS (MICROVOLTS)

-25	-25	-25	-25	-25	-25	-25	-25
-8	24	236	301	53	-10	-53	-41
-16	-22	117	178	-33	-25	-38	-24
-41	-12	51	8	-20	-80	-30	-48
-13	-13	-13	-13	-13	-13	-13	-13

EPICARDIAL POTENTIALS (10 MICROVOLTS)

-813	-813	-813	-813	-813	-813	-813	-813
-2686	1144	-26	1703	-1061	1755	-2053	2711
-92	-344	-12	-178	807	-1304	1273	-1541
141	68	53	3	-401	528	-727	359
24	24	24	24	24	24	24	24

FRAME 151

BODY-SURFACE POTENTIALS (MICROVOLTS)

-30	-30	-30	-30	-30	-30	-30	-30
-27	-25	211	346	60	-18	-62	-55
22	-32	138	235	-10	-32	-33	-30
-41	-12	80	24	-27	-51	-22	-41
-10	-10	-10	-10	-10	-10	-10	-10

EPICARDIAL POTENTIALS (10 MICROVOLTS)

-866	-866	-866	-866	-866	-866	-866	-866
-4419	1444	-53	1882	-1321	2054	-2668	3815
175	-452	4	-189	1243	-2525	2430	-2575
34	107	51	9	-665	1295	-1618	765
30	30	30	30	30	30	30	30

FRAME 161

BODY-SURFACE POTENTIALS (MICROVOLTS)

-38	-38	-38	-38	-38	-38	-38	-38
-16	-46	209	419	98	10	-76	-82
-33	-48	174	315	16	-4	-32	-38
-46	-18	115	51	0	-41	-13	-50
-6	-6	-6	-6	-6	-6	-6	-6

EPICARDIAL POTENTIALS (10 MICROVOLTS)

-975	-975	-975	-975	-975	-975	-975	-975
-5479	1652	-74	2171	-1573	2593	-3576	4852
278	-515	11	-201	1408	-2516	3010	-3250
18	129	74	11	-804	1560	-2066	982
49	49	49	49	49	49	49	49

FRAME 171

BODY-SURFACE POTENTIALS (MICROVOLTS)

-53	-53	-53	-53	-53	-53	-53	-53
-74	-96	220	536	150	12	-107	-124
-60	-67	201	447	48	10	-48	-72
-60	-38	146	101	55	-16	-16	-67
-8	-8	-8	-8	-8	-8	-8	-8

EPICARDIAL POTENTIALS (10 MICROVOLTS)

-1137	-1137	-1137	-1137	-1137	-1137	-1137	-1137
-7089	2031	-35	2452	-1173	2637	-4043	5935
483	-658	18	-198	1286	-2559	3617	-4173
-114	186	97	9	-371	1866	-2658	1349
76	76	76	76	76	76	76	76

FRAME 181

BODY-SURFACE POTENTIALS (MICROVOLTS)

-80	-80	-80	-80	-80	-80	-80	-80
-132	-138	217	687	212	22	-160	-196
-101	-124	240	628	117	13	-72	-114
-90	-72	132	178	51	-8	-27	-92
-13	-13	-13	-13	-13	-13	-13	-13

EPICARDIAL POTENTIALS (10 MICROVOLTS)

-1304	-1304	-1304	-1304	-1304	-1304	-1304	-1304
-7937	2258	-123	2943	-1462	3313	-5184	6994
520	-731	17	-205	1923	-3639	4970	-5174
-196	230	128	13	-1369	2607	-3814	1787
132	132	132	132	132	132	132	132

FRAME 191

BODY-SURFACE POTENTIALS (MICROVOLTS)

-106	-106	-106	-106	-106	-106	-106	-106
-189	-207	139	837	298	40	-212	-245
-130	-162	251	787	198	67	-76	-135
-101	-74	234	271	134	51	-12	-103
-6	-6	-6	-6	-6	-6	-6	-6

EPICARDIAL POTENTIALS (10 MICROVOLTS)

-1394	-1394	-1394	-1394	-1394	-1394	-1394	-1394
-9435	2545	-154	3325	-1078	3502	-6098	8125
723	-846	29	-204	1762	-3147	5756	-5868
-400	294	149	19	-1559	3403	-4826	2245
182	182	132	182	182	182	182	182

E.2 Solutions by Iterative Inversion

FRAME 1

BODY-SURFACE POTENTIALS (MICROVOLTS)

6	6	6	6	6	6	6	6
13	-24	0	-4	4	4	13	-12
-2	0	-8	-4	-6	36	24	4
-12	-6	-4	12	16	-6	0	33
0	0	0	0	0	0	0	0

EPICARDIAL POTENTIALS (10 MICROVOLTS)

3	3	3	3	3	3	3	3
-59	-0	-1	-8	8	5	15	13
-12	-2	-2	-2	-7	139	48	8
-9	-6	-4	-5	5	4	-6	-19
1	1	1	1	1	1	1	1

FRAME 11

BODY-SURFACE POTENTIALS (MICROVOLTS)

12	12	12	12	12	12	12	12
25	-10	8	0	10	18	25	12
16	10	2	16	2	20	38	6
0	10	-6	18	6	-8	16	48
8	8	8	8	8	8	8	8

EPICARDIAL POTENTIALS (10 MICROVOLTS)

6	6	6	6	6	6	6	6
-29	4	1	-3	16	14	27	23
-0	1	2	3	7	60	70	2
-4	-3	1	7	-7	-14	-6	-11
5	5	5	5	5	5	5	5

FRAME 21

BODY-SURFACE POTENTIALS (MICROVOLTS)

12	12	12	12	12	12	12	12
20	-25	-6	2	6	10	25	4
24	4	-12	40	4	10	32	8
13	20	6	20	32	0	18	32
8	8	8	8	8	8	8	8

EPICARDIAL POTENTIALS (10 MICROVOLTS)

5	5	5	5	5	5	5	5
-73	-7	-2	-3	-0	5	23	14
-22	-7	1	9	12	3	49	-3
-13	-17	1	23	2	-2	-9	-1
9	9	9	9	9	9	9	9

FRAME 31

BODY-SURFACE POTENTIALS (MICROVOLTS)

0	0	0	0	0	0	0	0
38	-4	-13	-8	0	2	2	4
51	51	48	64	12	30	50	30
57	103	59	64	88	30	57	62
27	27	27	27	27	27	27	27

EPICARDIAL POTENTIALS (10 MICROVOLTS)

-5	-5	-5	-5	-5	-5	-5	-5
-33	-17	-7	-29	-33	-14	-14	7
12	5	8	10	2	40	65	25
63	13	17	29	22	27	9	34
21	21	21	21	21	21	21	21

FRAME 41

BODY-SURFACE POTENTIALS (MICROVOLTS)

10	10	10	10	10	10	10	10
44	-51	-107	-53	4	10	22	0
88	94	30	85	51	60	74	60
110	110	106	92	83	62	107	101
53	53	53	53	53	53	53	53

EPICARDIAL POTENTIALS (10 MICROVOLTS)

-0	-0	-0	-0	-0	-0	-0	-0
-157	-92	-39	-120	-35	-9	3	11
-18	-14	-3	2	-0	130	101	86
92	28	27	39	29	27	44	90
29	29	29	29	29	29	29	29

FRAME 51

BODY-SURFACE POTENTIALS (MICROVOLTS)

12	12	12	12	12	12	12	12
16	-111	-146	-66	18	20	25	-30
55	0	10	57	55	69	76	41
66	67	74	92	76	72	100	80
50	50	50	50	50	50	50	50

EPICARDIAL POTENTIALS (10 MICROVOLTS)

1	1	1	1	1	1	1	1
-296	-120	-50	-139	5	0	11	-3
-108	-44	-21	-7	-4	188	114	50
9	-16	2	20	39	40	56	38
24	24	24	24	24	24	24	24

FRAME 61

BODY-SURFACE POTENTIALS (MICROVOLTS)

13	13	13	13	13	13	13	13
25	-53	-33	-32	8	8	30	-8
38	-18	-27	44	12	33	41	33
10	18	27	44	40	13	44	27
22	22	22	22	22	22	22	22

EPICARDIAL POTENTIALS (10 MICROVOLTS)

5	5	5	5	5	5	5	5
-145	-30	-16	-69	-2	2	24	16
-59	-21	-8	0	-6	83	62	55
-28	-33	-5	21	3	1	6	-16
13	13	13	13	13	13	13	13

FRAME 71

BODY-SURFACE POTENTIALS (MICROVOLTS)

8	8	8	8	8	8	8	8
20	-25	-2	-6	8	0	18	0
22	-32	-36	22	-30	2	12	13
0	-6	2	8	-16	-27	2	0
0	0	0	0	0	0	0	0

EPICARDIAL POTENTIALS (10 MICROVOLTS)

4	4	4	4	4	4	4	4
-67	-2	-2	-14	12	1	17	16
-38	-12	-3	3	-11	-9	16	25
-38	-29	-7	13	-50	-43	-26	-10
4	4	4	4	4	4	4	4

FRAME 81

BODY-SURFACE POTENTIALS (MICROVOLTS)

4	4	4	4	4	4	4	4
8	0	53	76	32	0	10	-38
27	-31	-10	74	-13	0	-10	-2
-27	-13	20	8	-33	-33	-6	-6
-2	-2	-2	-2	-2	-2	-2	-2

EPICARDIAL POTENTIALS (10 MICROVOLTS)

-0	-0	-0	-0	-0	-0	-0	-0
-14	37	27	131	56	-7	1	-4
-5	9	22	38	73	-50	-46	-40
-40	-20	8	49	-76	-82	-54	-68
13	13	13	13	13	13	13	13

FRAME 101

BODY-SURFACE POTENTIALS (MICROVOLTS)

66	66	66	66	66	66	66	66
-67	-776	-1831	-1689	521	484	132	-110
139	-270	-1250	164	1024	793	484	171
278	125	-12	687	943	771	602	324
300	300	300	300	300	300	300	300

EPICARDIAL POTENTIALS (10 MICROVOLTS)

9	9	9	9	9	9	9	9
-2023	-1462	-836	-3227	1055	226	47	-138
-1593	-932	-535	-446	-231	2655	760	104
-838	-1026	-422	-34	1219	847	570	85
138	138	138	138	138	138	138	138

FRAME 91

BODY-SURFACE POTENTIALS (MICROVOLTS)

-62	-62	-62	-62	-62	-62	-62	-62
-130	-278	-431	-148	257	130	-124	-223
-27	-146	-4	598	441	271	50	-50
38	38	221	481	447	274	178	36
88	88	88	88	88	88	88	88

EPICARDIAL POTENTIALS (10 MICROVOLTS)

-83	-83	-83	-83	-83	-83	-83	-83
-870	-436	-156	-402	343	-96	-294	-323
-474	-184	-31	83	345	405	-239	-607
-331	-177	40	299	218	35	-105	-346
181	181	181	181	181	181	181	181

FRAME 111

BODY-SURFACE POTENTIALS (MICROVOLTS)

106	106	106	106	106	106	106	106
115	-276	-618	-630	55	167	214	92
153	-85	-655	-301	139	209	235	182
125	24	-139	0	157	167	209	167
103	103	103	103	103	103	103	103

EPICARDIAL POTENTIALS (10 MICROVOLTS)

81	81	81	81	81	81	81	81
-604	-454	-270	-1128	222	206	300	220
-543	-361	-257	-242	-329	1044	603	633
-226	-419	-243	-200	395	371	356	296
-54	-54	-54	-54	-54	-54	-54	-54

FRAME 121

BODY-SURFACE POTENTIALS (MICROVOLTS)

4	4	4	4	4	4	4	4
25	-18	35	150	41	13	8	-16
30	-24	0	94	-18	-8	-12	30
-2	-8	30	0	-8	-36	12	0
6	6	6	6	6	6	6	6

EPICARDIAL POTENTIALS (10 MICROVOLTS)

-1	-1	-1	-1	-1	-1	-1	-1
-60	61	50	266	78	-0	-2	7
3	21	39	63	127	-89	-54	41
-32	-14	16	64	-64	-71	-48	-36
15	15	15	15	15	15	15	15

FRAME 141

BODY-SURFACE POTENTIALS (MICROVOLTS)

-25	-25	-25	-25	-25	-25	-25	-25
-8	24	206	301	53	-10	-53	-41
-16	-22	117	178	-33	-25	-38	-24
-41	-12	31	8	-20	-80	-30	-48
-13	-13	-13	-13	-13	-13	-13	-13

EPICARDIAL POTENTIALS (10 MICROVOLTS)

-24	-24	-24	-24	-24	-24	-24	-24
22	149	139	536	81	-45	-90	-57
91	87	95	124	232	-223	-141	-147
-12	52	63	118	-133	-153	-138	-129
31	31	31	31	31	31	31	31

FRAME 131

BODY-SURFACE POTENTIALS (MICROVOLTS)

-8	-8	-8	-8	-8	-8	-8	-8
0	2	135	260	38	-4	-16	-33
-2	-16	93	135	-46	-33	-33	-10
-38	-18	36	-16	-32	-72	-24	-30
-12	-12	-12	-12	-12	-12	-12	-12

EPICARDIAL POTENTIALS (10 MICROVOLTS)

-10	-10	-10	-10	-10	-10	-10	-10
-17	137	97	467	60	-22	-35	-25
75	74	30	103	188	-211	-110	-79
-8	40	49	95	-120	-125	-104	-97
20	20	20	20	20	20	20	20

FRAME 151

BODY-SURFACE POTENTIALS (MICROVOLTS)

-30	-30	-30	-30	-30	-30	-30	-30
-27	-25	201	346	60	-18	-62	-55
22	-32	138	235	-10	-32	-33	-30
-41	-12	30	24	-27	-51	-22	-41
-10	-10	-10	-10	-10	-10	-10	-10

EPICARDIAL POTENTIALS (10 MICROVOLTS)

-30	-30	-30	-30	-30	-30	-30	-30
-111	143	117	609	76	-62	-110	-87
65	89	108	149	287	-294	-156	-196
-23	55	77	154	-155	-171	-142	-156
44	44	44	44	44	44	44	44

FRAME 161

BODY-SURFACE POTENTIALS (MICROVOLTS)

-38	-38	-38	-38	-38	-38	-38	-38
-16	-46	209	419	98	10	-76	-82
-33	-48	174	315	16	-4	-32	-38
-46	-18	115	51	0	-41	-13	-50
-6	-6	-6	-6	-6	-6	-6	-6

EPICARDIAL POTENTIALS (10 MICROVOLTS)

-39	-39	-39	-39	-39	-39	-39	-39
-180	143	133	733	140	-64	-141	-102
54	98	131	187	381	-251	-186	-265
-41	63	97	202	-161	-192	-170	-202
62	62	62	62	62	62	62	62

FRAME 171

BODY-SURFACE POTENTIALS (MICROVOLTS)

-53	-53	-53	-53	-53	-53	-53	-53
-74	-96	220	536	150	12	-107	-124
-60	-67	201	447	48	10	-48	-72
-60	-38	146	101	55	-16	-16	-67
-8	-8	-8	-8	-8	-8	-8	-8

EPICARDIAL POTENTIALS (10 MICROVOLTS)

-57	-57	-57	-57	-57	-57	-57	-57
-334	141	157	926	219	-95	-204	-188
18	193	162	248	519	-310	-279	-437
-97	53	121	280	-176	-214	-221	-289
93	93	93	93	93	93	93	93

FRAME 181

BODY-SURFACE POTENTIALS (MICROVOLTS)

-80	-80	-80	-80	-80	-80	-80	-80
-132	-138	217	687	212	22	-160	-196
-101	-124	240	628	117	13	-72	-114
-96	-72	182	178	51	-8	-27	-92
-13	-13	-13	-13	-13	-13	-13	-13

EPICARDIAL POTENTIALS (10 MICROVOLTS)

-84	-84	-84	-84	-84	-84	-84	-84
-484	127	186	1177	301	-138	-302	-294
-38	104	202	329	711	-458	-412	-663
-193	38	153	385	-244	-325	-318	-427
136	136	136	136	136	136	136	136

FRAME 191

BODY-SURFACE POTENTIALS (MICROVOLTS)

-106	-106	-106	-106	-106	-106	-106	-106
-189	-207	139	837	298	40	-212	-245
-130	-162	251	787	198	67	-76	-135
-101	-74	234	271	134	51	-12	-103
-6	-6	-6	-6	-6	-6	-6	-6

EPICARDIAL POTENTIALS (10 MICROVOLTS)

-111	-111	-111	-111	-111	-111	-111	-111
-700	92	208	1424	443	-175	-399	-410
-117	90	233	405	910	-404	-503	-635
-273	5	172	472	-232	-337	-363	-539
179	179	179	179	179	179	179	179

E.3 Solutions from Perturbed Data

FRAME 1

BODY-SURFACE POTENTIALS (MICROVOLTS)

-2	-2	-2	-2	-2	-2	-2	-2
9	-28	9	-3	2	9	10	-6
-1	-5	-15	3	-0	26	18	10
-15	1	-9	20	24	-7	-1	35
4	4	4	4	4	4	4	4

EPICARDIAL POTENTIALS (10 MICROVOLTS)

-2	-2	-2	-2	-2	-2	-2	-2
-73	6	0	-9	0	2	9	10
-17	-2	-1	-0	-5	89	31	17
-19	-14	-6	-2	8	1	-14	-30
4	4	4	4	4	4	4	4

FRAME 11

BODY-SURFACE POTENTIALS (MICROVOLTS)

9	9	9	9	9	9	9	9
16	-0	8	2	18	21	22	18
23	4	1	13	2	16	42	7
5	3	-3	25	12	-17	10	44
13	13	13	13	13	13	13	13

EPICARDIAL POTENTIALS (10 MICROVOLTS)

4	4	4	4	4	4	4	4
-7	4	1	0	35	15	21	11
0	1	2	3	10	44	77	2
-10	-4	-0	4	-4	-19	-18	-5
6	6	6	6	6	6	6	6

FRAME 21

BODY-SURFACE POTENTIALS (MICROVOLTS)

2	2	2	2	2	2	2	2
13	-34	-14	0	-1	1	32	-4
32	4	-19	37	1	7	39	2
15	17	0	22	33	-7	9	29
6	6	6	6	6	6	6	6

EPICARDIAL POTENTIALS (10 MICROVOLTS)

-0	-0	-0	-0	-0	-0	-0	-0
-93	-13	-4	-6	-19	-3	31	9
-30	-11	-0	8	4	-5	63	-17
-18	-23	-2	20	0	-7	-20	6
9	9	9	9	9	9	9	9

FRAME 31

BODY-SURFACE POTENTIALS (MICROVOLTS)

-2	-2	-2	-2	-2	-2	-2	-2
46	1	-5	-14	6	-2	-1	0
54	56	56	63	11	35	40	28
54	98	76	64	91	26	64	70
35	35	35	35	35	35	35	35

EPICARDIAL POTENTIALS (10 MICROVOLTS)

-6	-6	-6	-6	-6	-6	-6	-6
-19	-10	-7	-41	-16	-18	-19	8
22	10	9	8	1	60	44	21
68	19	19	29	24	27	11	28
21	21	21	21	21	21	21	21

FRAME 41

BODY-SURFACE POTENTIALS (MICROVOLTS)

19	19	19	19	19	19	19	19
34	-42	-135	-59	12	15	19	1
97	90	39	81	50	55	79	67
100	115	135	101	77	52	109	93
55	55	55	55	55	55	55	55

EPICARDIAL POTENTIALS (10 MICROVOLTS)

5	5	5	5	5	5	5	5
-135	-90	-40	-130	-16	-9	-0	0
-12	-10	-3	-0	-2	109	112	105
96	35	28	34	22	15	39	75
29	29	29	29	29	29	29	29

FRAME 61

BODY-SURFACE POTENTIALS (MICROVOLTS)

14	14	14	14	14	14	14	14
33	-61	-30	-34	6	15	25	-4
39	-19	-25	36	12	40	51	31
1	12	34	47	41	23	45	18
12	12	12	12	12	12	12	12

EPICARDIAL POTENTIALS (10 MICROVOLTS)

6	6	6	6	6	6	6	6
-162	-27	-16	-73	-5	12	-20	17
-59	-19	-8	-2	-11	110	83	51
-26	-30	-6	15	6	10	14	-27
13	13	13	13	13	13	13	13

FRAME 51

BODY-SURFACE POTENTIALS (MICROVOLTS)

17	17	17	17	17	17	17	17
11	-103	-147	-72	23	21	31	-32
53	6	18	64	47	76	66	37
64	67	59	97	81	66	91	72
58	58	58	58	58	58	58	58

EPICARDIAL POTENTIALS (10 MICROVOLTS)

5	5	5	5	5	5	5	5
-279	-122	-32	-152	15	3	16	-12
-101	-43	-20	-7	-9	209	90	34
9	-12	5	23	31	35	43	33
26	26	26	26	26	26	26	26

FRAME 71

BODY-SURFACE POTENTIALS (MICROVOLTS)

17	17	17	17	17	17	17	17
28	-35	-8	-10	1	-4	23	-1[illegible]
19	-39	-30	30	-38	6	9	13
-4	-14	11	6	-13	-33	0	8
-0	-0	-0	-0	-0	-0	-0	-0

EPICARDIAL POTENTIALS (10 MICROVOLTS)

9	9	9	9	9	9	9	9
-92	-8	-5	-23	-5	0	23	28
-45	-12	-3	4	-19	5	9	22
-39	-26	-3	20	-58	-47	-32	-18
5	5	5	5	5	5	5	5

FRAME 81

BODY-SURFACE POTENTIALS (MICROVOLTS)

-5	-5	-5	-5	-5	-5	-5	-5
4	0	55	83	31	-4	1	-38
37	-34	-15	77	-21	0	-9	-4
-27	-7	19	15	-34	-33	-13	-4
-7	-7	-7	-7	-7	-7	-7	-7

EPICARDIAL POTENTIALS (10 MICROVOLTS)

-7	-7	-7	-7	-7	-7	-7	-7
-16	37	29	142	52	-9	-11	-16
-10	8	22	40	71	-57	-50	-52
-47	-25	6	49	-89	-88	-63	-73
15	15	15	15	15	15	15	15

FRAME 101

BODY-SURFACE POTENTIALS (MICROVOLTS)

57	57	57	57	57	57	57	57
-58	-767	-1827	-1681	513	491	126	-112
141	-271	-1250	156	1028	793	488	172
276	120	-5	697	945	777	607	327
297	297	297	297	297	297	297	297

EPICARDIAL POTENTIALS (10 MICROVOLTS)

4	4	4	4	4	4	4	4
-2002	-1459	-834	-3212	1034	231	39	-133
-1586	-928	-594	-445	-234	2649	768	103
-836	-1021	-422	-42	1221	850	576	81
139	139	139	139	139	139	139	139

FRAME 91

BODY-SURFACE POTENTIALS (MICROVOLTS)

-66	-66	-66	-66	-66	-66	-66	-66
-122	-287	-434	-157	262	132	-114	-214
-21	-140	-1	602	435	272	48	-54
34	31	223	477	452	274	176	41
83	83	83	83	83	83	83	83

EPICARDIAL POTENTIALS (10 MICROVOLTS)

-86	-86	-86	-86	-86	-86	-86	-86
-894	-431	-156	-420	355	-89	-284	-315
-472	-181	-30	82	342	406	-244	-619
-330	-175	42	303	216	39	-106	-352
181	181	181	181	181	181	181	181

FRAME 111

BODY-SURFACE POTENTIALS (MICROVOLTS)

114	114	114	114	114	114	114	114
116	-275	-600	-632	51	170	213	98
146	-85	-656	-296	131	211	226	179
117	24	-139	-3	155	163	207	169
96	96	96	96	96	96	96	96

EPICARDIAL POTENTIALS (10 MICROVOLTS)

87	87	87	87	87	87	87	87
-602	-449	-259	-1133	210	210	300	215
-536	-355	-255	-241	-336	1052	583	627
-222	-412	-239	-195	386	366	352	284
-54	-54	-54	-54	-54	-54	-54	-54

FRAME 121

BODY-SURFACE POTENTIALS (MICROVOLTS)

8	8	8	8	8	8	8	8
30	-15	37	143	38	7	3	-21
32	-16	8	93	-18	-4	-5	20
5	-3	28	8	-12	-39	9	9
1	1	1	1	1	1	1	1

EPICARDIAL POTENTIALS (10 MICROVOLTS)

1	1	1	1	1	1	1	1
-55	62	49	255	67	-6	-8	6
9	24	39	61	119	-79	-43	13
-27	-9	17	62	-71	-79	-54	-27
16	16	16	16	16	16	16	16

FRAME 141

BODY-SURFACE POTENTIALS (MICROVOLTS)

-31	-31	-31	-31	-31	-31	-31	-31
-16	23	205	296	44	-9	-53	-38
-19	-25	138	168	-40	-24	-29	-31
-32	-7	58	6	-19	-71	-20	-52
-5	-5	-5	-5	-5	-5	-5	-5

EPICARDIAL POTENTIALS (10 MICROVOLTS)

-27	-27	-27	-27	-27	-27	-27	-27
22	149	108	527	60	-37	-88	-63
87	85	92	120	217	-212	-120	-165
-10	47	58	111	-133	-142	-123	-111
30	30	30	30	30	30	30	30

FRAME 131

BODY-SURFACE POTENTIALS (MICROVOLTS)

1	1	1	1	1	1	1	1
-6	-3	195	265	37	-1	-7	-34
-2	-18	89	140	-37	-43	-32	-15
-44	-13	38	-16	-31	-62	-28	-34
-4	-4	-4	-4	-4	-4	-4	-4

EPICARDIAL POTENTIALS (10 MICROVOLTS)

-3	-3	-3	-3	-3	-3	-3	-3
-30	145	100	477	59	-25	-25	-31
77	78	93	106	198	-251	-107	-96
-4	43	52	99	-113	-118	-101	-106
20	20	20	20	20	20	20	20

FRAME 151

BODY-SURFACE POTENTIALS (MICROVOLTS)

-38	-38	-38	-38	-38	-39	-38	-38
-37	-33	136	353	68	-19	-52	-56
12	-27	129	239	-7	-24	-30	-35
-48	-20	75	24	-21	-42	-14	-45
-15	-15	-15	-15	-15	-15	-15	-15

EPICARDIAL POTENTIALS (10 MICROVOLTS)

-36	-36	-36	-36	-36	-36	-36	-36
-130	138	117	622	96	-59	-99	-98
59	85	108	152	298	-266	-151	-213
-32	48	74	155	-151	-163	-133	-167
45	45	45	45	45	45	45	45

FRAME 161

BODY-SURFACE POTENTIALS (MICROVOLTS)

-32	-32	-32	-32	-32	-32	-32	-32
-13	-45	239	424	106	15	-67	-74
-32	-43	131	321	10	-8	-24	-44
-42	-22	113	54	-9	-35	-13	-58
2	2	2	2	2	2	2	2

EPICARDIAL POTENTIALS (10 MICROVOLTS)

-36	-36	-36	-36	-36	-36	-36	-36
-180	142	134	740	158	-67	-132	-102
57	100	133	189	386	-272	-172	-285
-41	67	100	206	-177	-197	-168	-199
63	63	63	63	63	63	63	63

FRAME 181

BODY-SURFACE POTENTIALS (MICROVOLTS)

-77	-77	-77	-77	-77	-77	-77	-77
-125	-143	213	678	208	31	-169	-198
-34	-121	242	631	114	5	-78	-116
-88	-77	175	172	53	-17	-36	-87
-9	-9	-9	-9	-9	-9	-9	-9

EPICARDIAL POTENTIALS (10 MICROVOLTS)

-82	-82	-82	-82	-82	-82	-82	-82
-496	123	133	1160	294	-127	-312	-295
-39	103	201	328	704	-489	-425	-669
-195	41	136	389	-245	-330	-328	-424
136	136	136	136	136	136	136	136

FRAME 171

BODY-SURFACE POTENTIALS (MICROVOLTS)

-58	-58	-58	-58	-58	-58	-58	-58
-78	-104	228	539	158	18	-105	-116
-62	-59	197	447	47	15	-56	-72
-61	-47	138	111	49	-11	-19	-62
-6	-6	-6	-6	-6	-6	-6	-6

EPICARDIAL POTENTIALS (10 MICROVOLTS)

-60	-60	-60	-60	-60	-60	-60	-60
-356	148	150	931	238	-95	-202	-197
18	103	153	248	522	-296	-300	-443
-106	48	119	277	-187	-221	-224	-296
94	94	94	94	94	94	94	94

FRAME 191

BODY-SURFACE POTENTIALS (MICROVOLTS)

-112	-112	-112	-112	-112	-112	-112	-112
-189	-216	138	846	295	30	-207	-244
-122	-162	252	783	189	76	-72	-130
-96	-68	224	279	142	43	-20	-97
1	1	1	1	1	1	1	1

EPICARDIAL POTENTIALS (10 MICROVOLTS)

-116	-116	-116	-116	-116	-116	-116	-116
-723	90	209	1439	435	-179	-394	-406
-121	89	233	405	304	-373	-497	-823
-276	4	170	467	-234	-339	-375	-533
180	180	180	180	180	180	180	180

REFERENCES

Barnard, A.C.L., Duck, I.M. and Lynn, M.S. (1967). The application of electromagnetic theory to electrocardiography I. Derivation of the integral equations. Biophys. J. Vol. 7, p. 443-62.

Barnard, A.C.L., Duck, I.M., Lynn, M.S. and Timlake, W.P. (1967). The application of electromagnetic theory to electrocardiography II. Numerical solution of the integral equations. Biophys. J. Vol. 7, p. 463-91.

Barr, R.C., Pilkington, T.C., Boineau, J.P. and Spach, M.S. (1966). Determining surface potentials from current dipoles with application to electrocardiography. IEEE Trans. bio-med. Engng. BME-13, p. 88-92.

Barr, R.C., Pilkington, T., Boineau, J. and Rogers, C. (1970). An inverse electrocardiographic solution with an on-off model. IEEE Trans. bio-med. Engng. BME-17, p. 49-57.

Barr, R.C., Spach, M.S. and Herman-Giddens, G.S. (1971). Selection of the number and positions of measuring locations for electrocardiography. IEEE Trans. bio-med. Engng. BME-18, p. 125 -138.

Barr, R.C. and Spach, M.S. (1976). Inverse solutions directly in terms of potentials. In 'The theoretical basis of electrocardiology'. p. 294-304, Clarendon Press, Oxford.

Bellman, R., Collier, C., Kagiwada, H., Kaloba, R. and Selvester, R. (1964). Estimation of heart parameters using skin potential measurements. Communs. Asso. Comp. Mach. Vol. 7, p. 666-8.

Binns, K.J. and Lawrenson, P.J. (1973). Analysis and computation of electric and magnetic field problems. Pergamon Press, Oxford.

Burger, H.C. and van Milaan, J.B. (1946). Heart vector and leads. Br. Heart J. Vol. 8, p. 157-61; (1947). Vol. 9, p. 154-8; (1948). Vol. 10, p. 229-33.

Brody, D.A. and Hight, J. (1972). Test of an inverse electrocardiographic solution based on accurately determined model data. IEEE Trans. bio-med. Engng. BME-19, p. 221-8.

Durrer, D., Roos, J.P. and Buller, J. (1965). The spread of excitation in canine and human heart. In 'Electrophysiology of the heart', p. 203-214. Pergamon Press, Oxford.

Durrer, D., van Dam, R. Th., Freud, G.E., Janse, M.J., Meijler, F.L. and Arzbaecher, R.C. (1970). Total excitation of the isolated human heart. Circulation Vol.41, p. 899-912.

Fischmann, E.J. and Barber, M.B. (1963). Aimed electrocardiography. Model studies using a heart consisting of six electrically isolated areas. Am. Heart J. Vol. 65, p. 628-7.

Frank, E. (1952). Electric potential produced by two current sources in a homogeneous conducting sphere. J. Appl. Phys. Vol. 23, p. 1225.

Gabor, D. and Nelson, C.V. (1954). Determination of the resultant dipole of the heart from measurements on the body surface. J. Appl. Phys. Vol. 25, p. 413-16.

Gelernter, H.L. and Swihart, J.C. (1964). A mathematical-physical model of the genesis of the electrocardiogram. Biophys. J. Vol. 4, p. 285-301.

Geselowitz, D.B. (1960). Multipole representation for an equivalent cardiac generator. Proc. Inst. Radio Engrs. Vol. 48, p. 75-9.

Geselowitz, D.B. (1967). On bioelectric potentials in an inhomogeneous volume-conductor. Biophys. J. Vol. 7, p. 1.

Hamer, J., Boyle, D. and Sowton, E. (1965). The transmission of electrical forces from the heart to the body surface. Br. Heart J. Vol. 27, p. 365-73.

Hildebrand, F.B. (1968). Finite-difference equations and simulations. Prentice-Hall, New Jersey.

Horan, L. and Flowers, N. (1967). Simulation of the sequence of the ventricular activation and the choice of an inverse solution. Med. Res. Engng. Vol. 6, p. 28-35.

Karplus, W.J. (1958). Analog simulation. McGraw-Hill, New York.

Lanczos, C. (1956). Applied analysis. Prentice-Hall, New Jersey.

Lanczos, C. (1958). Iterative solution of large-scale linear systems. J. Soc. Indust. Appl. Math. Vol. 6, p. 91-109.

Lanczos, C. (1961). Linear differential operators. Van Nostrand, London.

Lo, G.C.C and Monro, D.M. (1976). Simulation of electric fields in the human thorax. In 'Advances in cardiology' Vol. 21, S. Karger, Basel.

Lynn, M., Barnard, A.C.L., Holt, J. and Sheffield, L. (1967). A proposed method for the inverse problem in electrocardiography. Biophys. J. Vol. 7, p. 925-45.

Martin, R.O. and Pilkington, T.C. (1972). Unconstrained inverse electrocardiography: Epicardial potentials. IEEE Trans. bio-med. Engng. BME-19, p. 276-85.

Milne, W.E. (1953). Numerical solution of differential equations. Wiley, New York.

Monro, D.M., Guardo, R.A.L., Bourdillion, P.J. and Tinker, J. (1974). A technique for simultaneous electrocardiographic surface mapping. Cardiovasc. Res. Vol. 8, p. 688-700.

Nelson, C.V. and Geselowitz, D.B. (1976). The theoretical basis of electrocardiology. Clarendon Press, Oxford.

Nicholson, P.W. (1967). Experimental models for current conduction in an anisotropic medium. IEEE Trans. bio-med. Engng. BME-14, p. 55.

Okada, R.H. (1956). Potential produced by an eccentric current dipole in a finite-length circular conducting cylinder. IRE Trans. Med. Electron. Vol. 7, p. 14.

Plonsey, R. (1966). Limitations on the equivalent cardiac generator. Biophys. J. Vol. 6, p. 163-173.

Plonsey, R. (1969). Bioelectric phenomena. McGraw-Hill, New York.

Plonsey, R. and Heppner, D.B. (1967). Considerations of quasi-stationarity in electrophysiological systems. Bull. Math. Biophys. Vol. 29, p. 657.

Rogers, C.L. and Pilkington, T.C. (1968). The solution of over-determined equations as a multistage process. IEEE Trans. bio-med. Engng. BME-15, p. 179-85.

Rush, S. (1970). An inhomogeneous anisotropic model of the human torso for electrocardiographic studies. Med. Biol. Engng. Vol. 9, p. 201-11.

Rush, S., Abildskov, J.A. and McFee, R. (1963). Resistivity of body tissues at low frequencies. Circulation Res. Vol. 12. p. 40-50.

Selvester, R.H., Palmersheim, J. and Pearson, R.B. (1971). VCG inverse model for prediction of myocardial diseases. In 'Vectorcardiography 2', p. 54-65, North-Holland, Amsterdam.

Spach, M.S. and Barr, R.C. (1975). Ventricular intramural and epicardial potential distributions during ventricular activation and repolarization in intact dog. Circulation Res. Vol. 37, p. 243-257.

Spach, M.S. and Barr, R.C. (1976). Analysis of ventricular activation and repolarization from intramural and epicardial potential distributions for ectopic beats in the intact dog. Circulation Res. Vol. 37, p. 830-843.

Symington, J. (1956). An atlas illustrating the topographical anatomy of the head, neck and trunk. Oliver and Boyd, London.

Taccardi, B. and Marchetti, G. (1965). Distribution of heart potentials on the body surface and in artificial conducting media. In 'Electrophysiology of the heart', p.203-214, Pergamon Press, Oxford.

Taccardi, B., Musso, E. and Ambroggi, L. (1971). Potential fields of normal and ischemic hearts during rest, ventricular excitation and recovery. In 'Vectorcardiography 2', p. 142-5, North-Holland, Amsterdam.

Terry, F. (1967). Comparison of iterative techniques for solving Neumann problems. Proc. 20th Ann. Con. Engng. Med. Biol. Vol. 9, p. 21.5.

Twomey, S. (1963). On the numerical solution of Fredholm integral equations of the first kind by inversion of the linear system produced by quadrature. J. Asso. Comp. Mach. Vol. 10, p. 97-101.

Twomey, S. (1965). The application of numerical filtering to the solution of integral equations encountered in indirect sensing measurements. J. Franklin Inst. Vol. 279, p. 95-109.

Twomey, S. and Howell, H.B. (1963). A discussion of indirect sounding methods, with special reference to the deduction of vertical ozone distribution from light scattering measurements. Mon. Weather Rev. Vol. 91, p. 659-664.

Vitkovitch, D. (1966). Field analysis. Van Nostrand, London.

Volynskii, B.A. and Bukhman, V.Ye. (1965). Analogues for the solution of boundary-value problems. Pergamon Press, Oxford.

Yeh, G.C. and Martinek, J. (1957). The potential of a general dipole in a homogeneous conducting prolate spheroid. Ann. New York Acad. Sci. Vol. 19, p. 293-308.

Yeh, G.C., Martinek, J. and de Beaumont, H. (1958). Multipole representation of current generators in a volume conductor. Bull. Math. Biophys. Vol. 20. p. 203-16.